The Thesis Committee for Roman J. Shor
Certifies that this is the approved version of the following thesis:

Modeling Proppant Flow in Fractures using LIGGGHTS, a Scalable
Granular Simulator

APPROVED BY
SUPERVISING COMMITTEE:

Supervisor:

Mukul M. Sharma

Jon E. Olson

Modeling Proppant Flow in Fractures using LIGGGHTS, a Scalable Granular Simulator

by

Roman J. Shor, B.A.; B.S.E.; M.S.E.

Thesis

Presented to the Faculty of the Graduate School of

The University of Texas at Austin

in Partial Fulfillment

of the Requirements

for the Degree of

Master of Science in Engineering

The University of Texas at Austin
May 2014

Dedication

Dedicated to the vision and forbearance of my parents and to the patience and wisdom of all.

Acknowledgements

Abstract

Modeling Proppant Flow in Fractures using LIGGGHTS, a Scalable Granular Simulator

Roman J. Shor, M.S.E.

The University of Texas at Austin, 2014

Supervisor: Mukul M. Sharma

Proppant flowback in fractures under confining pressures is not well understood and difficult to reproduce in a laboratory setting. Improper management of proppant flowback leads to flow restrictions near the well bore, poor fracture conductivity and costly production equipment damage. A simple, scalable model is developed using a discrete element method (DEM) particle simulator, to simulate representative cubic volumes consisting of fracture openings, fracture walls and the confining formation. The effects of fracture width, confining stress, fluid flow velocity and proppant cohesion are studied for a variety of conditions. Fracture width is found to be dependent on confining stress and fluid flow velocity while proppant production is also dependent on cohesion. Three regimes are observed, with complete fracture evacuation occurring at high flow rates and low confining stresses, fully packed fractures occurring at high confining stresses and open but mostly evacuated fractures occurring in-between. From these observations, a recommended flowback rate can be estimated for a given set of conditions. A slow and controlled well flowback is recommended to improve proppant pack stability. The rate ramp-up time is dependent on the leak-off coefficient.

Table of Contents

List of Figures

x

List of Illustrations

1.   INTRODUCTION

With unconventional formations producing an ever-increasing fraction of the world's oil and gas, hydraulic fracture treatments in horizontal wells are becoming standard industry practice for production wells around the world. A majority of new onshore hydrocarbon production within the United States comes from tight, or low permeability, formations that require stimulation, such as hydraulic fracturing, to be produced economically. Over the past fifty years, hydraulic fracturing treatments have become widespread and increasing complex, often involving dozens of stages in extended reach horizontal wells. Typical treatments conclude with the injection of slurries laden with proppants that remain trapped in the fractures to maintain the width of and to increase the permeability of generated fractures. These proppants can vary from common sand, sorted by size to suit treatment parameters, to manufactured polymer beads and can be coated with resins or other surface modification agents to improve proppant pack cohesion, to improve proppant and pack compressive strength and permeability and to reduce erosion during flowback or production. The production of fracture or formation fluids add additional stresses to these proppant packs and in many cases cause a portion of the proppant to be produced back to the surface. Mitigation techniques to reduce proppant production during flowback vary vastly by operator and service company and include various shut-in or flowback procedures, proppant treatments and screens.

The mechanics of proppant packing and pack failure have been studied, both in industry and academia, for over fifty years, but disagreement still exists about the

mechanics of pack failure, the influences of the various formation and proppant grain properties and the effect of flowback rates. The lack of agreement has led to varied, and often conflicting, flowback practices and policies in the field without one cohesive, industry wide standard that is able to maximized proppant placement and fracture conductivity. This thesis will begin with a survey of current insights and understandings of proppant pack stability, including the various modeling approaches, and the experimental and field studies. A discrete element model, built upon an open source particle simulator, of proppant packs in simple hydraulic fractures using a granular formulation will be presented. The underlying particle model will be based on a soft sphere contact model used extensively for particle and molecular simulations. An investigation and a sensitivity analysis of the stability of these packs will follow that will attempt to infer the effects of fracture width, confining stress, pressure drop and proppant cohesion on proppant pack stability. Finally, a recommendation on flowback procedure is presented.

2. LITERATURE REVIEW

Over the last fifty years, a suite of tools has been developed by industry to mitigate proppant flowback that includes forced closure – rapid flowback of fracturing fluids on fracturing treatment completion, slow flowback – slower flowback of fracture fluid, resin coated sands – to increase cohesion of proppant grains, deformable proppants – to increase contact area between grains, mechanical screens and frac-packs – to keep proppants and formation fines out of the wellbore, resin injection – to increase cohesion of proppants near the wellbore, and surface modification agents (Trela et al., 2008; Nguyen & Jaripatke, 2009). The range of conditions recommended for each of these is less well understood, often leading to suboptimal fracturing treatments. As a case and point, there are no standard industry practices or recommendations available currently for well flowback to maximize well productivity and proppant placement while minimizing flowback of proppant.

Hydraulic fracture treatments involve the pumping of high-pressure fluids to propagate fractures in the target formations and include stages where slurries containing proppants and other additives with the goal of propping open the induced fractures on completion, as empty fractures would close upon treatment completion since the fracture fluid is carrying the formation stresses and often do not provide the desired improvement in permeability. The fracturing fluid pressure must overcome the in situ geologic stresses, both near the wellbore and in the far field, and the strength of the formation to propagate the fracture. During the treatment, the carrier fluids carry confining stresses,

but once pumping is stopped and flowback begins, the confining stress are transferred to the proppant packs deposited. Proppant settling is a major concern, and depending on carrier fluid viscosities, proppant size and treatment duration, proppant settling can lead to very little proppant placement in the top of the fracture or far within the fracture. To reduce settling of the proppant within the fracture, and to lock proppant-packs into upper or far field portions of the fracture, forced closure – with rapid flowback of fracturing fluids – has been proposed and applied successfully as a mitigation technique (Ely, 1996; Weaver et al., 1999). During forced closure, once the proppant slurry is pumped into the fracture, the fluid is rapidly produced back to surface in an effort to quickly close the fracture and lock the proppant within it. However, due to the high fracture fluid flow velocities, due to the large pressure drops, proppant pack erosion near the wellbore, especially near the perforations, where fluid velocities are greatest, has been observed.

To improve the cohesion between proppant grains – and thus improving pack strength, resin coatings, surface modification agents and injection of resins have all been proposed as mitigating techniques and have been actively applied to reduce proppant pack erosion. Resin coatings of proppant grains, applied before pumping at the surface, improves cohesion between the grains within a proppant pack and has been shown, dependent on the formulation of resin being used, to improve the compressive strength, permeability and resistance to flow erosion of the pack. Resin coatings must be allowed to cure within the fracture once pumping is complete for set periods of time prior to fracture fluid flowback, but there is evidence that some flowback must occur prior to

4

completion of the curing process to ensure proper grain to grain contact is established within the proppant packs (Nguyen et al., 1998). Treatments involving resins must be carefully designed due to the sensitivity of the resin – including curing time and final strength – to carrier and formation fluid properties, pressures and temperatures (Dewprashad et al., 1993). Conventional proppant packs and weak or unconsolidated formations with tendencies to produce formation fines have also been strengthened with surface modification agents and resin injections (Trela et al., 2008).

There have been successful applications of deformable proppants where either high production flow rates or low confining stresses have caused conventional proppant packs to erode rapidly. In shallow formations with low confining stresses and formation rock strength, treatments where deformable proppant was mixed in with standard sands have shown improved resistance to pack erosion. The higher static friction of the deformable proppants – through increased inter-grain contact areas – improved the cohesion of the packs in the presence of low confining pressures (Stephenson et al., 2003). In high pressure, high temperature (HPHT) scenarios where high confining stresses, high flow rates and extreme temperatures typically reduce the pack strength of conventional proppants, deformable proppants have shown promise by improving the compressive strengths of packs and resisting erosion due to high fluid flow (Stephenson et al., 2002; Brannon et al., 2003).

Formations with tendencies to produce formation fines – typically unconsolidated or poorly consolidated sands and sandstones – are typically treated using frac-packs,

gravel packs or screens to reduce production of fines and reduce surface equipment damage. Each of these techniques serves as a filter to restrict flow to formation fines while continuing to allow formation fluids to be produced (Nguyen & Jaripatke, 2009; Trela et al., 2008). While pumping proppant slurries, through fractures that intersect formations containing highly permeable zones, such as natural fractures, tip screenouts have been shown to occur due to the formation of proppant packs in the zones of high leakoff (Weng & Klein, 1998).

2.1   Previous Work

Efforts to model and understand the behavior of proppants in slurries and in proppant packs began in the 1950s and 1960s with the application of broad correlations that related predicted pack stabilities from fluid flow velocities, proppant transport and settling velocities. Much of this work – especially the correlations between proppant transport and fluid flow – was the application of pioneering work done in sedimentology and geomorphology to understand sediment transport – as functions of grain size and fluid velocity – in rivers and deltas in the earlier part of the century (Baker & Pyne, 1978). Continued industry application of hydraulic fracturing has necessitated a rapid increase in the understanding of the complexity of fracture networks and proppant transport, distribution and packing.

Early efforts sought to understand, quantify and predict the placement and transport of placement in fractures. The importance of proppant transport and placement in fractures was systematically documented in a study of different proppant placement strategies in over 200 wells (Gadde & Sharma, 2005) and several alternative strategies for proppant placement have been suggested (Liu et al., 2007; Malhotra et al., 2013). In 1977, Novotny presented a model that accounted for the geometry of the fracture, fluid leakoff to the formation and fluid heating in simple planar fractures. Using analytic solutions for the settling velocity of proppant grains – in Newtonian fluids – and by deriving extensions for flow between smooth parallel plates, the significance of proppant settling on proppant pack distribution was shown to be significant. Correlations

7

developed from laboratory experiments extended this analysis to non-Newtonian fluids and it was shown that the shearing properties – especially shear thickening behavior – of the carrier fluids had great impacts on retaining proppants in suspension during the shut-in stage of proppant treatments (Novotny, 1977). In experiments conducted using glass plates, it was found that stable proppant packs – of single proppant grain widths – could only be formed when proppant diameters were the same size as the fracture width. This showed that fracture wall roughness – glass plates being smooth – was integral to formation of wider proppant pack and that channeling within stable proppant packs accelerated proppant production by increasing fluid velocity within the channels (Barree & Conway, 2001).

These simple types of two-dimensional models were unable to adequately explain or predict proppant placement, so three-dimensional models were developed, such as the one presented by Settari and Cleary (1984). Their model was used to predict the placement of proppant throughout an entire fracture, but it was hindered by its simplistic view of fracture geometry – limited to simple planar fractures – and by limited available field data with which to construct a realistic model for a specific field case. Proppant placement and gravitational settling was noted to be highly dependent on the closure period and on the breakdown characteristics of any gels used in the fracture fluids. Increased closure period, or equivalently slower flowback of fracture fluid, caused greater settling while longer gel breakdown deterred settling .

Later work began to use probabilistic methods to determine the failure of individual two dimensional grid blocks of proppant packs in fractures. The inferred flow velocity, confining loads and proppant properties determined proppant pack failure in each grid block based upon a set of failure criteria. A critical flow velocity was found to cause catastrophic pack failure and was dependent on proppant size and closure stress. Large proppants had higher critical flow velocities. Higher closure stress led to lower critical flow velocities. The addition of resin coatings or surface modification agents increased the critical flow velocities and reduced catastrophic pack failure, but instead formed channels within the proppant packs (Parker et al., 1999; van Batenburg et al., 1999).

A different approach was introduced shortly after Novotny's work in which the movement of individual proppant grains was described and modeled. By modeling individual proppant grains as simple spheres with inherent masses and velocities and allowing for their interaction, proppant distribution, flow and packing could be investigated at a granular scale. Until acted upon by an external force, such as a fluid force, a sphere would continue moving along its velocity vector until contact is made with a boundary or another sphere. On contact, reactive forces are calculated from each sphere's relative mass, velocity and spin, through a simple spring and dashpot model. The spring and dampening coefficients are calculated from material and fluid properties. These models did not model the effects of fluids directly, but instead added point drag forces to grains to simulate the viscous effect of fluid. Verifications with laboratory data

for sand packing and confining strength were carried out (Cundall & Strack, 1979; Tamura et al., 1994). A similar approach has been applied to sand production from weak formations (O'Connor et al., 1997).

Asgian et al. (1995) performed a series of eight simulations of proppant packs within fractures using granular fracture walls in a variety of conditions. From their limited data set, they concluded that cohesionless proppant packs are stable in fractures narrower than 5.5 proppant diameters in the presence of flowbacks less than 75 psi / ft. They note that flowbacks experienced in the field typically range from 10 to 30 psi / ft and hence a majority of narrow fractures are stable with ordinary sand. These forms of models have been extended to simulate multiphase flows (Dartevelle, 2004). A detailed survey of these models is presented by (Herrmann & Luding, 1998).

3.   MODEL FORMULATION

Existing proppant transport and stability models for fractures can be separated into two general categories, the finite element models and the discrete element models. Finite element models treat volumes of the fracture – in either two dimensions or three dimensions – as grid blocks for a finite calculation mesh and use continuum equations, correlations, or laws – or a combination thereof – to model a continuous phenomenon. The basic principles of this type of model rely on exchange of mass or energy across gradients on mesh block boundaries. Discrete element models use the basic physical interaction between discrete model elements – proppant grains and fracture walls in this case – and appropriate boundary conditions to achieve a similar result. Instead of using gradients in energy or concentration, energy is directly exchanged between elements and the movement of mass is discretely tracked. For example, an FEM model of diffusion would track the gradient in concentration across a mesh over time as mass or energy flows to balance the gradient. A DEM model of the same phenomenon could track the distribution of the individual point masses as collisions between elements acted to move mass.

Fracture and proppant models presented in the previous section can be categorized into these two broad categories based on their method of computation: finite element models (Novotny, 1977; Settari & Cleary, 1984; Mangeney et al., 2007; van Batenburg et al., 1999; Parker et al., 1999) and discrete element models (Cundall & Strack, 1979; Tamura et al., 1994; Asgian et al., 1995). Discrete methods have the

advantage of simulating phenomena from base principles while finite element methods are able to simulate much larger systems. The major disadvantage of DEM models is the computation intensity of the simulation, since computation time grows as a function of particle count – which can be quite large for fracture-proppant models. This thesis will present a continuation of the discrete work presented by Asgian et al. (1995) using a new open source granular simulator.

The following work has been presented and published at the 2014 Hydraulic Fracturing Conference in the Woodlands, Texas (Shor & Sharma, 2014).

3.1   Discrete Element Model

The base model is built upon an open source granular simulator called LIGGGHTS, **L**AMMPS **I**mproved for **G**eneral **G**ranular and **G**ranular **H**eat **T**ransfer **S**imulations, and is described in detail by Kloss (Kloss & Goniva). It is a simple soft sphere contact model, where spherical particles interact due to an overlap, δ, between particles, causing tangential and normal forces to be transferred through a spring-dashpot system that abstracts material properties. The normal force, F_n, is given by

$$\vec{F}_n = -k_n\vec{\delta} + c_n\overrightarrow{\Delta v_n}$$

where δ is the spatial overlap and Δv_n is the normal relative velocity at the contact point.

The tangential force, F_t, is given by

$$\overrightarrow{F_t} = k_t \left| \int_{t_{c,0}}^{t} \Delta v_t(\tau)d\tau \right| \vec{t} + c_t \overrightarrow{\Delta v_t}$$

where Δv_t is the relative tangential velocity, t is the tangential vector at the contact point, and $t_{c,0}$ is the time at which contact between particles begins. The magnitude of the tangential force is bounded by the frictional force,

$$\max\left(\left|\overrightarrow{F_t}\right|\right) = \left|\mu \overrightarrow{F_n}\right|.$$

The integration of force balance is carried out using the Lagrangian method for the particle phase, as described by Cundall and Strack, and evaluates the following basic equation of state (Cundall & Strack, 1979).

$$m_p \overrightarrow{\ddot{x}_p} = \overrightarrow{F_n} + \overrightarrow{F_t} + m\vec{g}$$

The point drag force on each proppant grain is calculated from the drag force from the viscous fluid and from the inertia of the particle. Asgian et al. (1995) calculate an upper bound for this force from base principles as

$$F_d = \frac{8}{3}\pi r^3 \frac{dP}{dx}$$

Where r is the radius of the particle and $\frac{dP}{dx}$ is the pressure drop within the fracture.

The simulator maintains neighbor lists for each discrete element and updates whenever the element moves a specified distance. Each element is only interacting directly with its neighbors and computation time is drastically reduced.

13
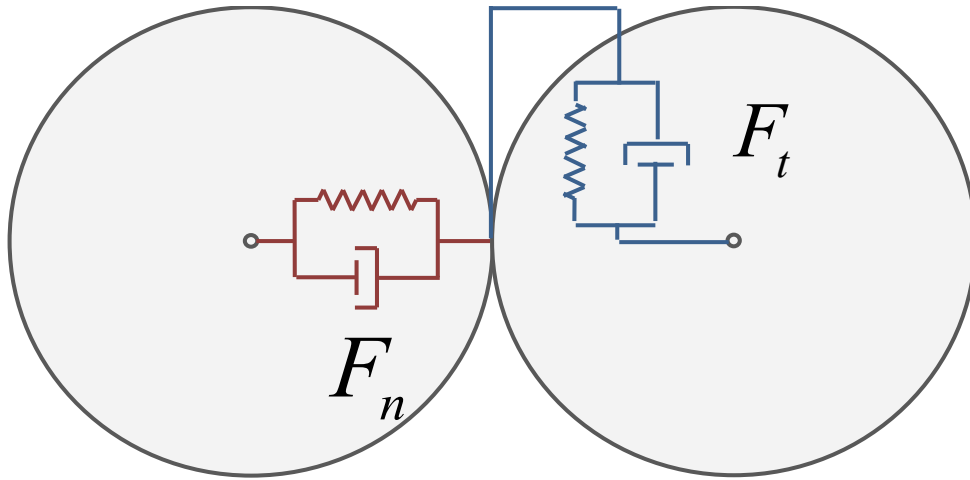
Illustration 1 Linear spring and dashpot model used for the soft sphere contact model. Once spheres overlap, normal and tangential forces are exchanged. The spring constants and dampening parameters are functions of material properties of the grain material, the viscosity of the surrounding medium and the cohesion between particles. Dampening increases with viscosity and cohesion while the spring constant increases with material stiffness.
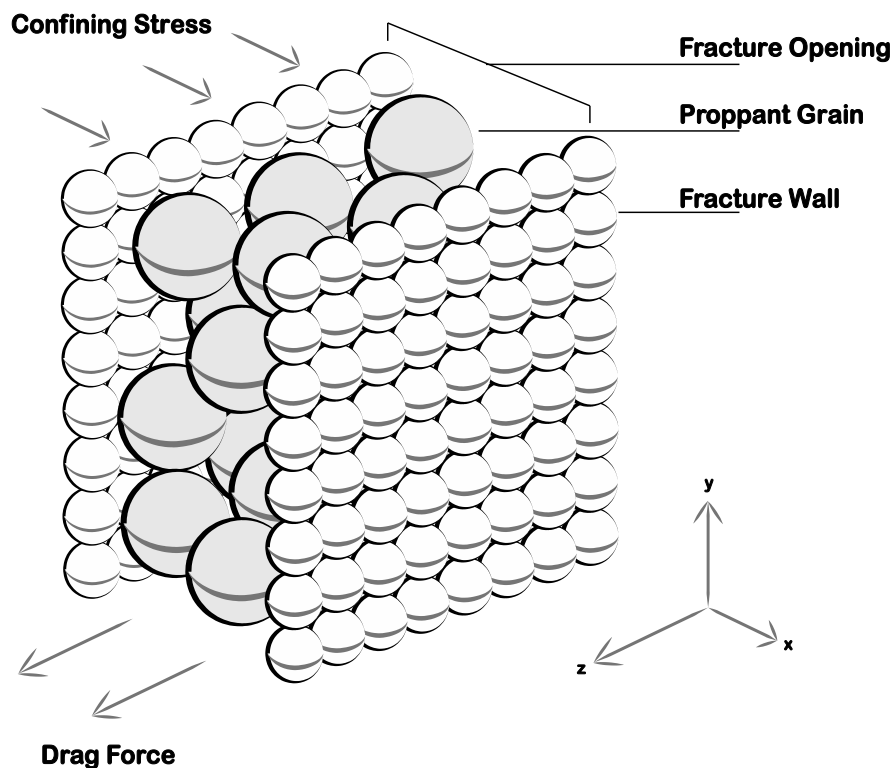
Illustration 2 A representative volume from within a fracture. The representative volume contains fracture walls that measure 3 mm by 3 mm and the initial width varies from 0.25 mm to 1.5 mm. Walls are modeled as square lattices of spherical grains while the proppant pack is a random packing of spherical grains between them. Confining stress from the formation acts normal to the plane of the fracture walls, represented as square lattices of smaller spheres. Fluid flow exerts a point drag force on proppant grains and acts perpendicular to the normal force. An open boundary allows proppant to flow out of the fracture and be produced..
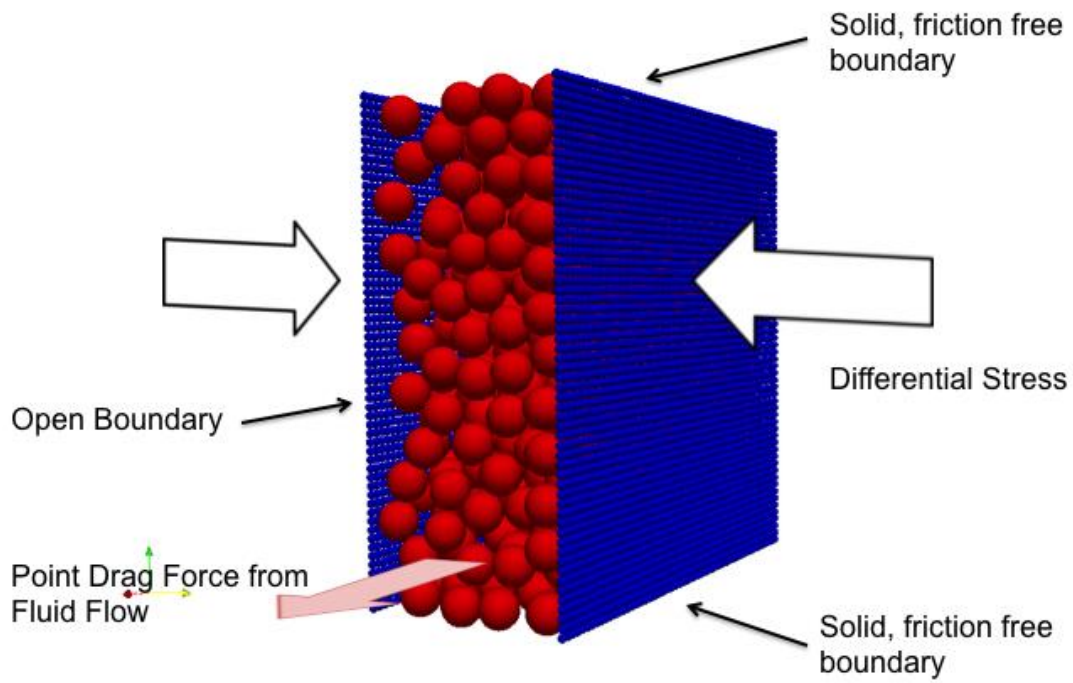
Illustration 3 The same volume, this time as simulated. Red spheres are the proppant grains, blue spheres are the square lattice representing the fracture walls.

3.2   Simulation Procedure

The simulation entails the creation of a proppant pack and then the application of confining pressure from the formation.

1.   Before the simulation can begin, a simulation volume and boundary conditions need to be defined in the model space. For the intents of this study, all simulations are run in a 3 mm cube with no flux boundary conditions in the y and z directions and a periodic boundary condition in the y direction. Given the small size of the simulation, the periodic condition simulates a fracture whose height is much greater than its width, as is expected. Once proppant packing is completed, the fixed boundary in the positive z direction is relaxed and becomes an open boundary to allow proppant to be produced.

2.   A random proppant pack is generated in the previously defined fracture void volume and is allowed to relax and lose energy, in the form of granular vibration, as proppant would in the presence of a carrier liquid. The random packing is dependent on a generating seed, allowing multiple simulations with identical packs to be performed.

3.   Fracture walls are inserted as square lattices of smaller spherical particles in rigid bodies. These walls are assumed to remain parallel and immobile except in the normal direction throughout the simulation.   The only force interactions allowed are in normal forces in the x direction and the lattices are allowed to move in the x direction as the fracture opens or closes. This condition allows the lattice walls to feel no torque or equivalently

maintain a rotational infinite moment of inertia, details and derivation may be found in earlier work (Mondal et al., 2011).

4. A normal force is applied to the fracture walls in the x direction and the proppant pack is allowed to consolidate within the fracture. This normal force is directly equivalent to the net pressure exerted on the pack by the formation and is balance of minimum horizontal stress, pore pressure and wellbore / fracture fluid pressure.

5. A point drag force is applied to each proppant particle and the front boundary condition is eased and allowed to become an open boundary. Proppant that is produced leaves the simulation, so computation time per time step decreases as the simulation continues.

   In the set of simulations presented in this thesis, the proppant is not replaced once it flows out and the fracture is allowed to empty rather than be replaced with new proppant. This was done to study the tendencies of the proppant to form stable proppant bridges at the onset of flowback and the assumption that bridges would not form without some form of flow constriction once the entire pack is mobile.

6. The simulation is allowed to continue until the system is at equilibrium and no more proppant can be produced under current conditions.

These simulations were run on a dual quad core Xeon processor with 4GB of memory. Typically two simulations can be run simultaneously with each simulation running in parallel on four cores on a single processor to reduce data communication between the two processors. Simulations take anywhere from four to eight hours to execute to completion with this hardware.
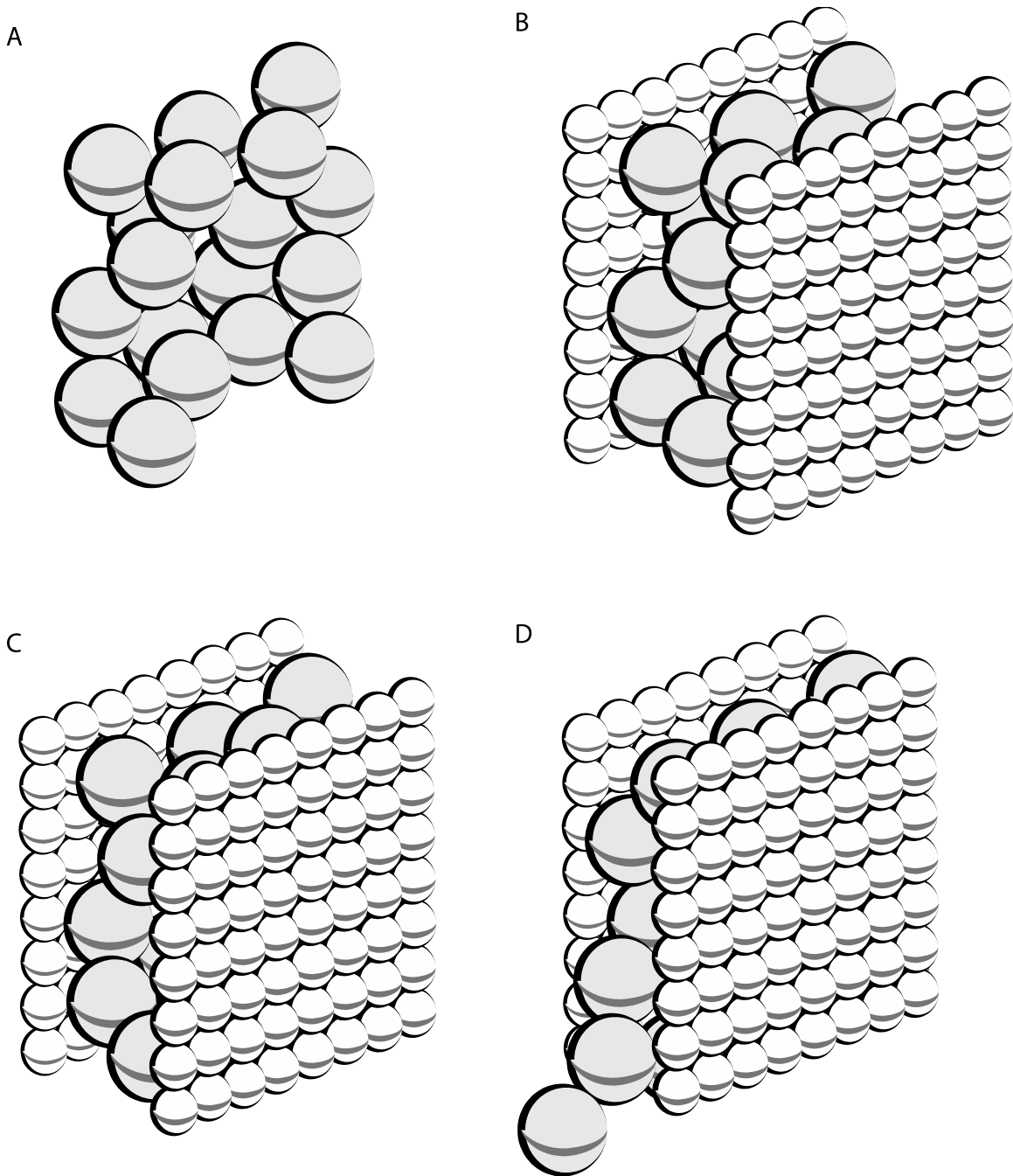
Illustration 4 The simulation procedure begins with the generation of a proppant pack

(A), addition of fracture walls (B), compaction (C) and application of

fluid flow and proppant production (D)

3.3   Choice of Simulation Conditions

A first approximation of for the pressure gradient experienced inside a planar fracture with a stable proppant pack is the Kozeny-Carmen model for flow through a packed bed of spherical particles.

$$\frac{dp}{dl} = \frac{180\mu v (1 - \epsilon)^2}{d_s^2 \epsilon^3}$$

where v is the interstitial velocity, μ is the fluid viscosity, ϵ is the porosity and d_s is the sphere diameter. The three general types of fluids used in fracture treatments today are slickwater fracs, with fluid viscosities between 1 and 3 centipoise, linear gels with viscosities between 10 and 30 centipoise, and crosslinked gels with viscosities up to 1000 centipoise. Assuming a fracture that is 5mm wide, 100 meters tall with 250 micron proppant and a flowrate of 1000 BBL / day and taking three fluid viscosities of 1, 10 and 100 centipoise, the pressure gradients as a function of the distance from the wellbore can be calculated and are shown in Figure 1.
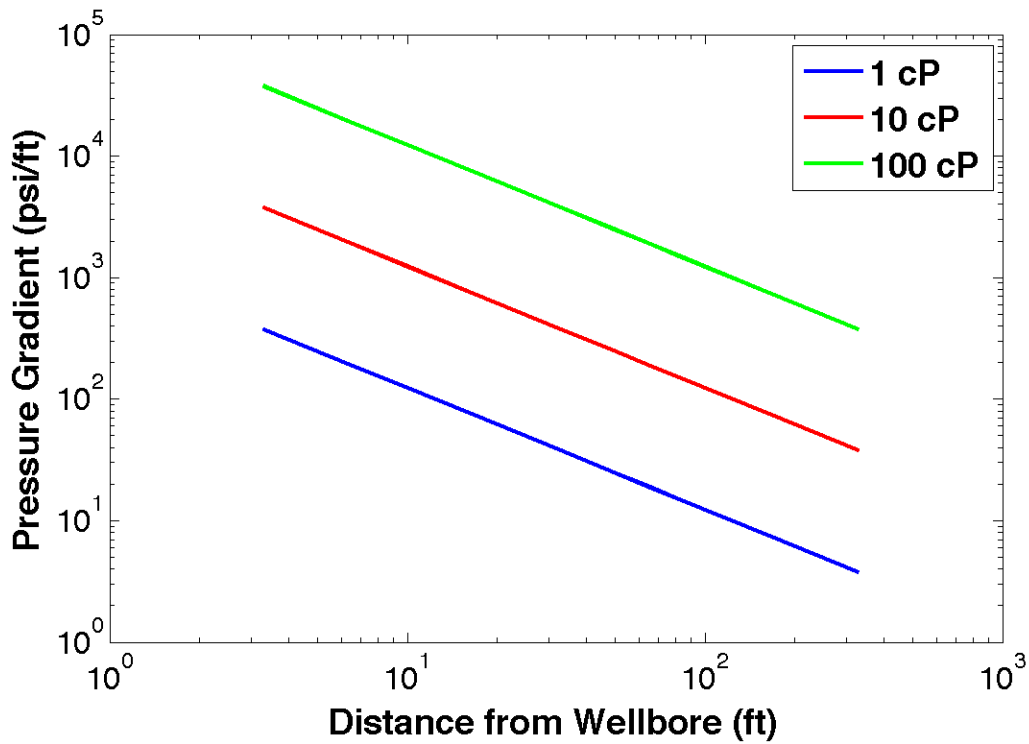
Figure 1 Pressure gradients within a planar fracture, as calculated using the Kozeny-Carmen model for flow in a packed bed of spherical particles. The fracture is uniformly 5 mm wide, 100 meters tall, contains 250 micron proppants and is subject to a 1000 bbl / day flow rate.

4.   RESULTS

Presented herein are results from over two thousand simulations representing well over 8000 hours of computer time. The contour and surface plots presented are constructed from the interpolation of discreet simulation results, each run for a specified set of initial and boundary conditions, specified on the x and y axes. Fracture widths are normalized by the diameter of the proppant, in the case of monodisperse proppants, or the maximum diameter of proppant, in the case of polydisperse proppants.

$$Width_d = \frac{Width_{final}}{D_{proppant}}$$

Mass fractions of produced proppant are normalized to the original mass of proppant placed in the fracture opening at the start of the simulation.

$$Mass_d = \frac{Mass_{final}}{Mass_{initial}}$$

To simulate the conditions in all parts of a fracture, a representative volume is taken and the confining stress, fluid pressure gradient, and initial fracture width is taken to represent expected conditions in desired location in the fracture. For example, to simulate a farfield location in a fracture at the moment of shut-in – when the mud pumps are shut off – a narrow initial fracture with zero net confining stress would be chosen since the fracture fluid is carrying the entire closure stress. Hundreds of these simulations are then run with varied pressure gradients in the flowing fluid and net confining stresses on the fracture walls, representing conditions in various locations in a

fracture to create a picture of conditions throughout. The results are presented in plots that follow and show the mass fraction of proppant produced once steady state is reached – where a stable proppant pack has formed or no proppant remains – which is implemented as a constant simulation mass criterion. Simulations were run starting with a fracture width of 2, 3 or 4 proppant diameters and fracture flow pressure gradients ranging from 0 to 400 psi / ft, as typically seen in planar fractures in horizontal wells. A simple application of the Kozeny-Carmen model for fluid flow through packed beds, as presented previously, shows that pressure gradients from fractures normal to the wellbore display pressure gradients over 100 psi / ft within 15 feet of the wellbore and drop to below 10 psi / ft 75 feet away from the wellbore. The ranges of net confining stresses represent conditions experienced during flowback with low net confining stresses immediately after shut-in and higher net confining stresses after fracture closure. Clear trends are seen that illustrate that proppant flowback is dependent on initial fracture width, net confining stress, pressure gradient of the fluid flowing and proppant cohesion.

4.1   Monodisperse Proppant

The first set of simulations use a monodisperse proppant, 235 microns in diameter in a variety of initial widths, net confining stresses and flowback pressure gradients. Figure 2 shows a contour plot of final fracture width for a fracture that is initially two proppant diameters in width as a function of net confining pressure in psi and the fracture flow gradient in psi / ft. For low net confining stresses, on the left side of the plot, the fracture width increases to three proppant diameters due to the set up of the simulation – the small net confining stress is unable to counterbalance the lateral forces imparted from collisions with the proppant grains, thus pushing the fracture walls apart and widening the fracture. This is not expected to occur in nature and is an artifact of the model setup. Moving from left to right, the net confining stress increases from 1 psi (simulating a fracture where the fracture fluid is carrying the stress while the fracture remains pressurized) to 3000 psi. Once the net confining stress reaches 1 psi, the fracture falls to two proppant diameters wide. As the pressure continues to increase, the fracture begins to collapse to a single proppant diameter in width, becoming 1.5 proppant diameters wide at 500 psi and a single proppant diameter wide at 2000 psi. There is little change to the final fracture width as the pressure gradient increases (y-axis), except at low net confining stresses. When there is little net confining stress, proppant grains are free to be produced at high pressure gradients, above 100 psi / ft for a net confining stress of 1 psi or less, and the fracture collapses.

Figure 3 presents the same information as Figure 2, but instead shows final fracture width as a function of net confining stress for several pressure gradients. This plot shows three distinct regions: (1) at low net confining stresses, the final fracture width is highly dependent on pressure gradient – collapsing to one at high pressure gradients, (2) between 1 and 100 psi, the final fracture width is independent of both net confining pressure and pressure gradient and (3) above 100 psi where the final fracture width decreases with increasing net confining pressure due to proppant pack reorganization and compaction.

Figure 4 shows a contour plot of the fraction of proppant produced in the same conditions as the previous two figures: a fracture initially two proppant diameters wide with net confining stress and the pressure gradient being varied. The behavior of this plot is more dependent on the pressure gradient than the previous one, as is expected. An increasing pressure gradient will carry more proppant grains out of a fracture, but may not necessarily reduce its width if there are stable proppant bridges propping it open. At low net confining stresses, below 2 psi at low (less than 10 psi / ft) pressure gradients and below 10 psi at high (greater than 100 psi / ft) pressure gradients , 90% of the proppant is produced out of the fracture. As net confining stress increases, so does proppant retention and the fraction of proppant produced decreases to less than 20% when the net confining stress exceeds 100 psi for all flow pressure gradients. The fraction of proppant produced also varies with the pressure gradient, so for a set net confining stress, the fraction produced will increase with an increased pressure gradient.

For example, at 10 psi of net confining stress, the fraction of proppant produced increases from just 30% in a 0.1 psi / ft pressure gradient to 100% in a 100 psi / ft pressure gradient.

Another way to view the proppant mass fraction produced is shown in Figure 5, which presents the fraction of proppant produced as a function of net confining stress for several pressure gradients. At low net confining stresses, nearly all the proppant is produced regardless of pressure gradient. Between 1 and 500 psi, the fraction produced varies greatly with the pressure gradient. And above 500 psi, very little proppant is produced, regardless of the pressure gradient. The top line (in pink) shows production with a 316 (=$10^{2.5}$) psi / ft pressure gradient – proppant only begins to remain within the fracture once a net confining stress of 10 psi is reached. The bottom line (in red) shows that production with a 1 psi / ft pressure gradient is limited to less than 30% with the same 10 psi net confining stress.

Figure 6 and Figure 7 present the same information – final fracture width – as Figure 2 and Figure 3, but for a fracture that is originally three proppant diameters in width. The final fracture width remains largely independent of the pressure gradient except at low net confining stresses, where the fracture collapses if the pressure gradient is over 100 psi / ft and the net confining stress is below 1 psi. However, at flowbacks over 100 psi / ft, the final fractures become limited at two proppant grains in width, showing that a proppant bridge greater than two proppant grains is not stable in a high flowback situation. Figure 7 shows the same flat behavior between 1 and 100 psi of net

26

confining stress as did Figure 3, but begins to shift downward – towards a narrower fracture – as the pressure gradient increases.

Figure 8 and Figure 9 present the mass fraction of proppant produced for a fracture originally three proppant diameters in width (comparable to Figure 4 and Figure 5 for the two proppant width fracture). A similar trend is observed, where the fraction of proppant produced increases with higher flowback pressure gradients and decreases with increasing net confining stress. The limits remain similar, with over 90% of the proppant being produced at low net confining stresses, or less than 1 psi for a 1 psi / ft flowback to less than 10 psi for a 100 psi / ft flowback. Less than 20 % of proppant is produced for a net confining stress of 50 psi for a 1 psi / ft flowback or 100 psi net confining stress for a 100 psi / ft flowback. The dependence of proppant production on the flowback pressure gradient is shown again in Figure 9 where the fraction of proppant produced is plotted as a function of net confining stress for discrete flowback pressure gradients. Once again, over 90% of proppant is produced in a 1 psi net confining stress while less than 20% is produced for a 1000 psi net confining stress, regardless of flowback. Between 1 and 1000 psi, the fraction of proppant produced increases with pressure gradient for a set net confining stress.

The data for a fracture initially four proppant diameters wide is presented as well. Figure 10 and Figure 11 present the final fracture widths and Figure 12 and Figure 13 present the fraction of proppant produced. The trends are similar as for a three proppant diameter wide fracture, where the fracture continues to collapse down to a two proppant

diameter wide fracture with a flowback of 100 psi / ft or greater. The fraction of proppant produced is shifted to the left slightly, where more proppant is produced for a stress-gradient combination than for a three diameter wide fracture, simply due to a greater number of proppant grains and a wider opening from which to be produced..

All these simulations have been for the case of proppants without cohesion (representing sand or bauxite), the simulated fractures collapse to widths of two proppant diameters at lower net confining stresses, regardless of original fracture width, indicating that stable bridges containing at least two proppant grains have formed. These fractures begin to narrow to a single proppant diameter in width as the net confining pressure increases, due to proppant bridges collapsing and additional proppant being produced. In all cases, fractures remain two diameters wide until the net confining stress exceeds 100 psi and begin to narrow significantly once it reaches 300 psi. At low net confining stresses, a propped fracture is formed, but most proppant is still produced, due to sparse bridges forming and propping open the fracture. At higher net confining stresses, a propped and packed fracture is formed, as the net confining stress allows more bridges to form and additional proppant is trapped. Fracture width is widely not affected by fluid flow within the fracture until the pressure drop equals 100 psi / ft or greater, at which point the fracture collapses at low net confining stresses. Fraction of proppant remaining in the fracture is dependent on fracture flow velocity, with more proppant remaining with lower flow for equal net confining stresses, as is expected, with remarkably log linear behavior.

An inverse correlation between final fracture width and the fraction of proppant produced can be noted, with wide fractures occurring at low net confining stresses also exhibiting high proppant production. Increased net confining stresses increase the fraction of proppant remaining by first facilitating the creation of stable bridges, up to 100 to 300 psi, at which point the bridges begin to collapse and the fracture begins to narrow. At this point, a fully packed fracture is exhibited and proppant production is minimized.
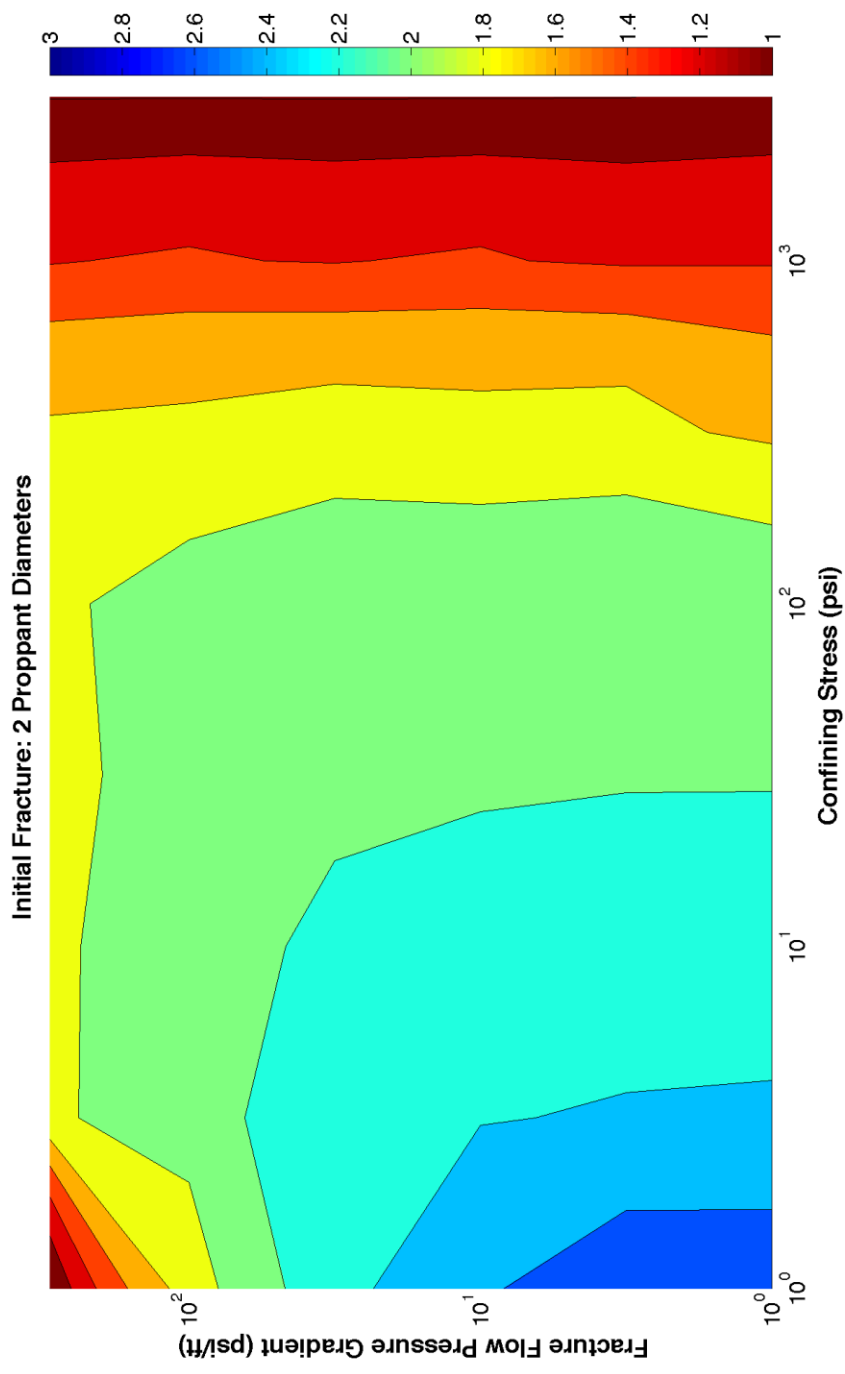
Figure 2 Final fracture width, normalized by proppant diameter, for a fracture initially two proppant diameters wide and a monodisperse 235 micron proppant.
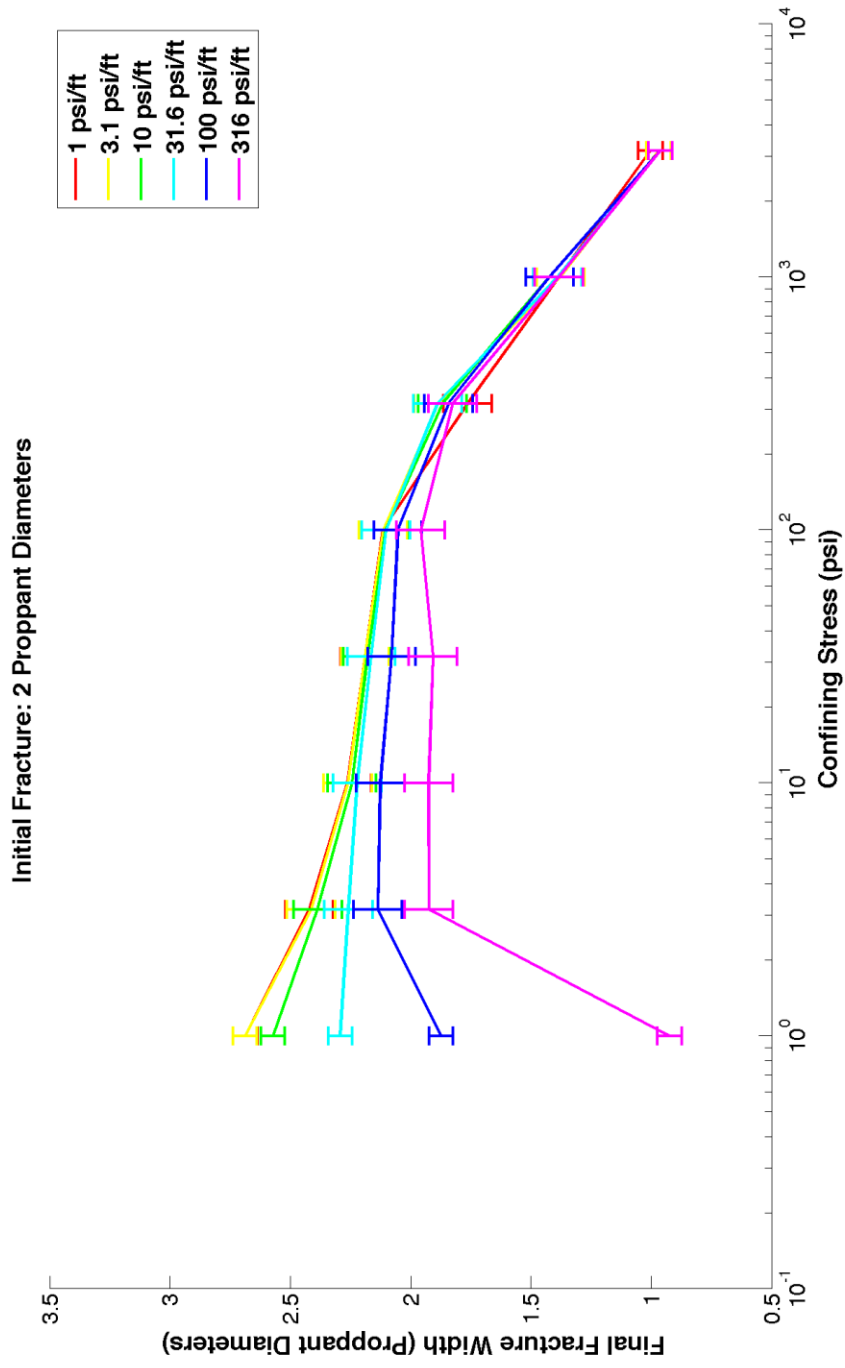
Figure 3 Final fracture width, normalized by proppant diameter, for a fracture initially two proppant diameters wide and a monodisperse 235 micron proppant.

Figure 4 Mass fraction of proppant produced for a fracture initially two proppant diameters wide with a monodisperse 235 micron proppant.
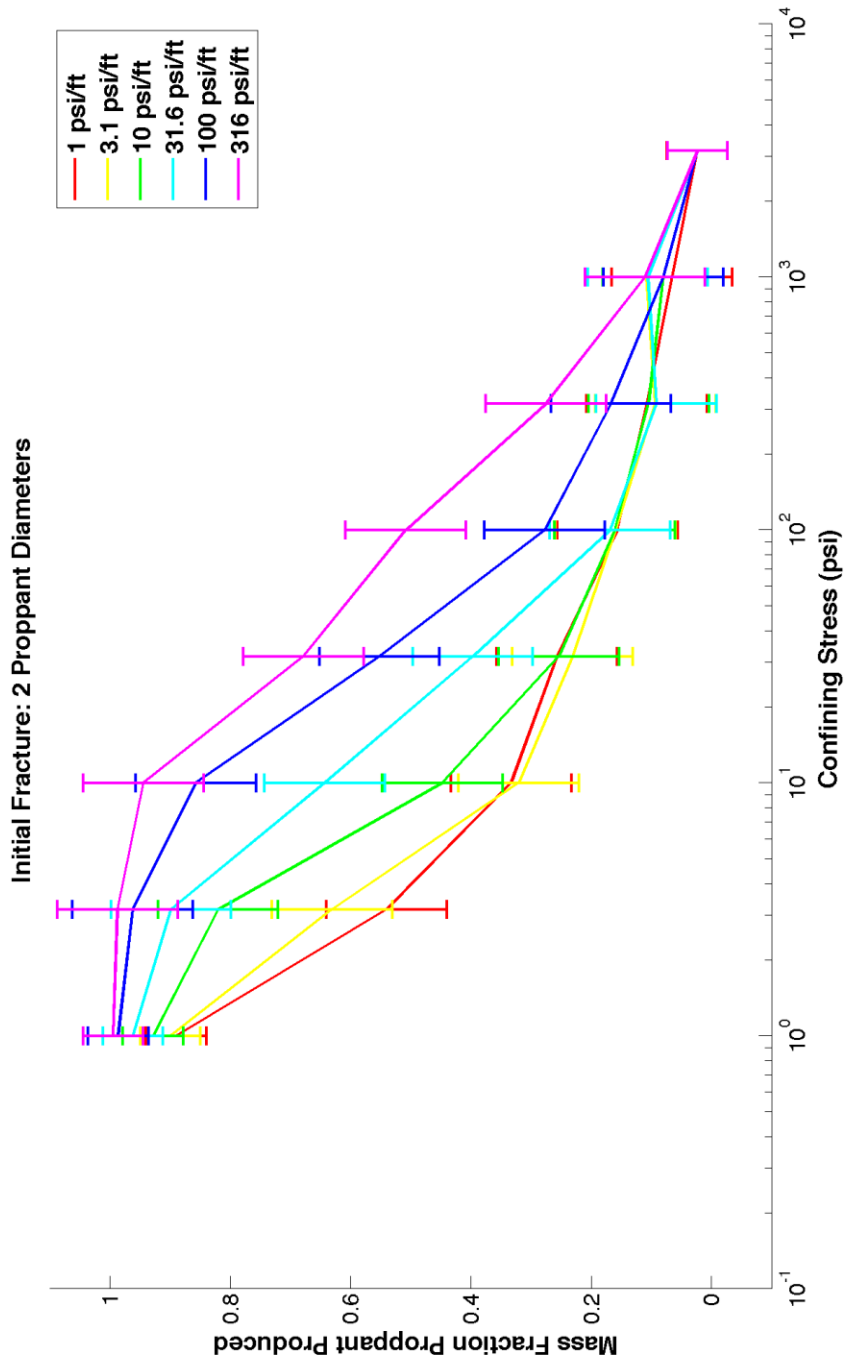
Figure 5 Mass fraction of proppant produced for a fracture initially two proppant diameters wide with a monodisperse 235 micron proppant
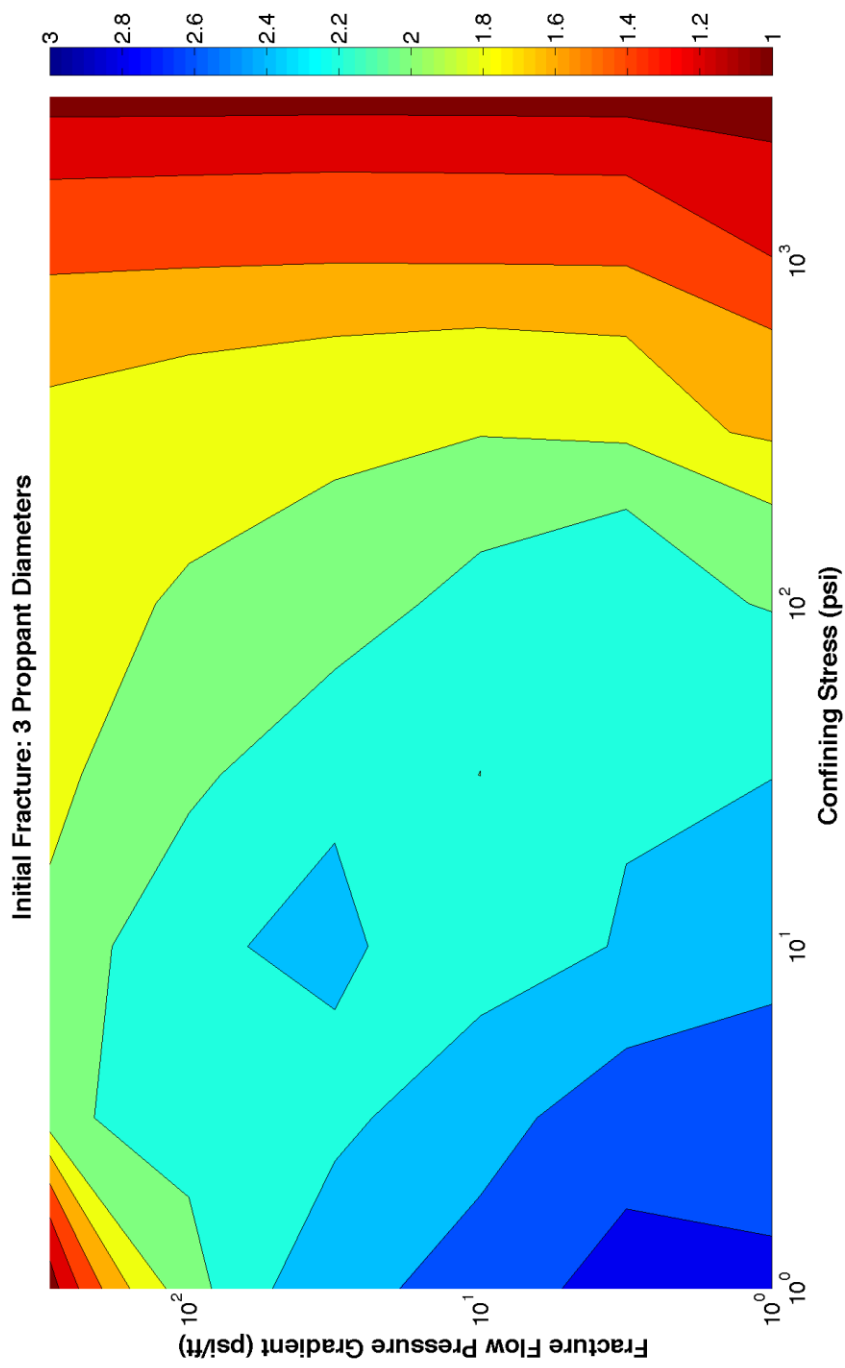
Figure 6 Final fracture width, normalized by proppant diameter, for a fracture initially three proppant diameters wide and a monodisperse 235 micron proppant.
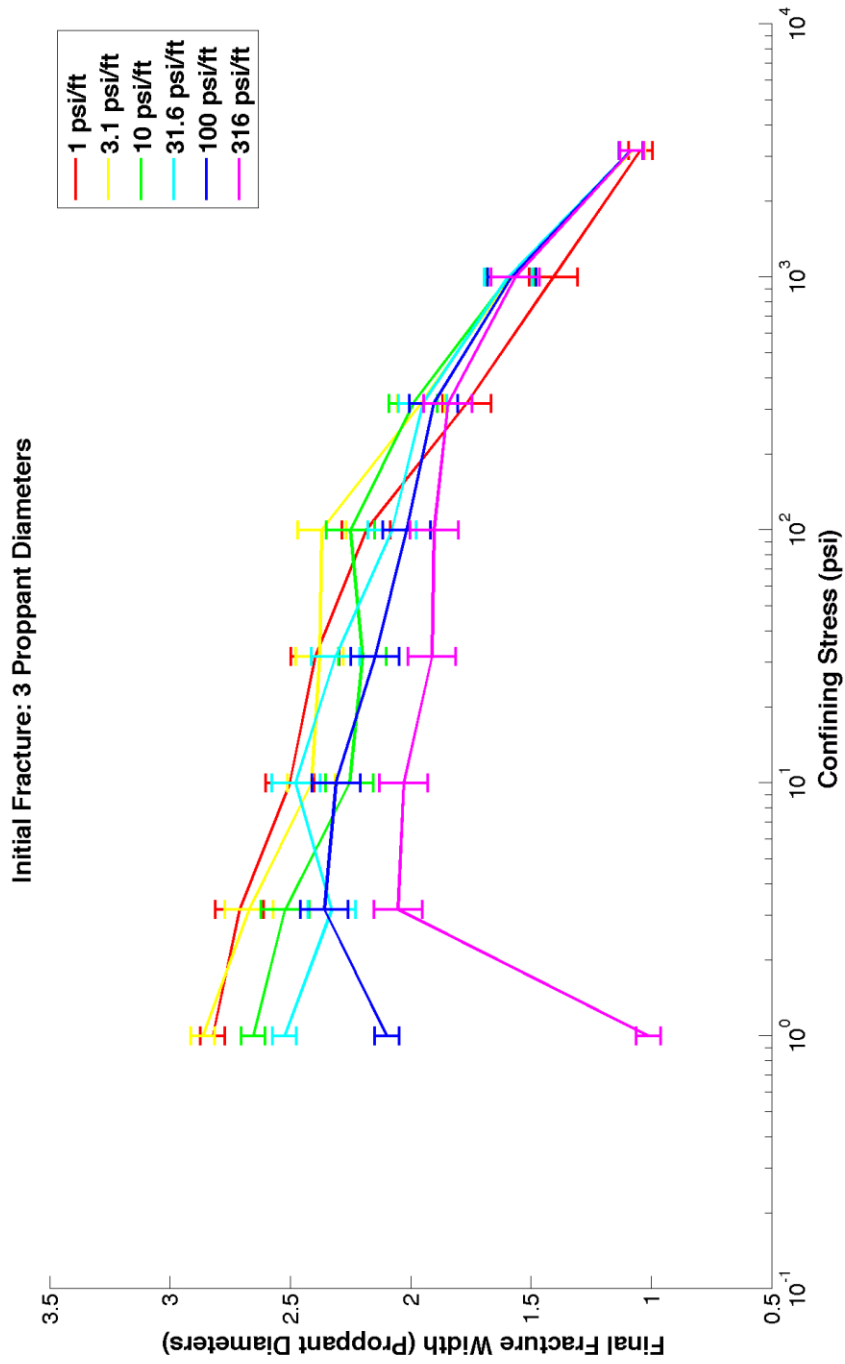
Figure 7 Final fracture width, normalized by proppant diameter, for a fracture initially three proppant diameters wide and a monodisperse 235 micron proppant.
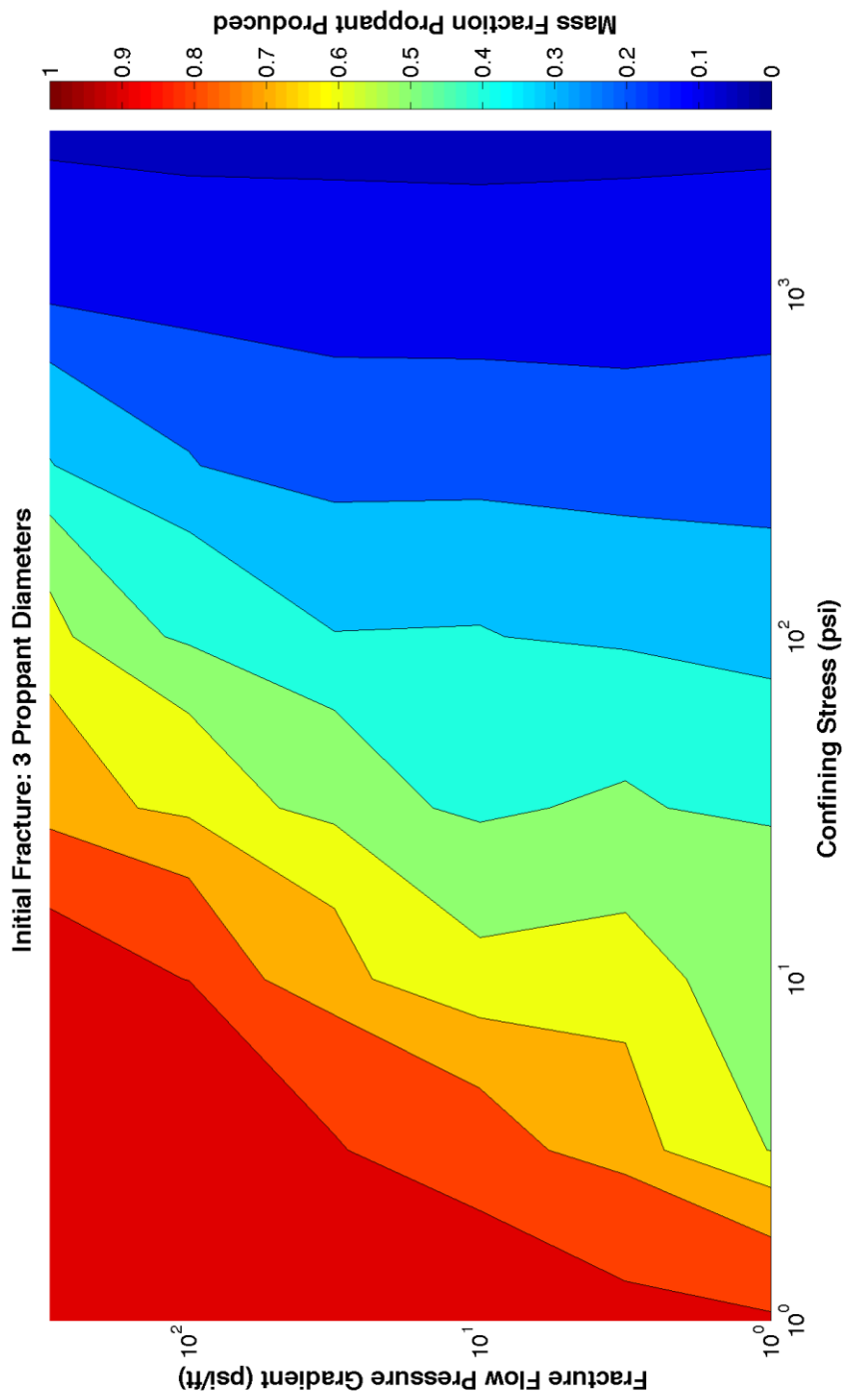
Figure 8 Mass fraction of proppant produced for a fracture initially three proppant diameters wide with a monodisperse 235 micron proppant
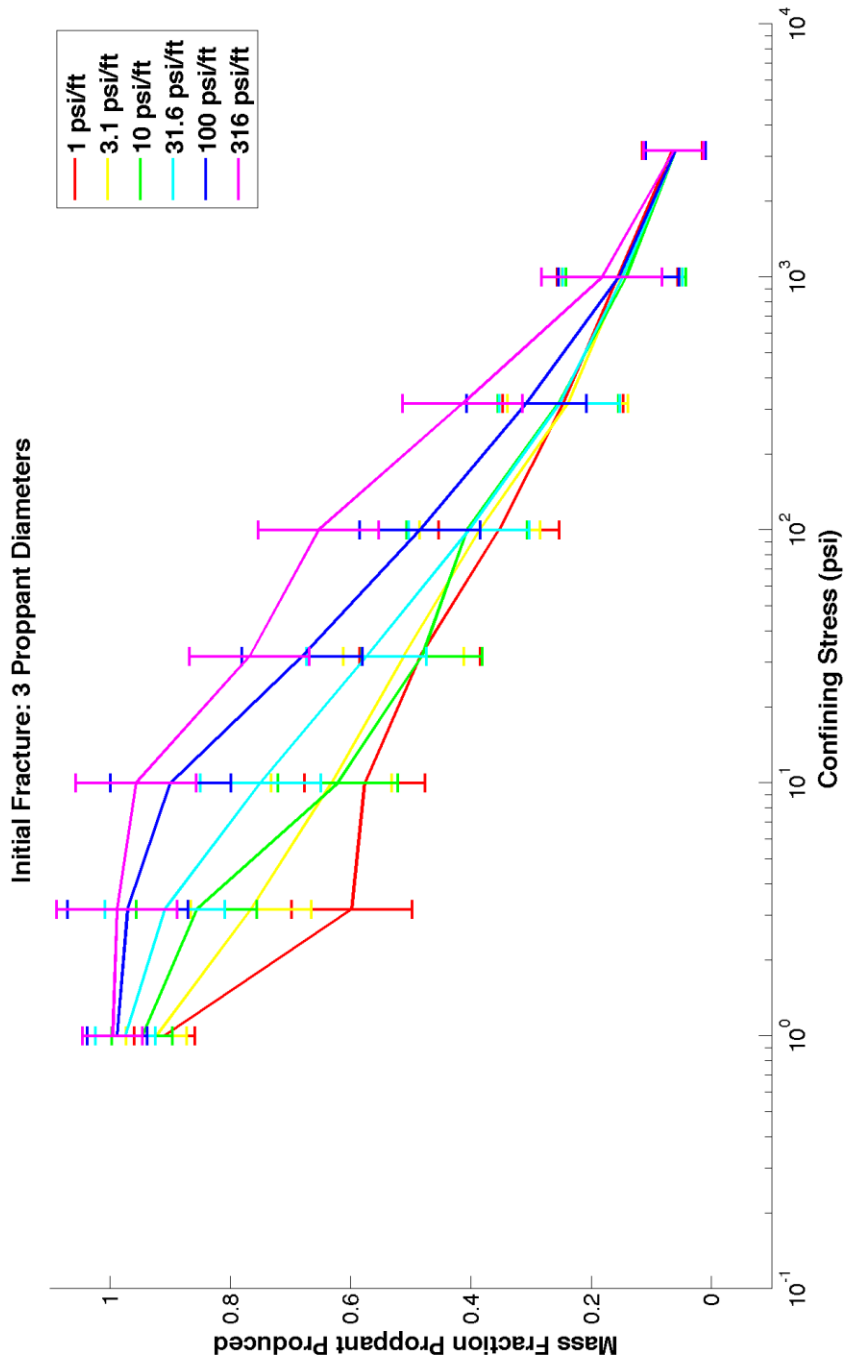
Figure 9 Mass fraction of remaining proppant for a fracture initially three proppant diameters wide with a monodisperse 235 micron proppant
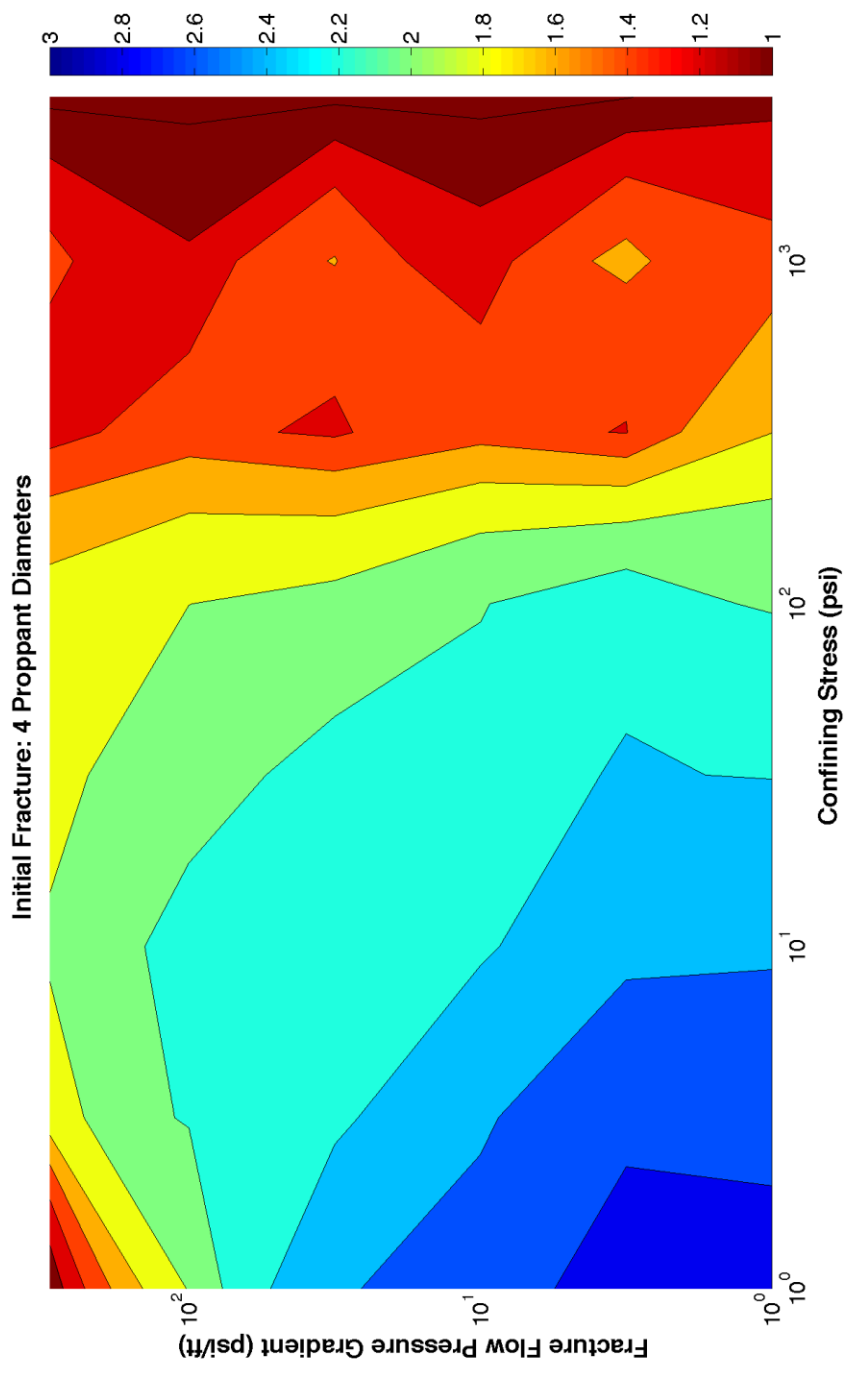
Figure 10 Final fracture width, normalized by proppant diameter, for a fracture initially four proppant diameters wide and a monodisperse 235 micron proppant.
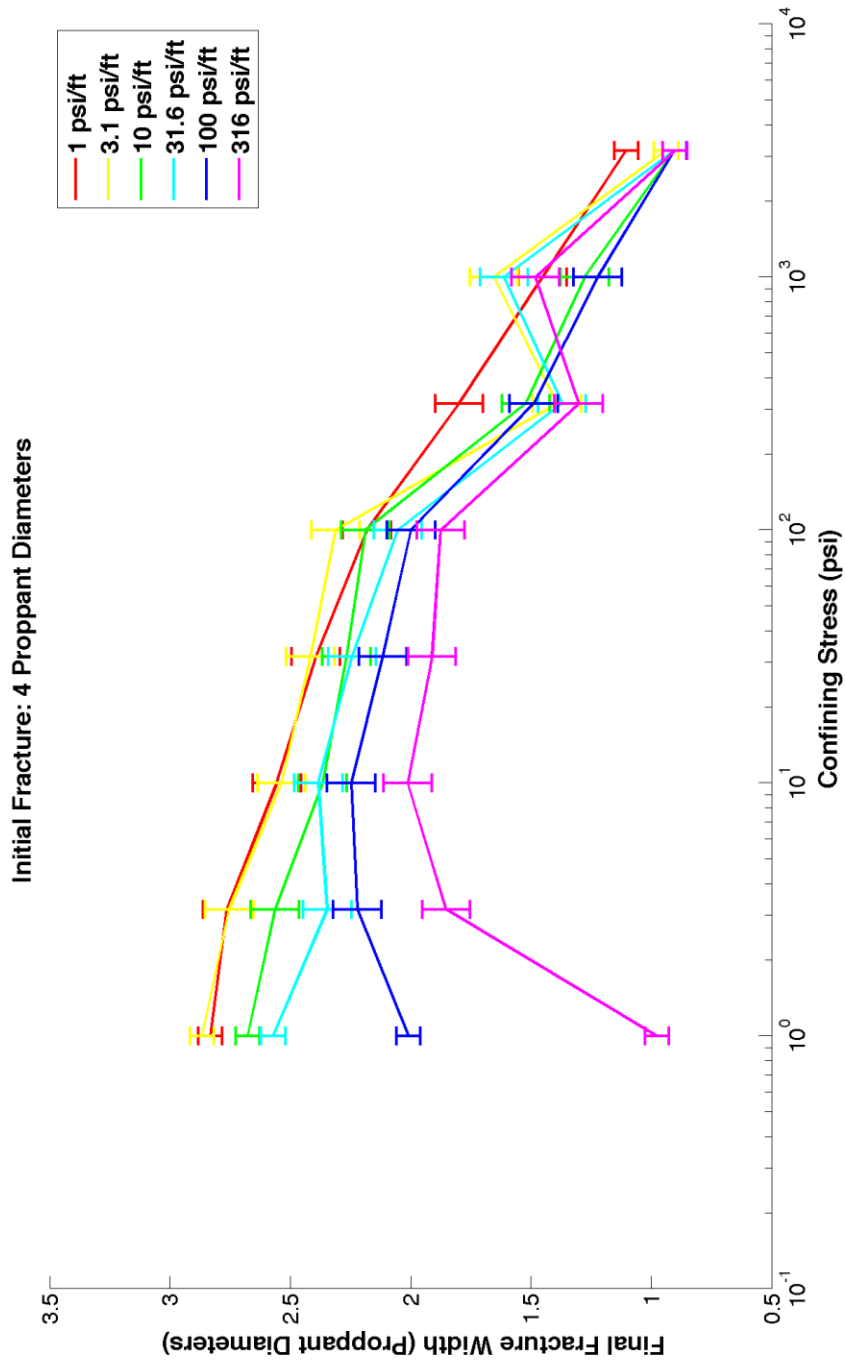
Figure 11 Final fracture width, normalized by proppant diameter, for a fracture initially four proppant diameters wide and a monodisperse 235 micron proppant.
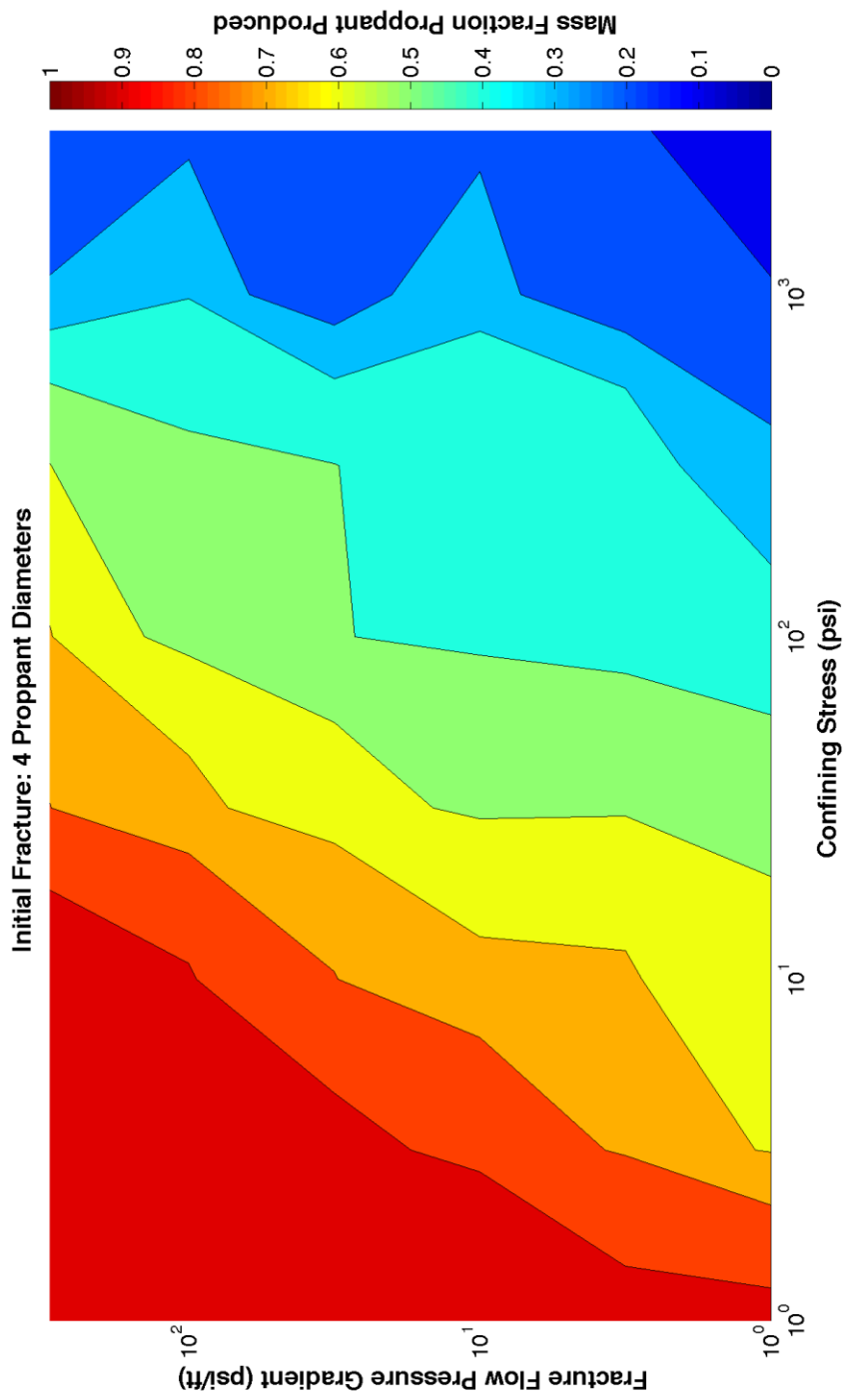
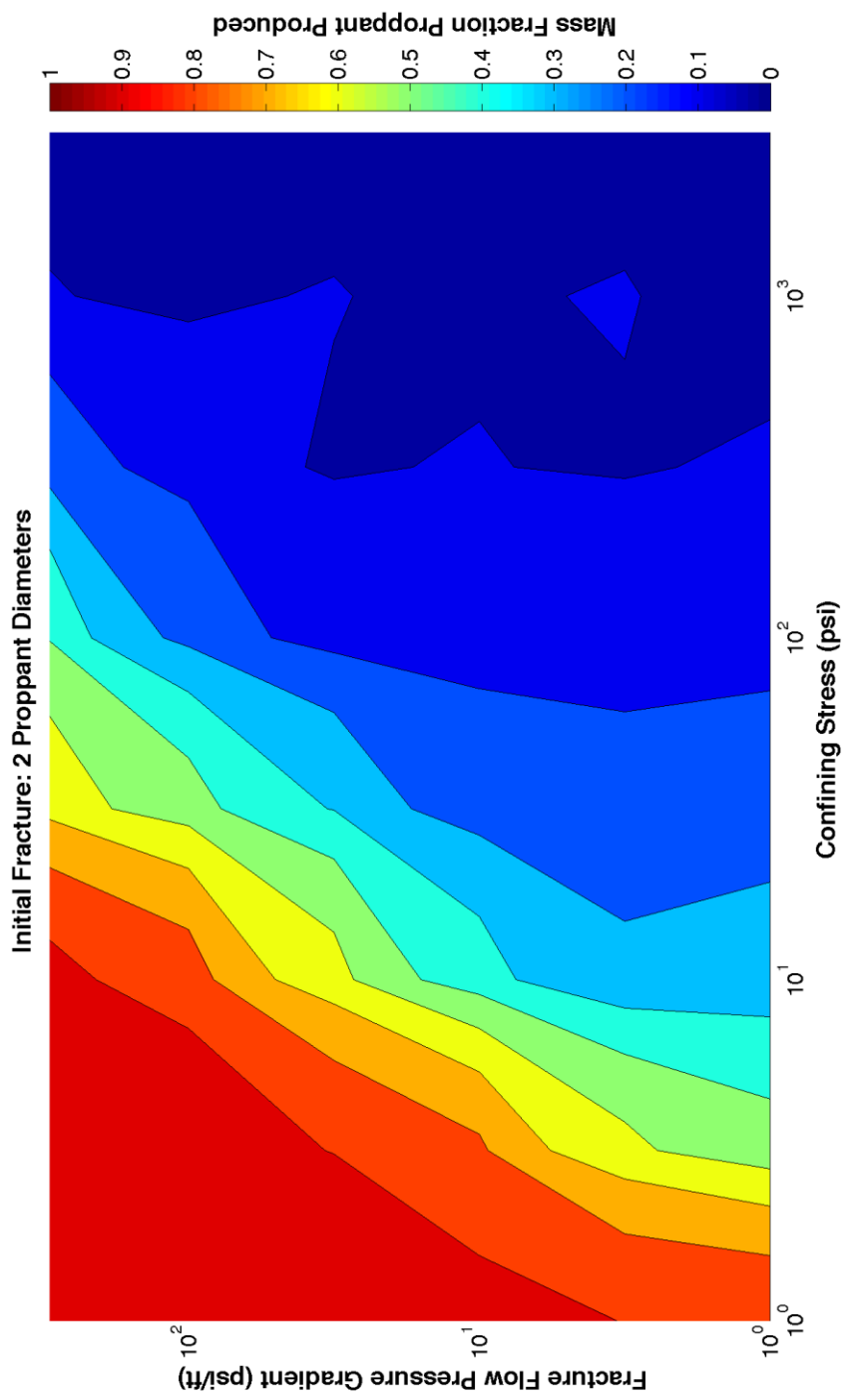Figure 12 Mass fraction of remaining proppant for a fracture initially four proppant diameters wide with a monodisperse 235 micron proppant
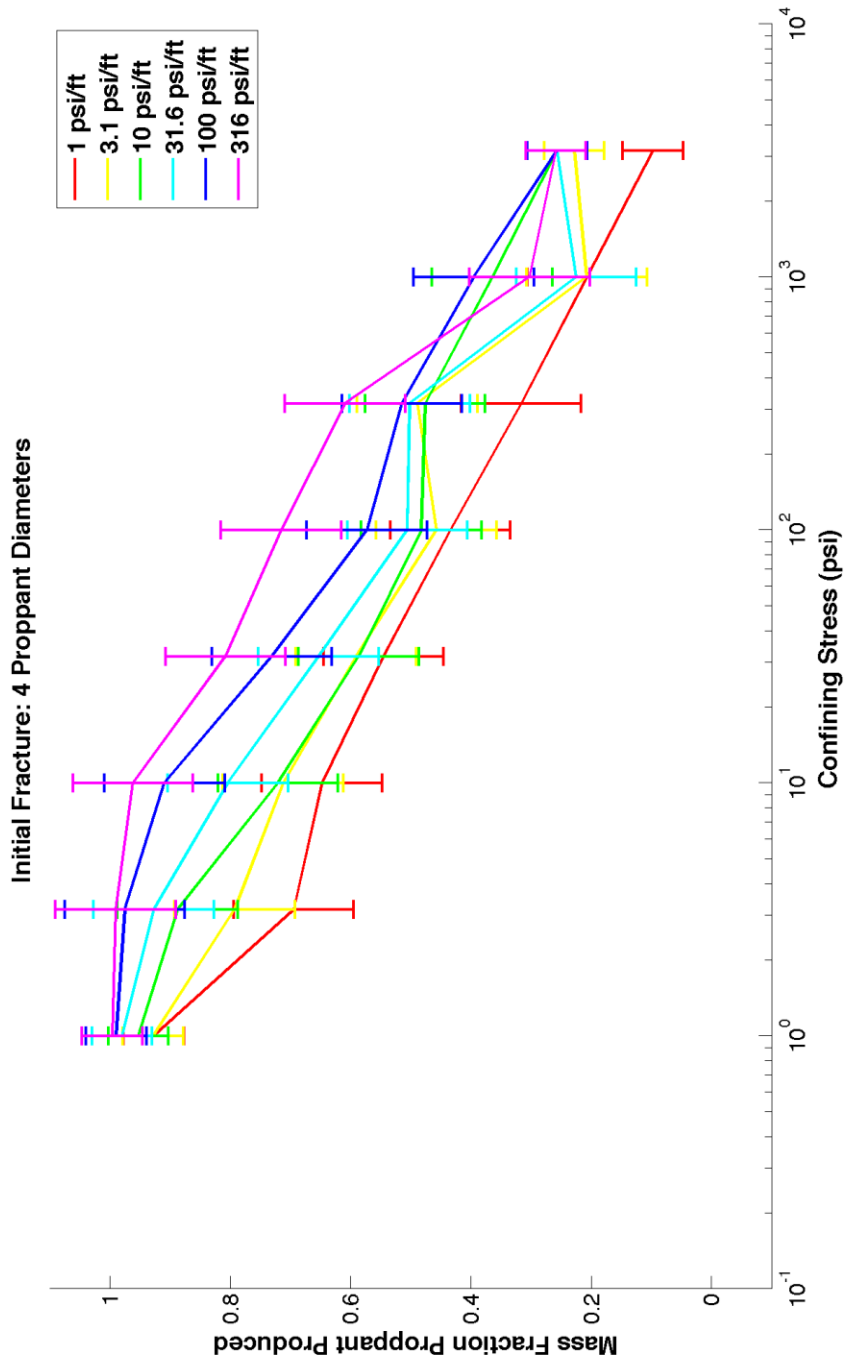
Figure 13 Mass fraction of remaining proppant for a fracture initially four proppant diameters wide with a monodisperse 235 micron proppant

4.2   Proppants with Cohesion

Additional simulations were repeated under identical conditions for the monodisperse proppants with the addition of cohesion between proppant grains and between the proppant grains and fracture walls. This cohesive strength was defined to be $1\,Pa$ or $1.45 \times 10^{-4}\,psi$, or an extremely weak cohesive coating. The general trend remained the same: final fracture widths are largely unaffected, with the fractures still collapsing to two proppant diameters or smaller. For net confining stresses up to 100 psi up to this transition point, cohesive proppants retain 20 to 30% more proppant within the proppant pack that ordinary proppant. Increasing the proppant cohesion allows other proppant particles to stick to stable brings rather than be swept away by the fluid flow.

Figure 14 presents a contour plot of the final fracture width as a function of net confining stress in psi and pressure gradient psi / ft. The plot is quite similar to the non-cohesive case (Figure 2), but the simulation artifact where the fracture widens at net confining stresses of 1 psi is absent. This is likely to grains sticking to each other on contact rather than bouncing off at low net confining stresses and thus not pushing the fracture walls apart. Otherwise, the fracture remains two proppant diameters wide until the net confining stress exceeds 100 psi, after which point the fracture gradually closes to a single proppant diameter in width at 1000 psi. As before, the fracture collapses at a high flowback, over 100 psi / ft, and a low net confining stress, less than 1 psi. Figure 15 presents this data again, but shows the final fracture width as a function of net confining stress for several flowback pressure gradients. Here, it is clearly seen that the final fracture width is a function of net confining stress for net confining stresses over 10 psi

and that final width decreases with increasing flowback for net confining stresses below 10 psi.

Figure 16 presents a contour plot of the fraction of proppant produced as a function of net confining stress and flowback pressure gradient. Less than 20% of proppant is produced at net confining stresses greater than 5 psi, similar to the case without cohesion. However, at low net confining stress, a larger fraction of the proppant remains within the fraction – only 70% is produced at 1 psi net confining and a 1 psi / ft flowback to 90% at 100 psi / ft flowback. Comparing this with the non-cohesive case where over 90% of proppant is produced at net confining stresses below 2 psi, the advantage of using resin becomes clear. Figure 17 presents the same data, but with final fracture width as a function of net confining stress, and both the log linear relationship between final width and net confining stress as well as the dependence on width on flowback are apparent and correspond to those observed with the non-cohesive proppants.

Figure 18 and Figure 19 show the final fracture width for a fracture initially three proppant diameters wide and similar trends are seen as for a fracture initially two proppant diameters wide. Of note, the maximum final fracture width is now only 2.5 proppant diameters, which means that bridges of three proppant grains do not form in a cohesive environment. This may be explained by the tendency of grains to form a triangular rather than linear bridge to increase contacts between grains but could also be an artifact of the simulation. Comparing with the non-cohesive case, proppant production at a 2 psi net confining stress is reduced at least 80% (increasing to 100% with higher flowback) to 70% (increasing to only 80% with higher flowback). Again, this shows the

advantage of using a resin coating, especially at low net confining stresses to retain more proppant.

For all these cases, as would be expected, the fraction of proppant produced is significantly reduced for net confining stresses between 10 and 1000 psi and all fracture flow pressure gradients, but interestingly is significantly reduced for cases of high fracture flow gradient and low net confining stresses. The latter may be attributed to cohesive groups of proppant grains that exit the fracture together instead of forming or even annihilating stable bridges. This is clearly shown in the change in final fracture width, with fractures reducing in width significantly at low net confining stresses and high fracture flow velocities. This suggests that aggressively flowing back a well too early (before fracture closure) will result in proppant flowback even when resin coated proppant is used.

Figure 14 Final fracture width, normalized by proppant diameter, for a fracture initially two proppant diameters wide and a monodisperse 235 micron proppant with enhanced proppant cohesion

Figure 15 Final fracture width, normalized by proppant diameter, for a fracture initially two proppant diameters wide and a

monodisperse 235 micron proppant with enhanced proppant cohesion
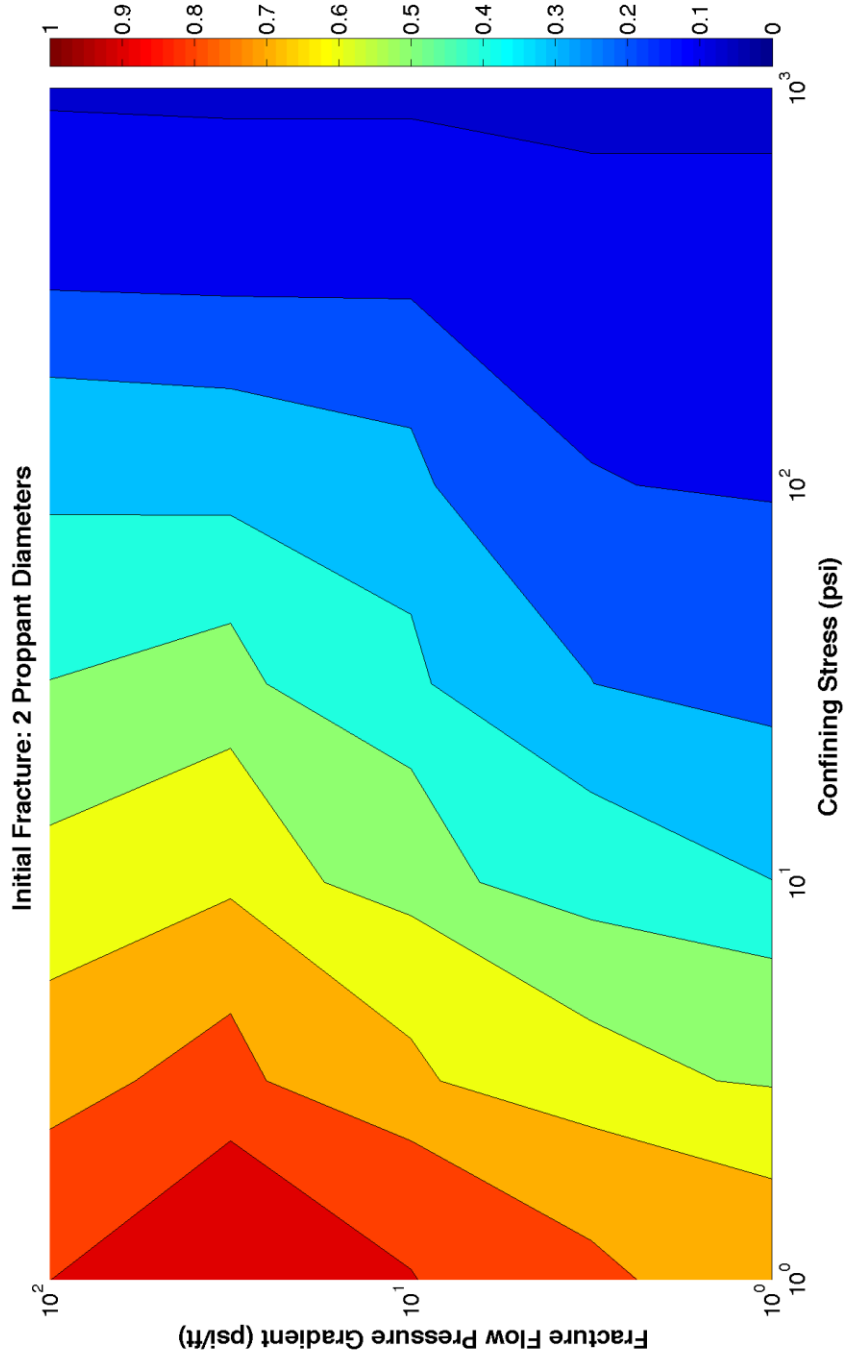
Figure 16 Mass fraction of proppant produced for a fracture initially two proppant diameters wide with a monodisperse 235 micron proppant with enhanced cohesion
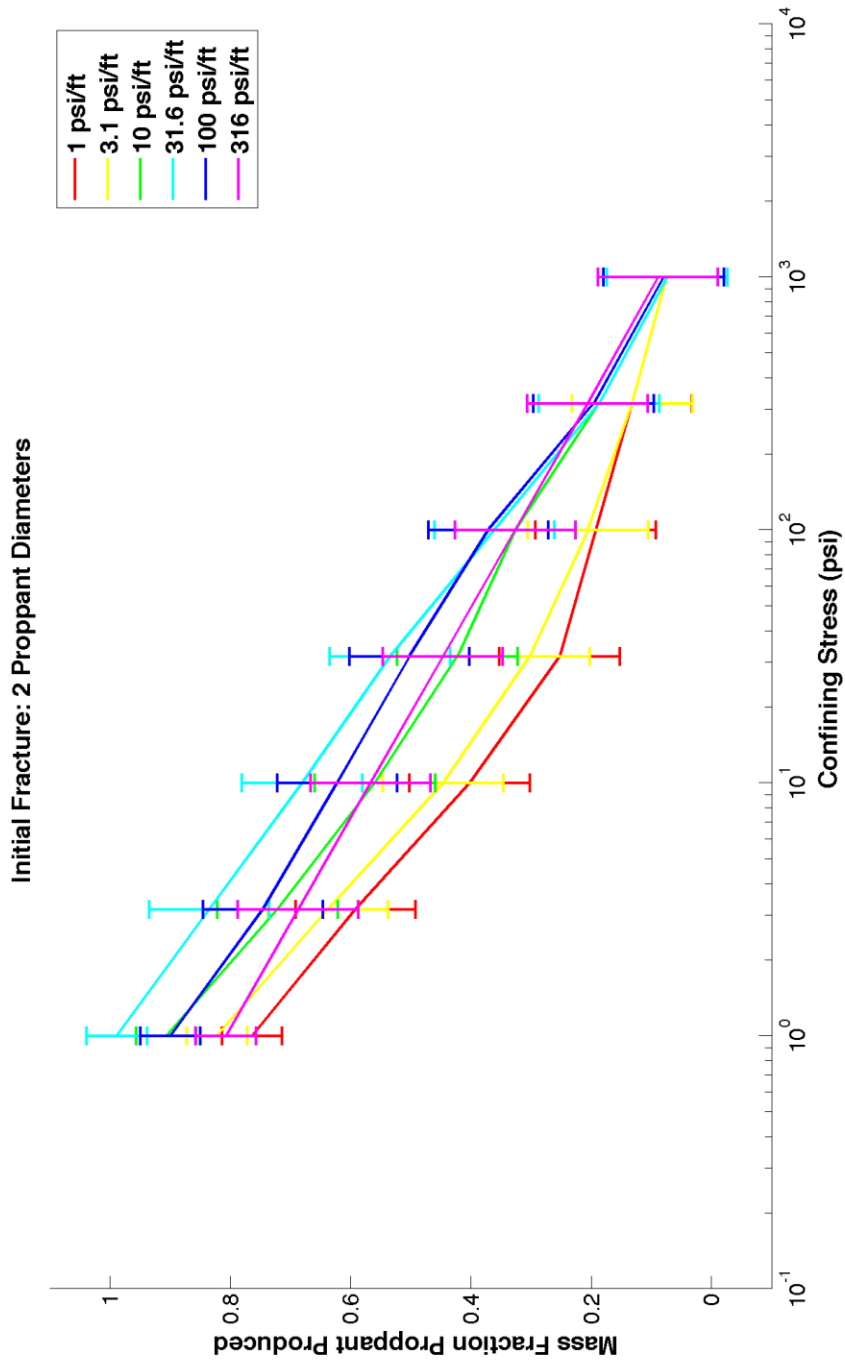
Figure 17 Mass fraction of proppant produced for a fracture initially two proppant diameters wide with a monodisperse 235 micron proppant with enhanced cohesion

Figure 18 Final fracture width, normalized by proppant diameter, for a fracture initially three proppant diameters wide and a monodisperse 235 micron proppant with enhanced proppant cohesion

Figure 19 Final fracture width, normalized by proppant diameter, for a fracture initially three proppant diameters wide and a monodisperse 235 micron proppant with enhanced proppant cohesion

Figure 20 Mass fraction of proppant produced for a fracture initially three proppant diameters wide with a monodisperse 235 micron proppant with enhanced cohesion

Figure 21 Mass fraction of proppant produced for a fracture initially three proppant diameters wide with a monodisperse 235 micron proppant with enhanced cohesion

4.3   Polydisperse Proppant

The experiments described in 4.1, which simulate proppants with a monodisperse 235 micron diameter, are repeated with addition of a second proppant size. The new experiments, which are run over a more limited 1 to 100 psi net confining stress and a 1 to 100 psi / ft flowback pressure gradient, have two proppant grains size – 118 micron and 235 micron – which are equally distributed by mass.

Figure 22 presents the contour plot of final fracture width as a function of the net confining stress and the flowback pressure gradient. Due to the low upper limit on maximum net confining stress, fracture narrowing is not seen in the data but is still expected to occur. As before in the non-cohesive proppant case, fracture widening is seen at low net confining stresses, below 10 psi, due to energy of proppant movement being transferred to the fracture walls. Figure 23 presents the same information, but plots the final fracture width as a function of the net confining stress for specific flowback pressure gradients. A similar behavior is seen, where final fracture width is independent of net confining stress between 10 and 100 psi but decreases slightly with increased pressure gradients.

Figure 24 presents the contour plot for the fraction of proppant produced as a function of the net confining stress and the pressure gradient. For net confining stresses over 50 psi, less than 20% of the proppant is produced, just as in the case with the monodisperse proppant, but with lower net confining stresses, a higher fraction is produced due to the smaller proppant grains escaping around and through any bridges that form. Figure 25 presents the same information but with the fraction produced being

a function of net confining stress for certain pressure gradients. A similar trend is seen, with proppant production increasing with increased pressure gradients.

Figure 26 and Figure 27 present the final fracture widths for an initially three proppant diameter wide fracture while Figure 30 and Figure 31 do the same for an initially four proppant diameter fracture as functions of net confining stress and pressure gradient. Figure 28 and Figure 29 present the fraction of proppant produced from an initially three proppant diameter wide fracture while Figure 32 and Figure 33 present the same for an initially four proppant diameter fracture as functions of net confining stress and pressure gradient. In each case, the results are similar to those with a monodisperse proppant, but with greater production of proppant at low net confining stresses (below 10 psi) and high pressure gradients (above 10 psi / ft).

In general, the addition of poly-disperse proppant increases fracture width at low net confining stresses but decreases the fraction of proppant remaining within the fracture. Multiple proppant sizes facilitate the formation of stable bridges and allow wider bridges to be formed, but the smaller proppants tend to be produced more readily than larger grains, so even in the presence of a proppant pack, smaller proppants are still able to escape and reduce the remaining mass fraction.
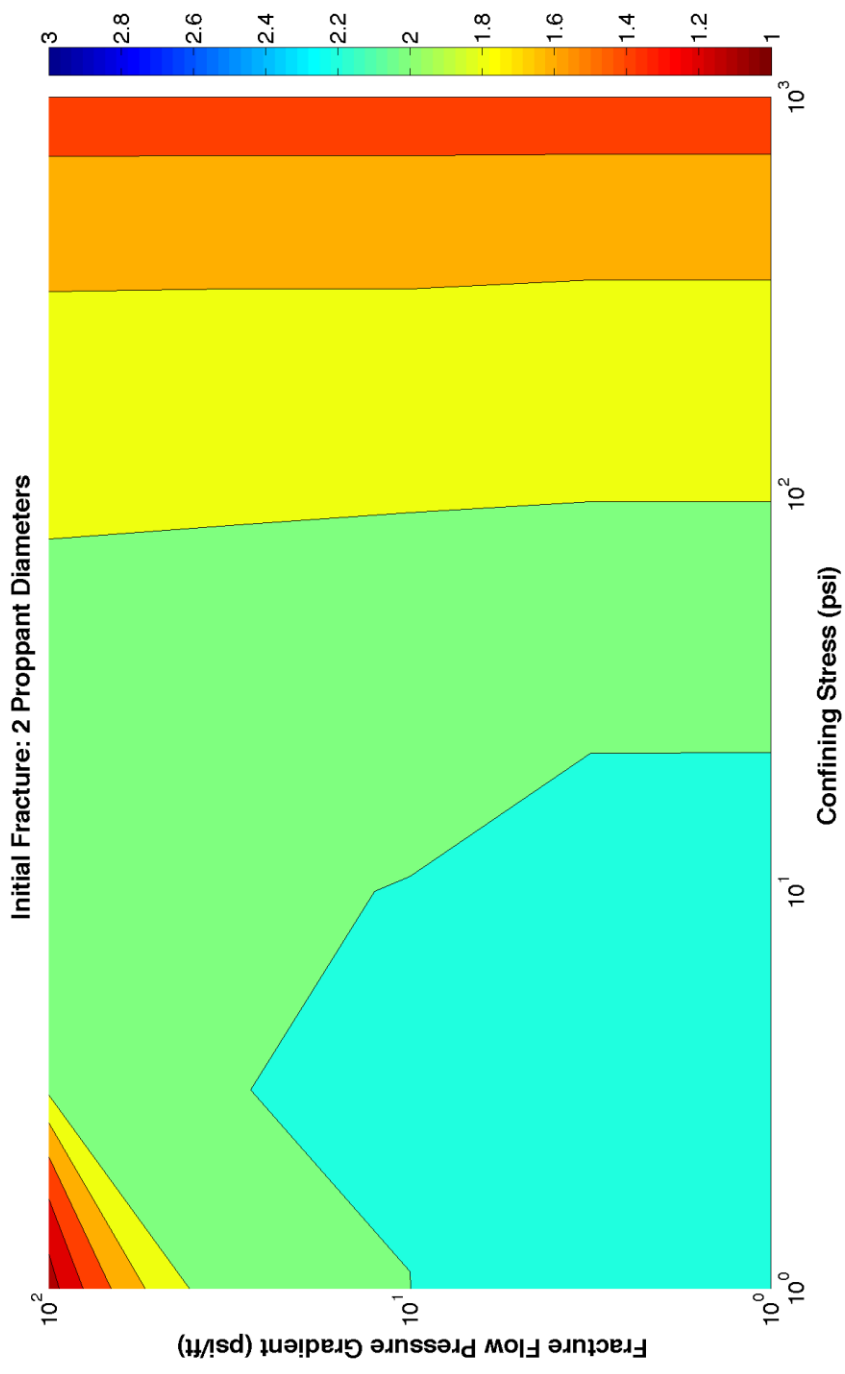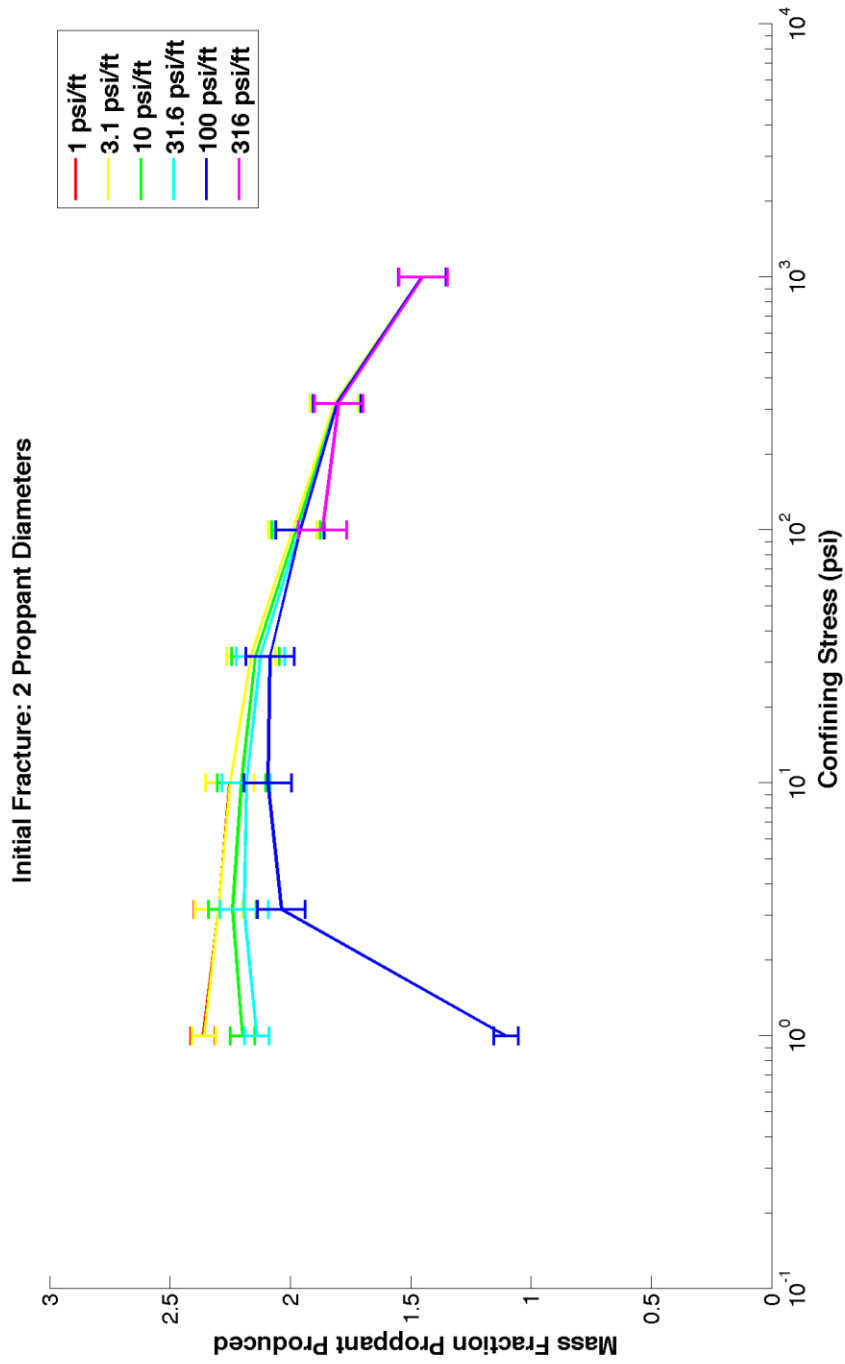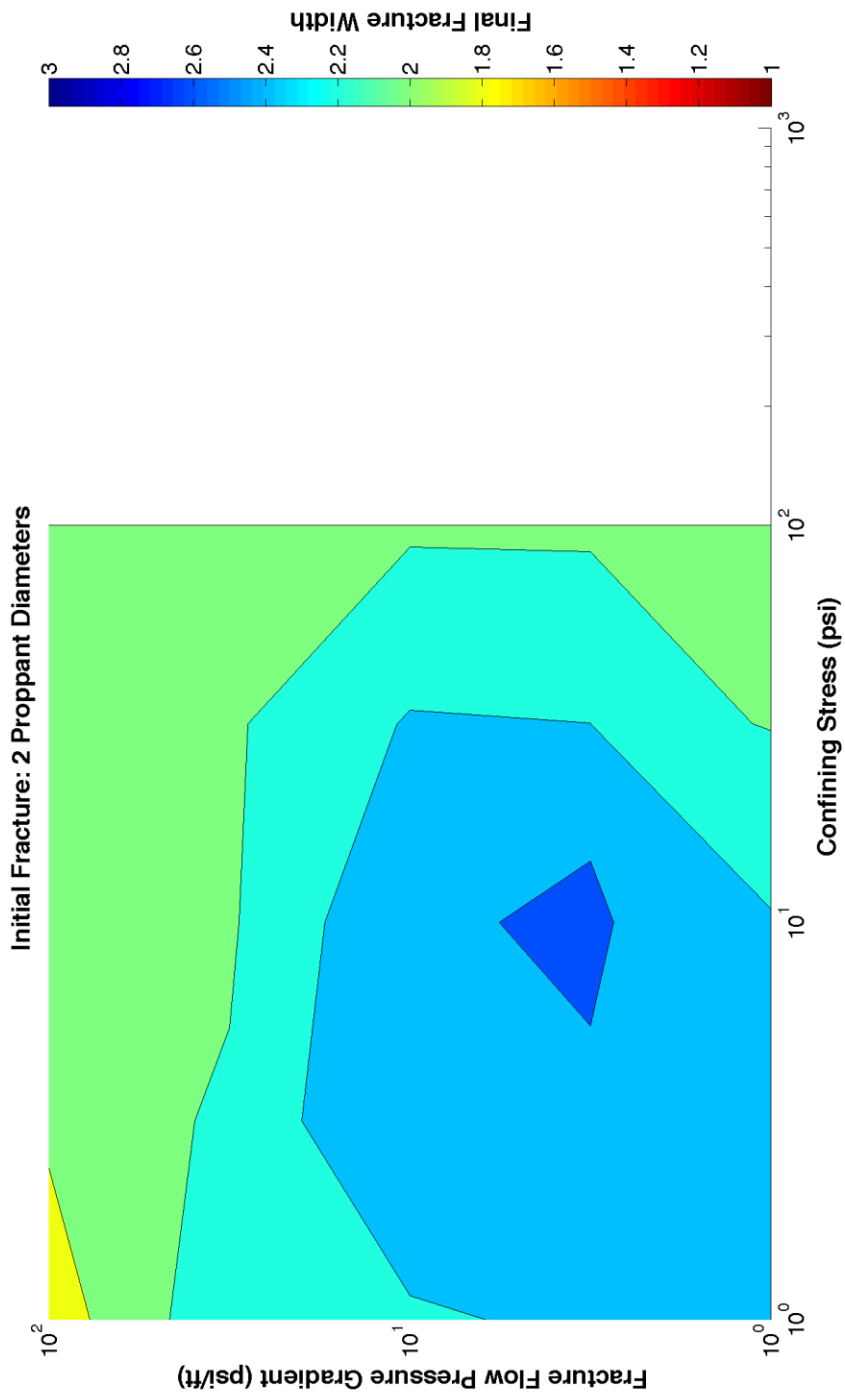
Figure 22 Final fracture width, normalized by proppant diameter, for a fracture initially two maximum proppant diameters wide and a polydisperse 118 and 235 micron proppant
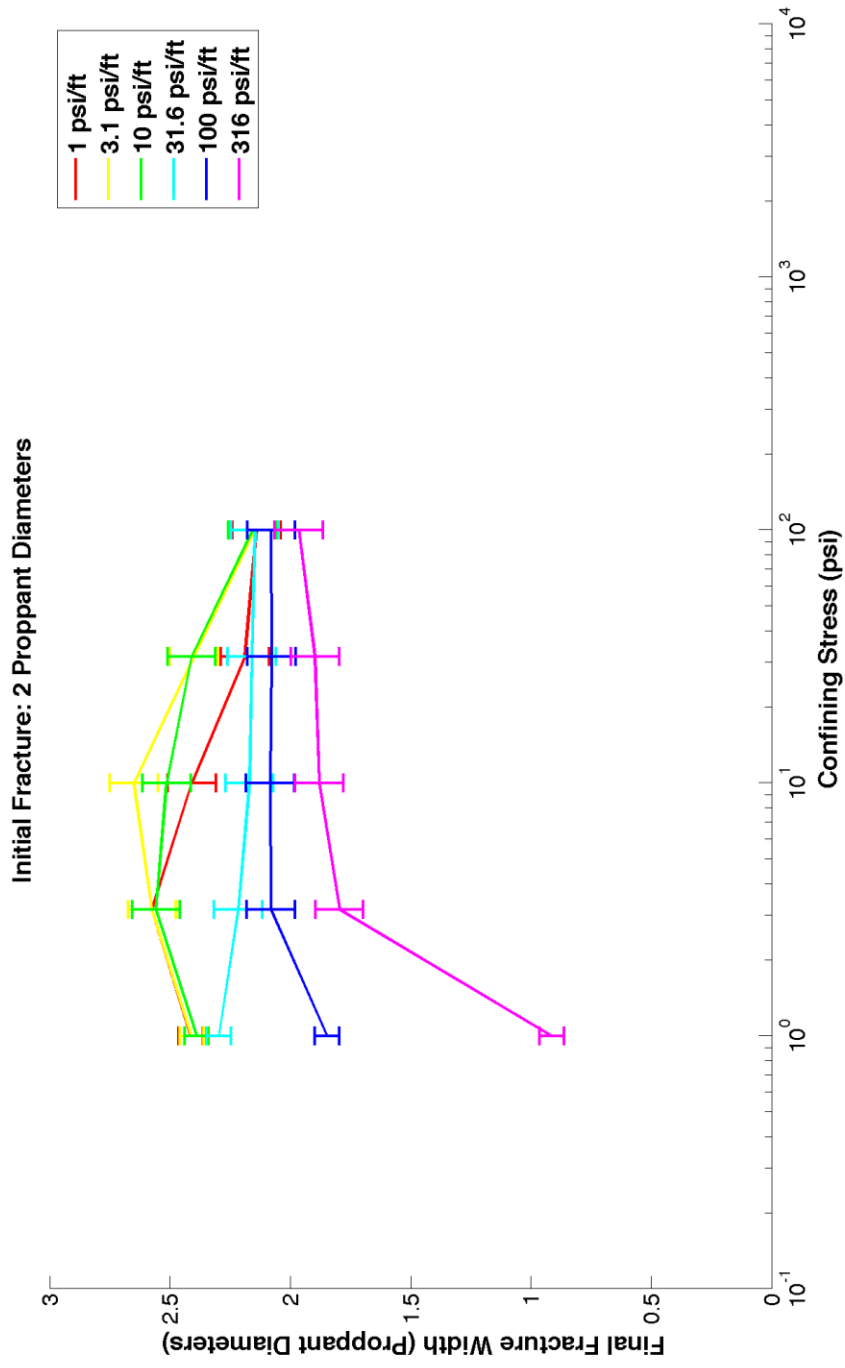
Figure 23 Final fracture width, normalized by proppant diameter, for a fracture initially two maximum proppant diameters wide and a polydisperse 118 and 235 micron proppant
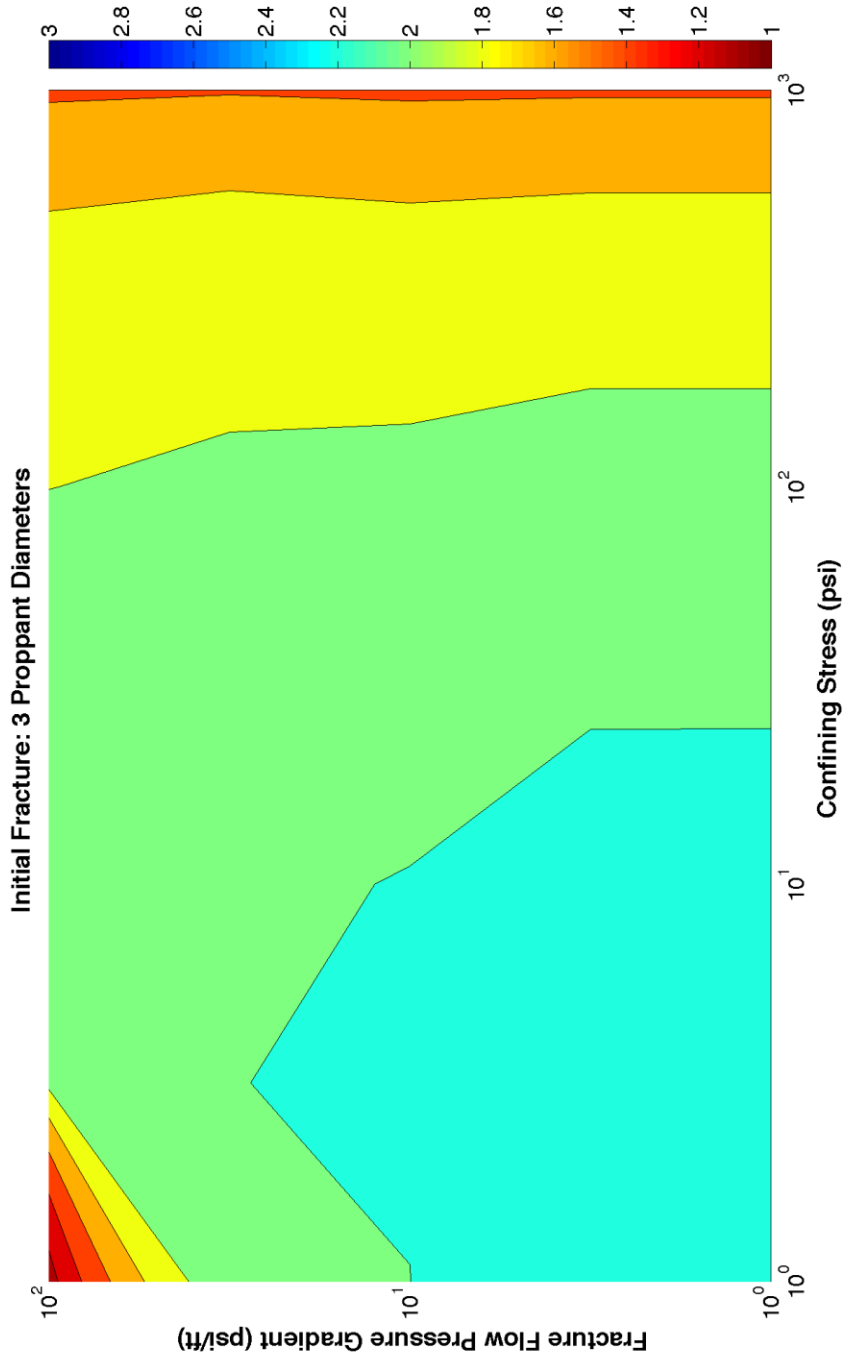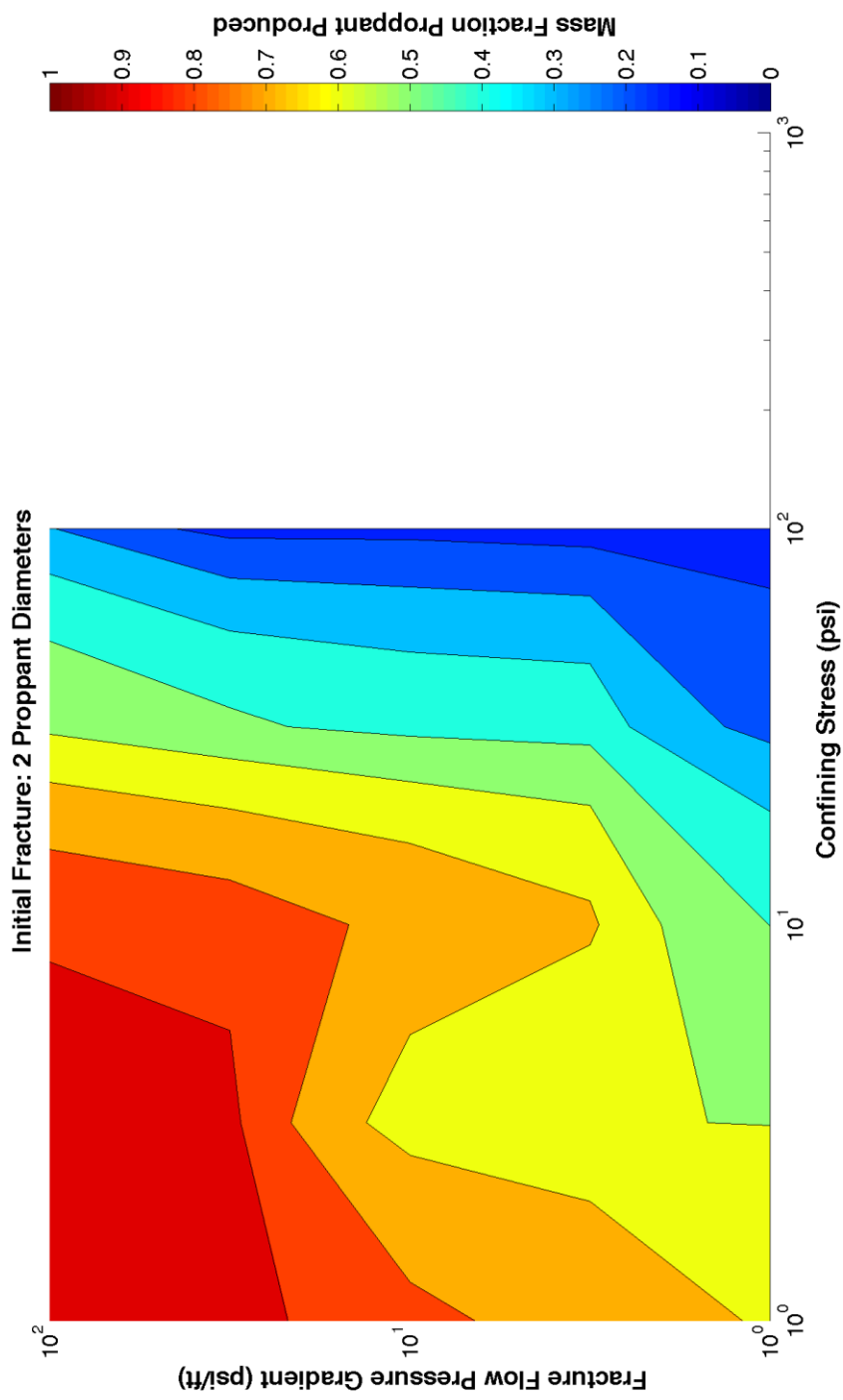
Figure 24 Mass fraction of proppant produced for a fracture initially two proppant diameters wide with a polydisperse 118 and 235 micron proppant
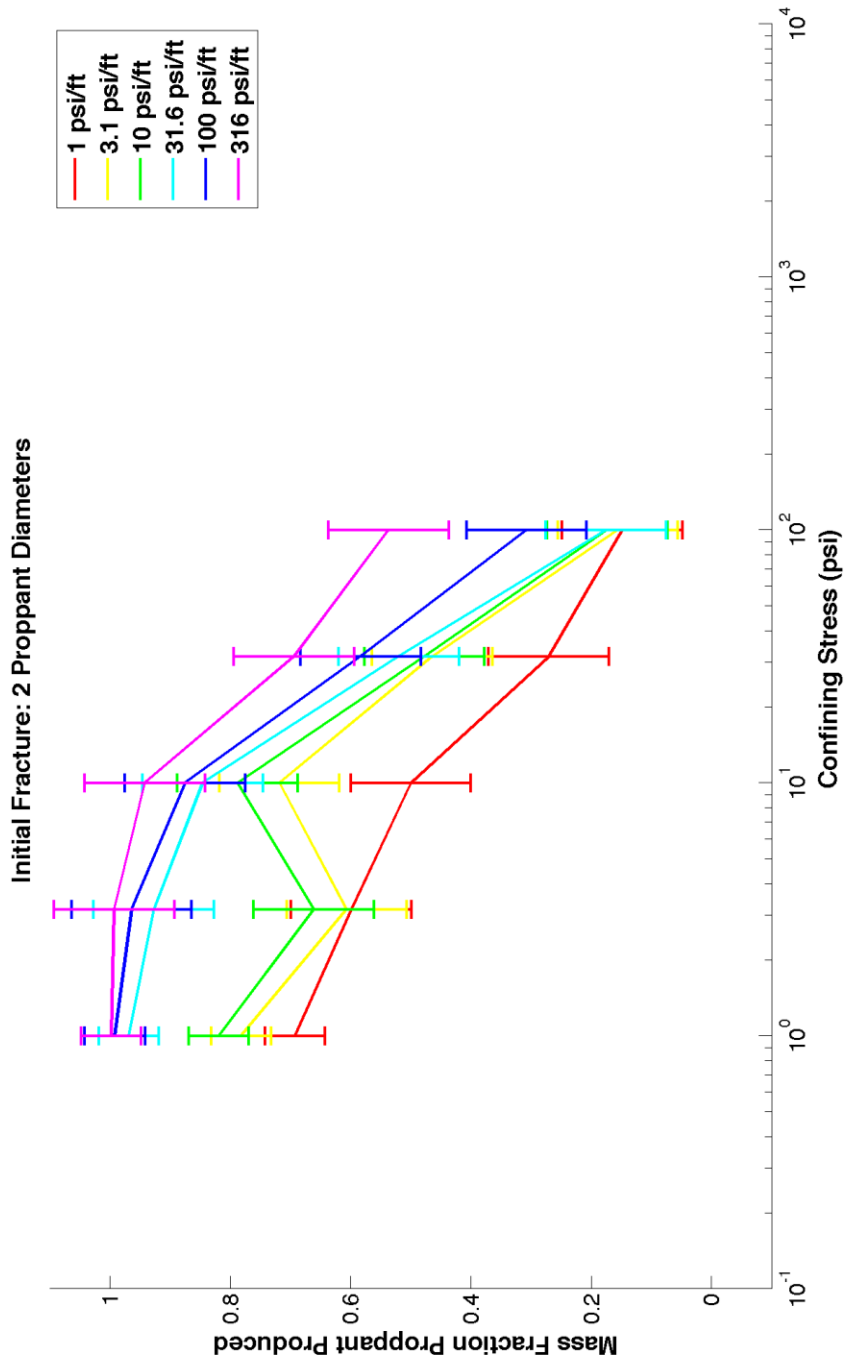
Figure 25 Mass fraction of proppant produced for a fracture initially two proppant diameters wide with a polydisperse 118

and 235 micron proppant
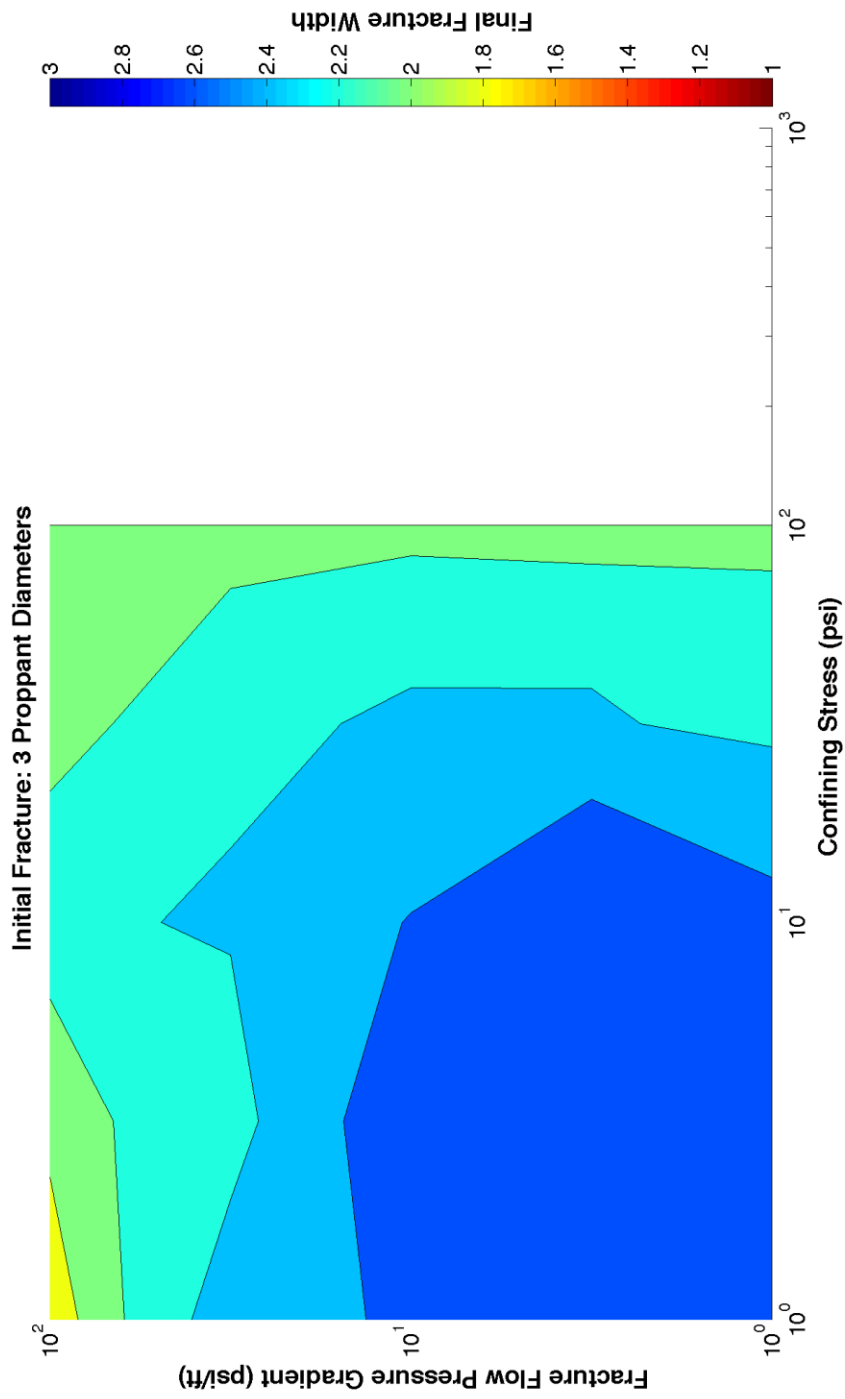
Figure 26 Final fracture width, normalized by proppant diameter, for a fracture initially three maximum proppant diameters wide and a polydisperse 118 and 235 micron proppant
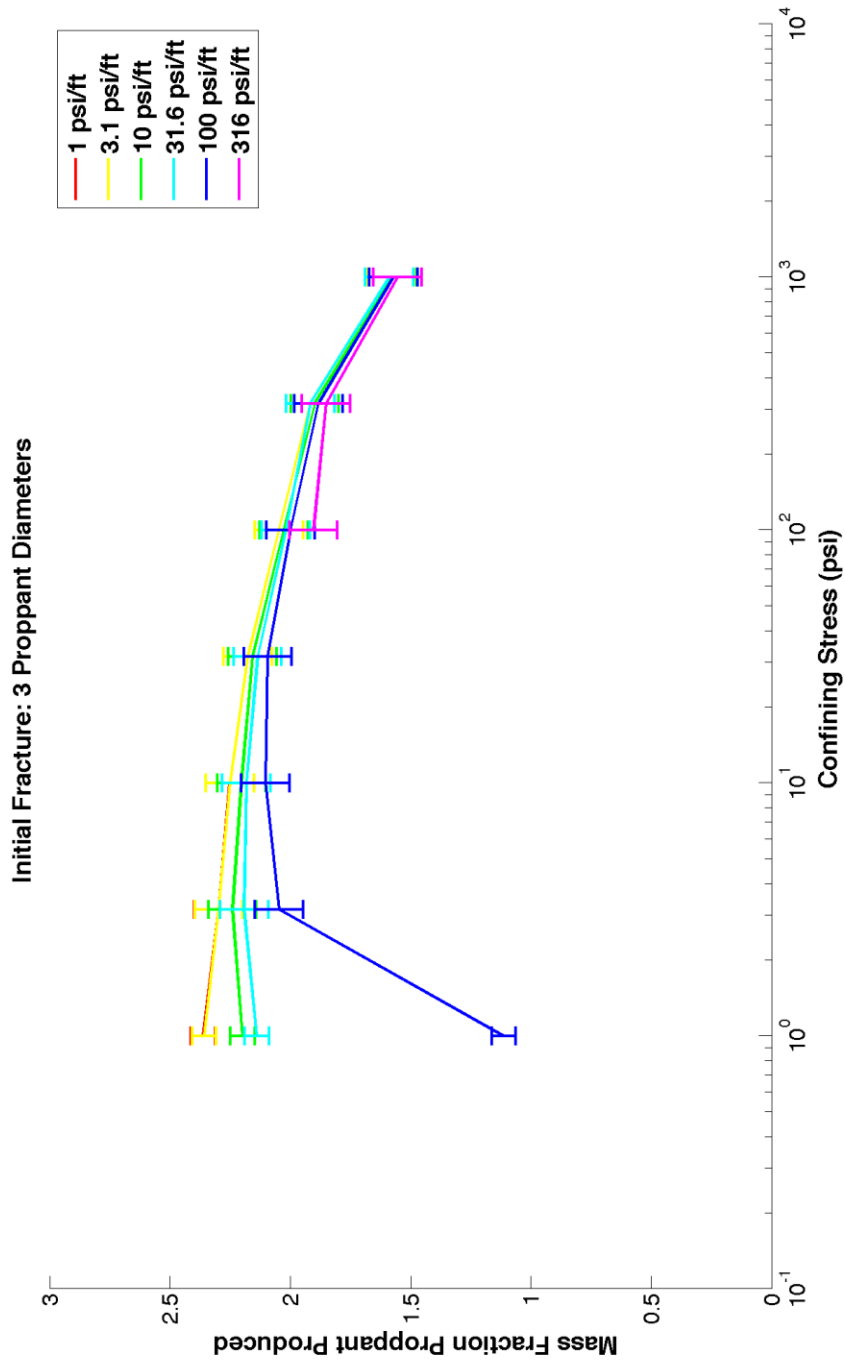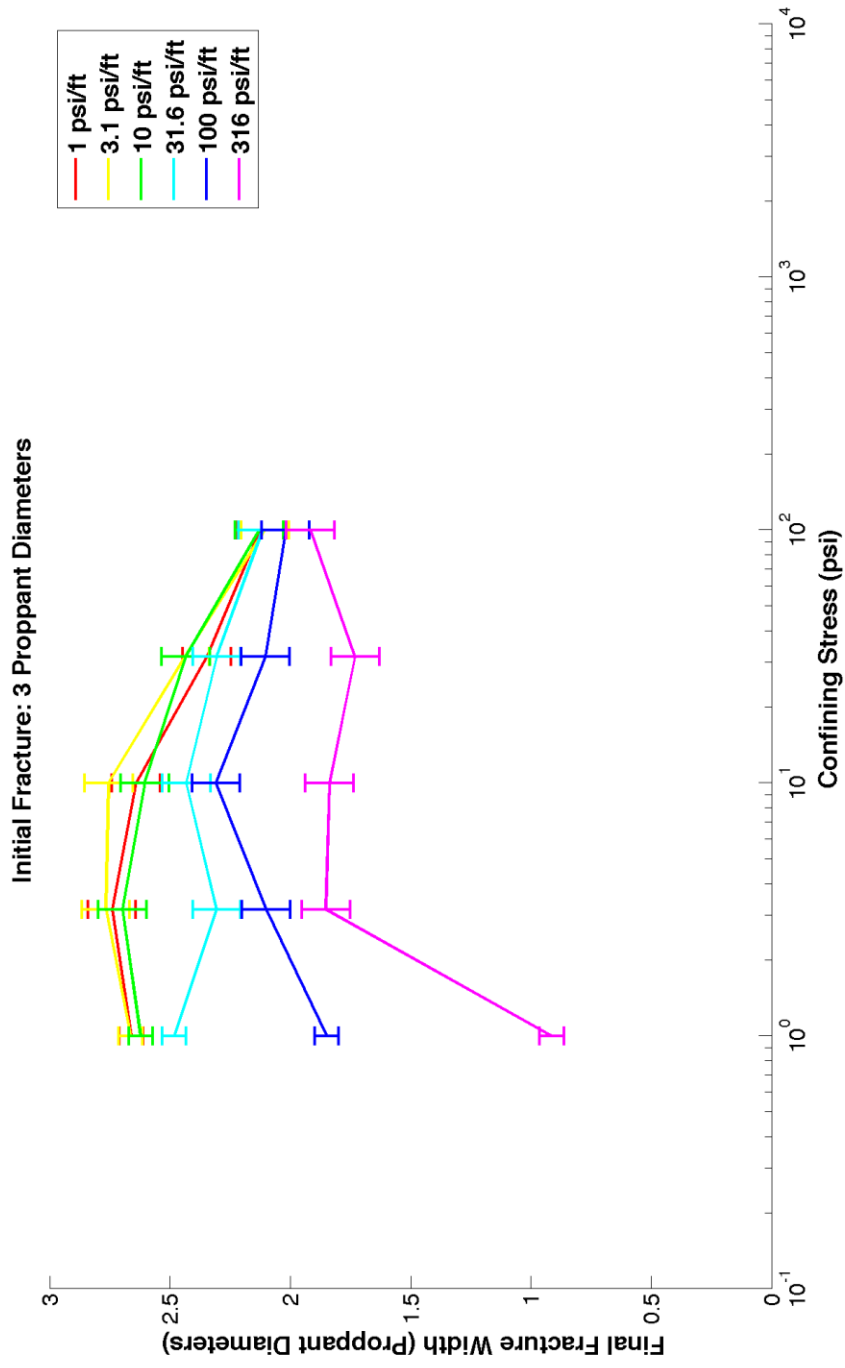
Figure 27 Final fracture width, normalized by proppant diameter, for a fracture initially three maximum proppant diameters wide and a polydisperse 118 and 235 micron proppant
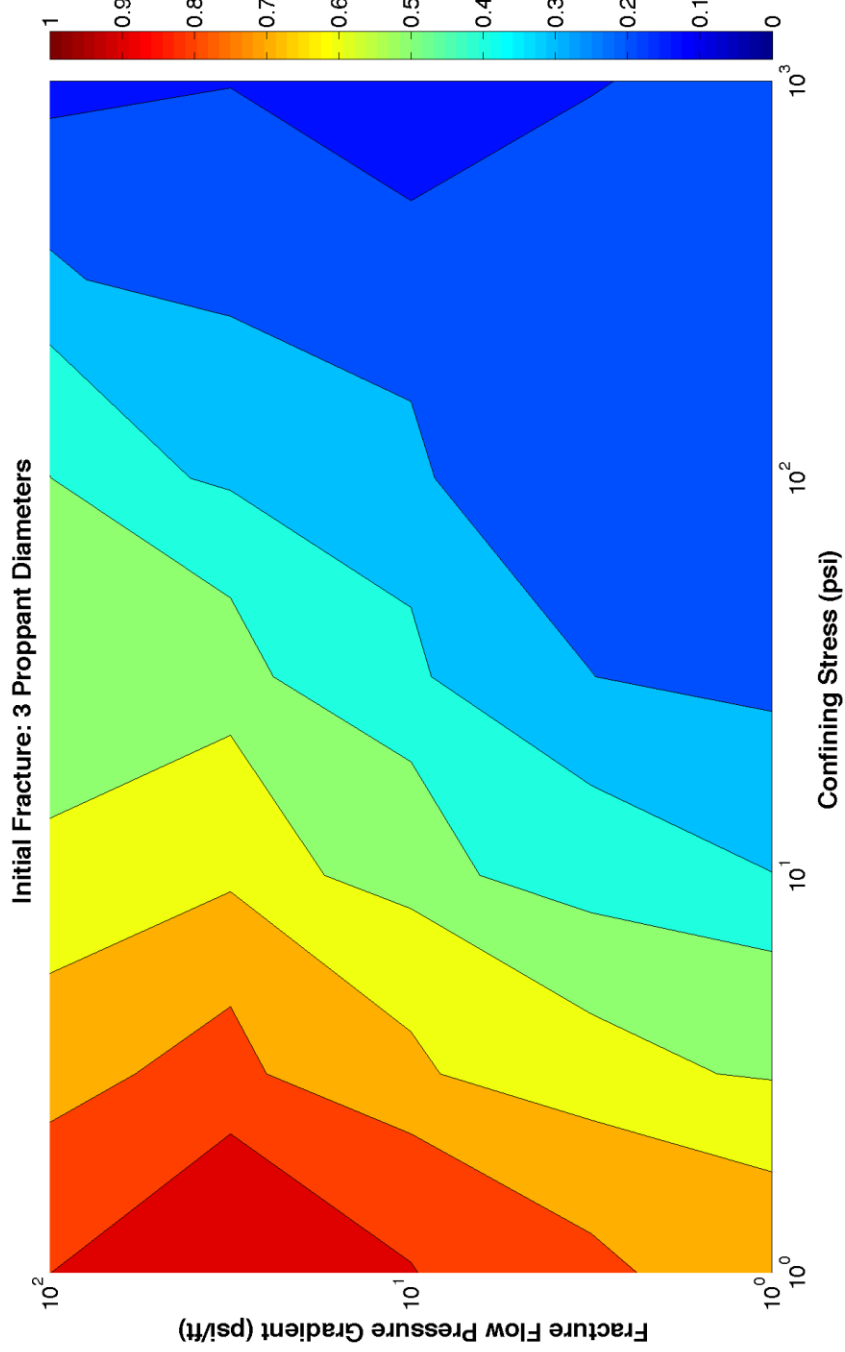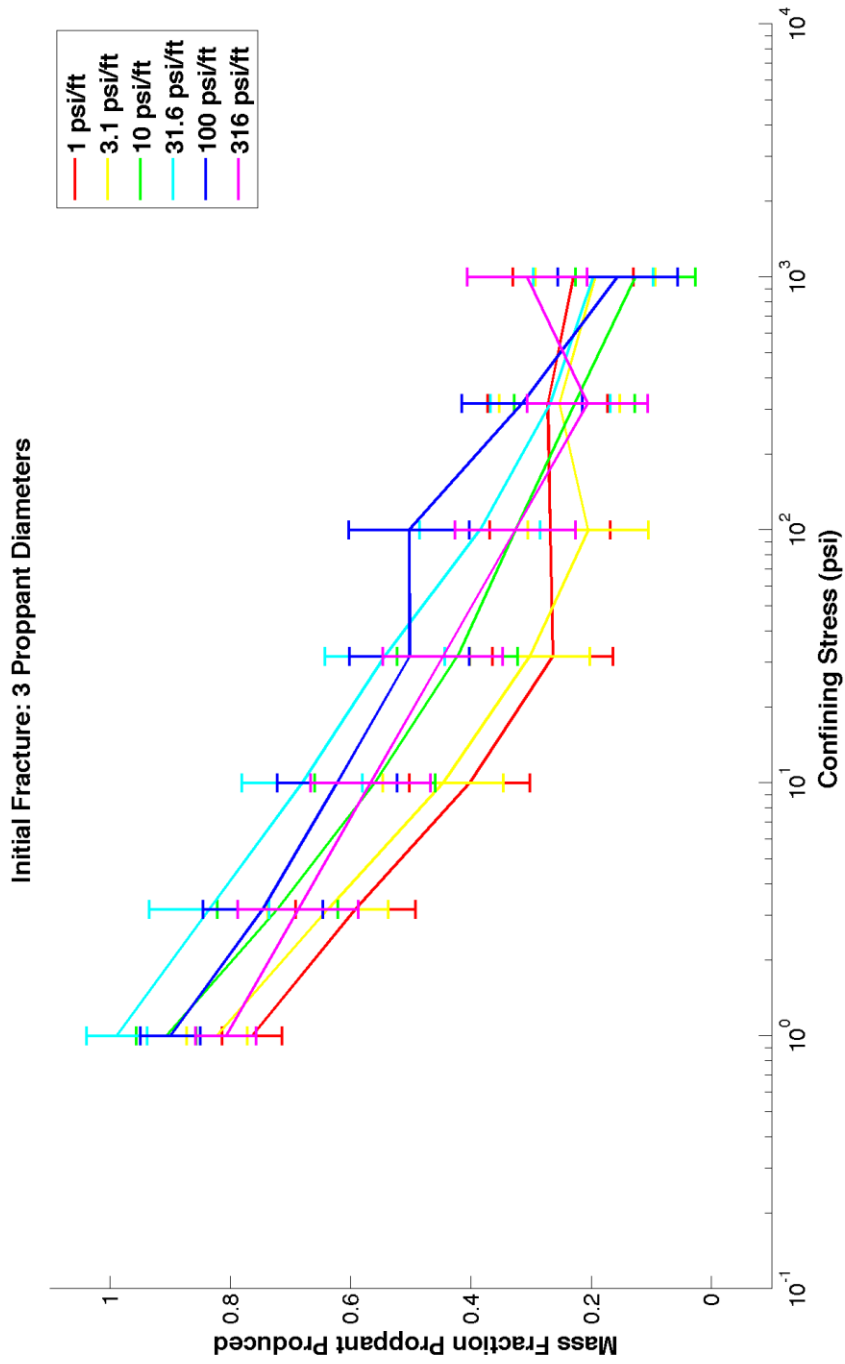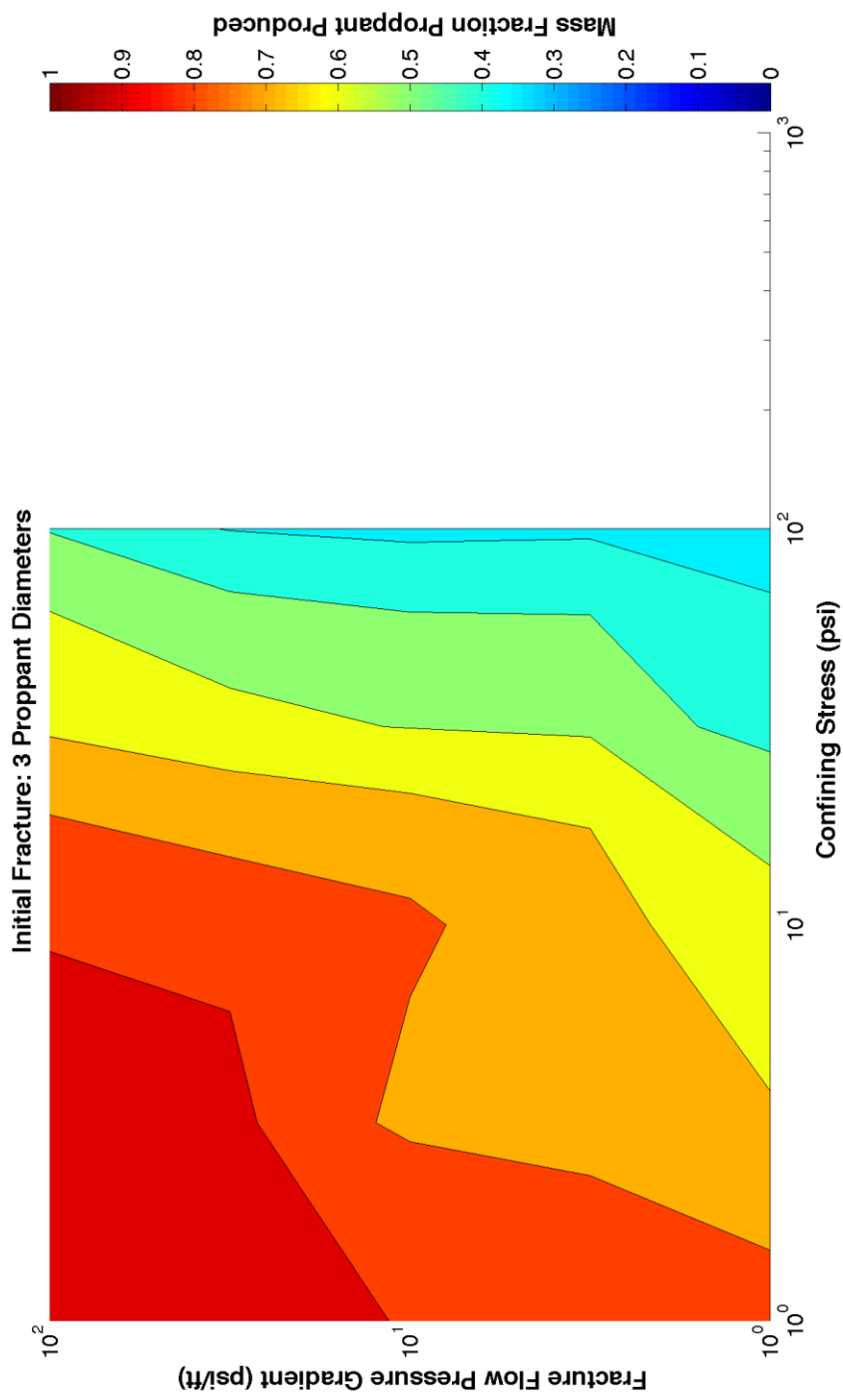
Figure 28 Mass fraction of proppant produced for a fracture initially three proppant diameters wide with a polydisperse 118 and 235 micron proppant
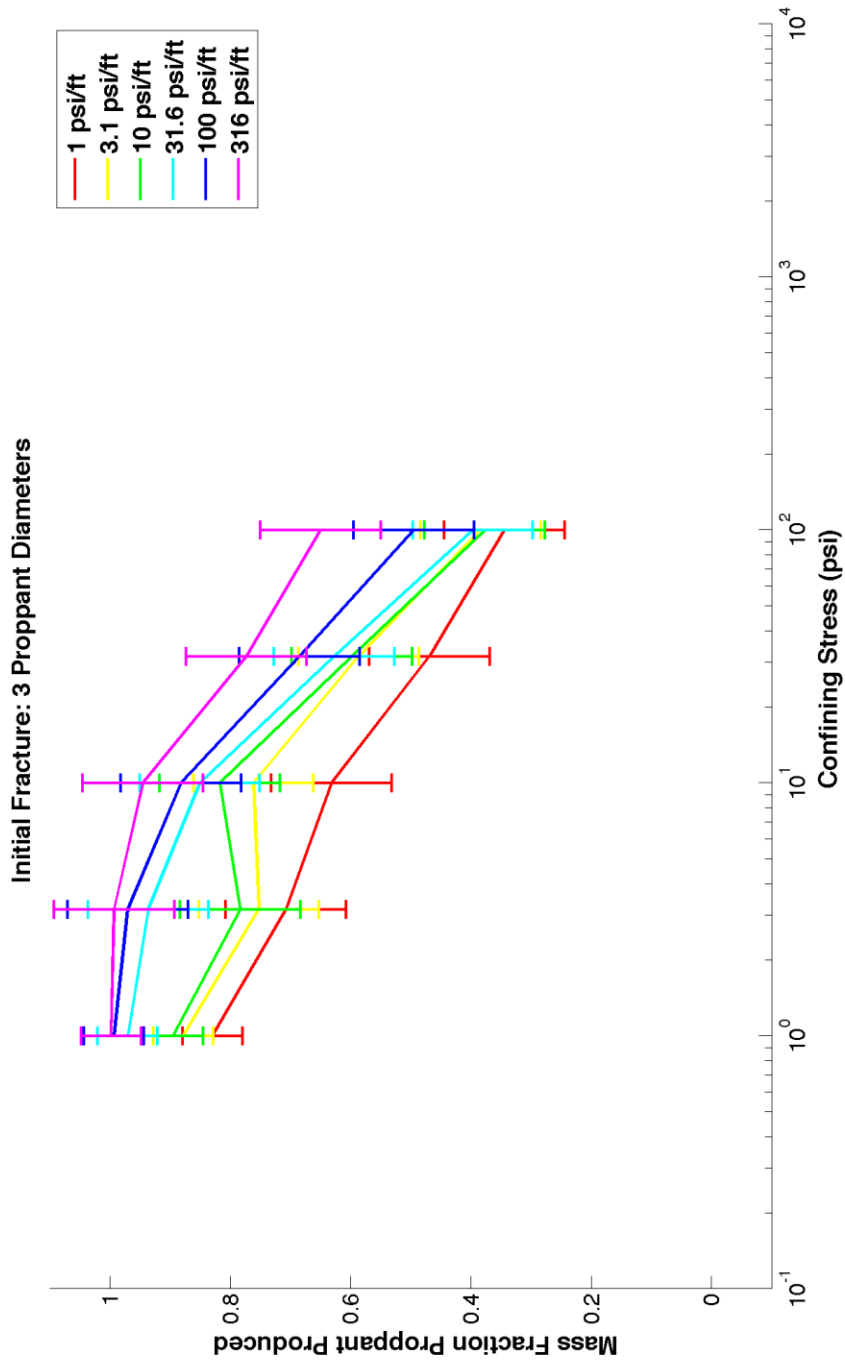
Figure 29 Mass fraction of proppant produced for a fracture initially three proppant diameters wide with a polydisperse 118

and 235 micron proppant
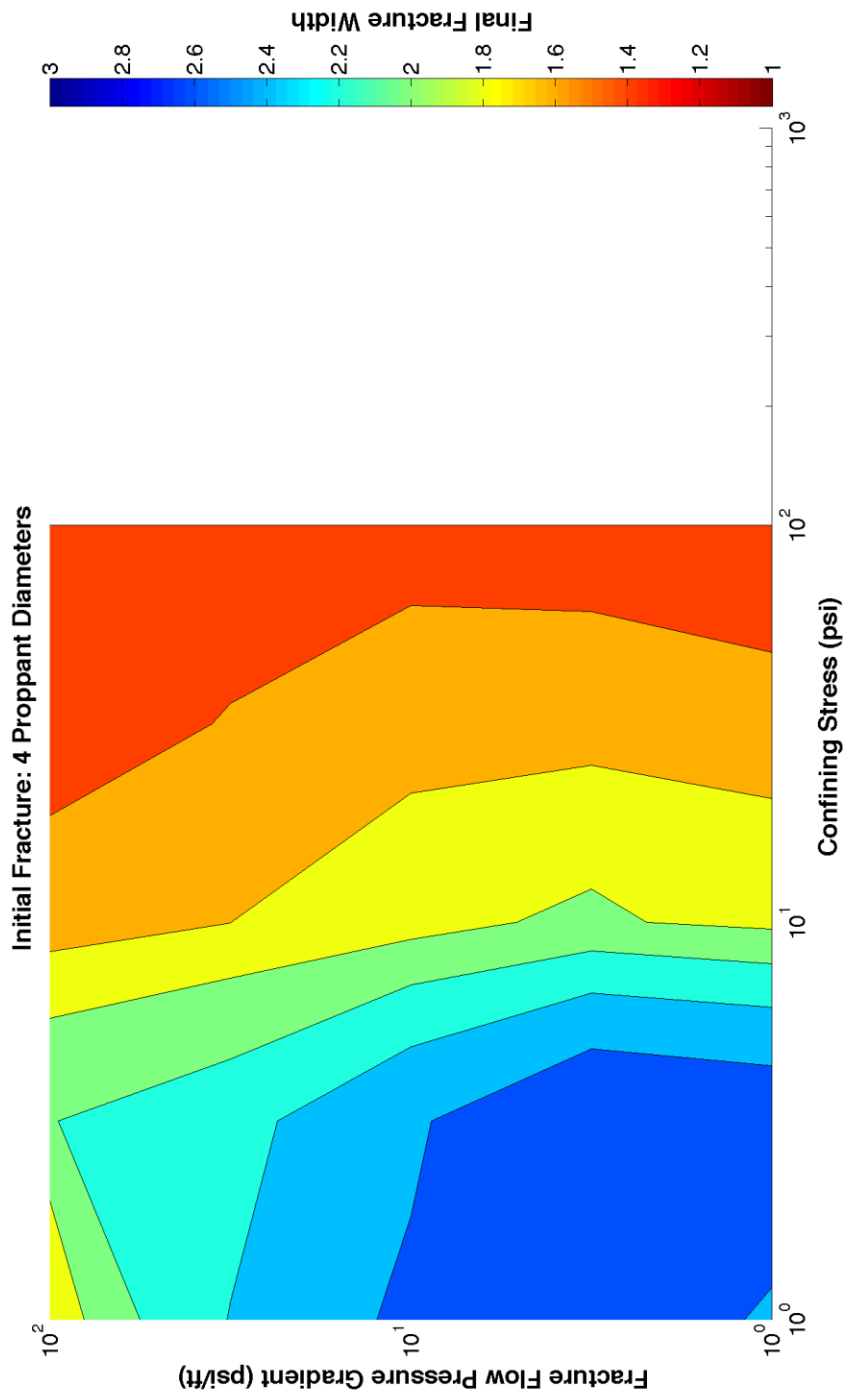
Figure 30 Final fracture width, normalized by proppant diameter, for a fracture initially four maximum proppant diameters wide and a polydisperse 118 and 235 micron proppant
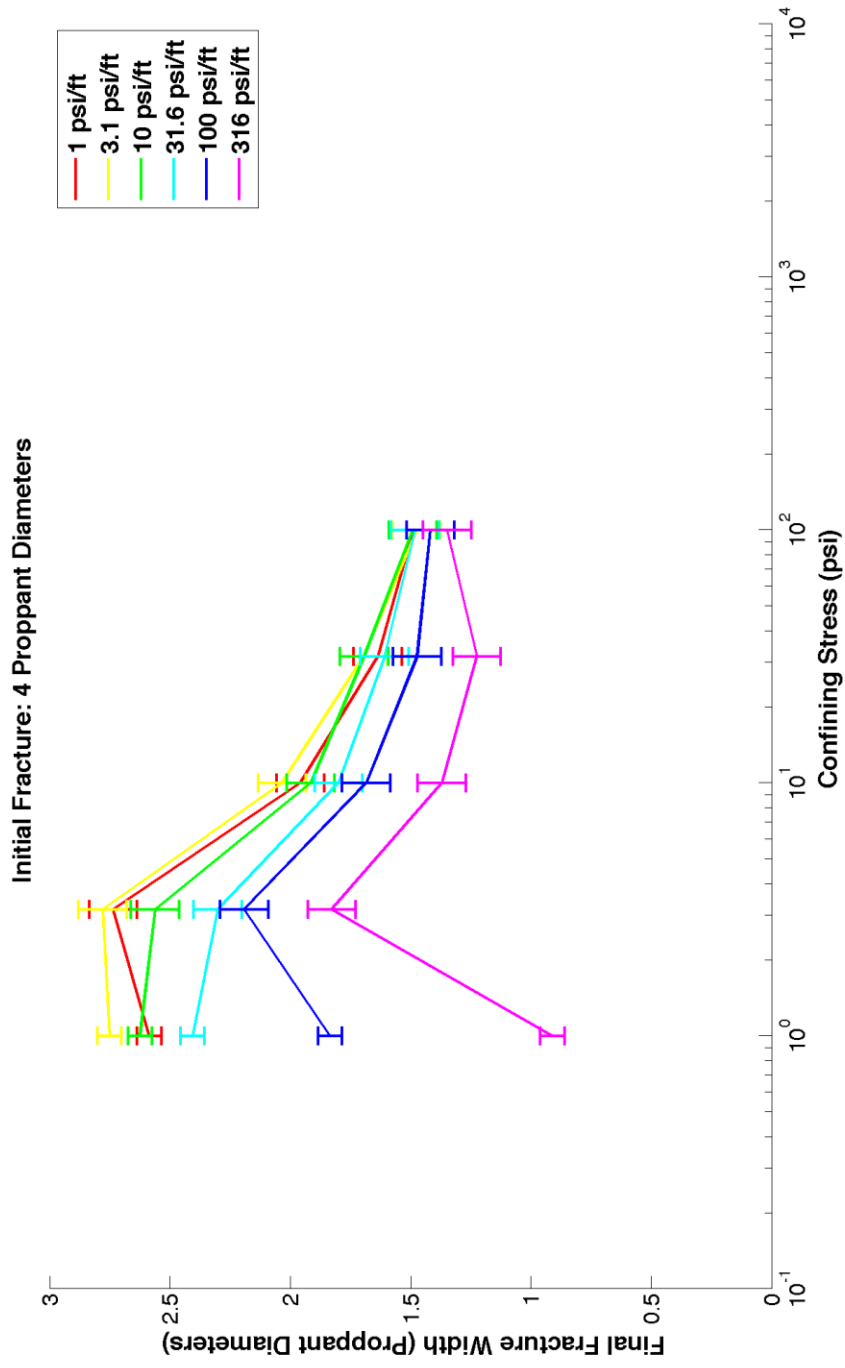
Figure 31 Final fracture width, normalized by proppant diameter, for a fracture initially four maximum proppant diameters wide and a polydisperse 118 and 235 micron proppant
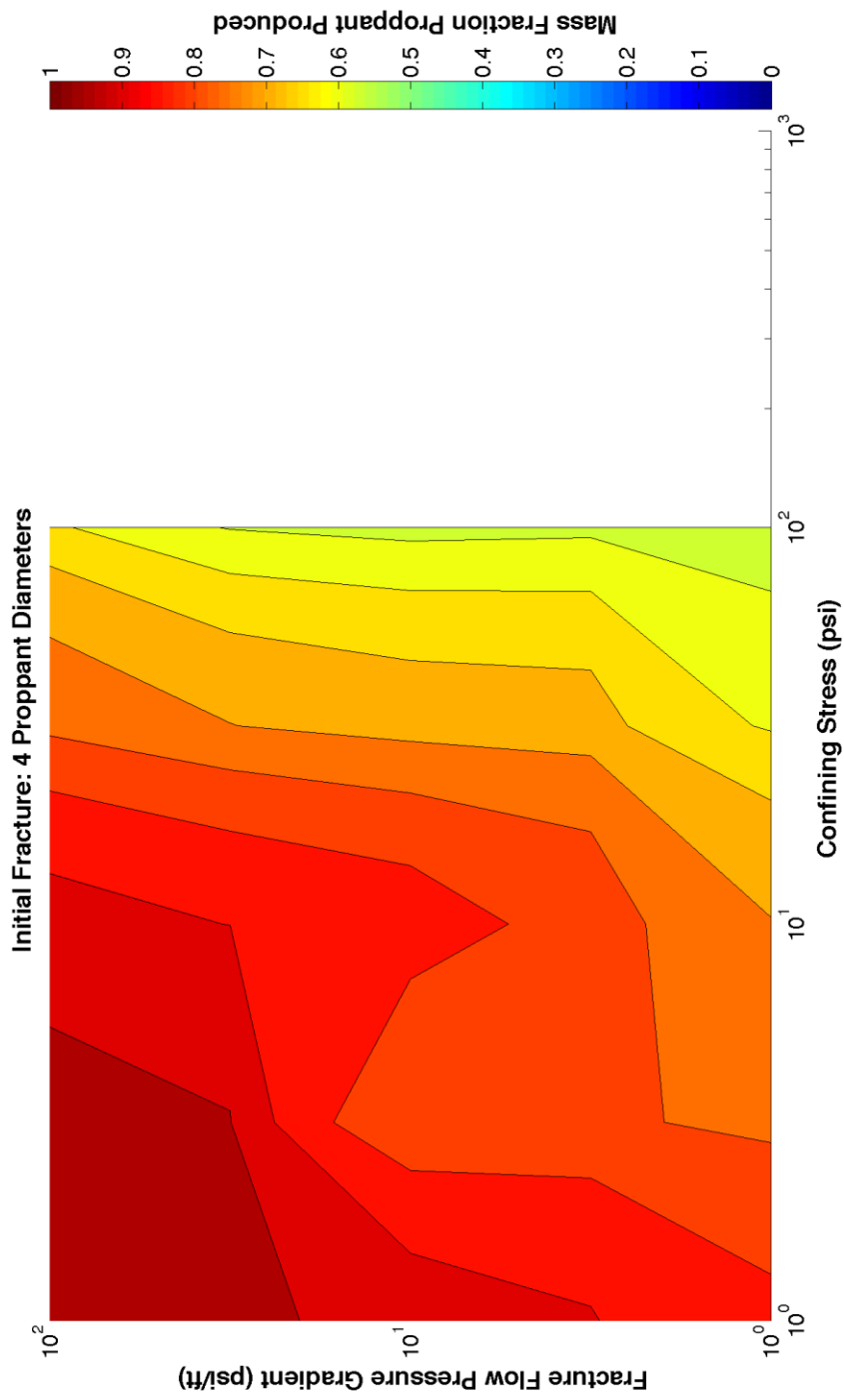
Figure 32 Mass fraction of proppant produced for a fracture initially four proppant diameters wide with a polydisperse 118 and 235 micron proppant
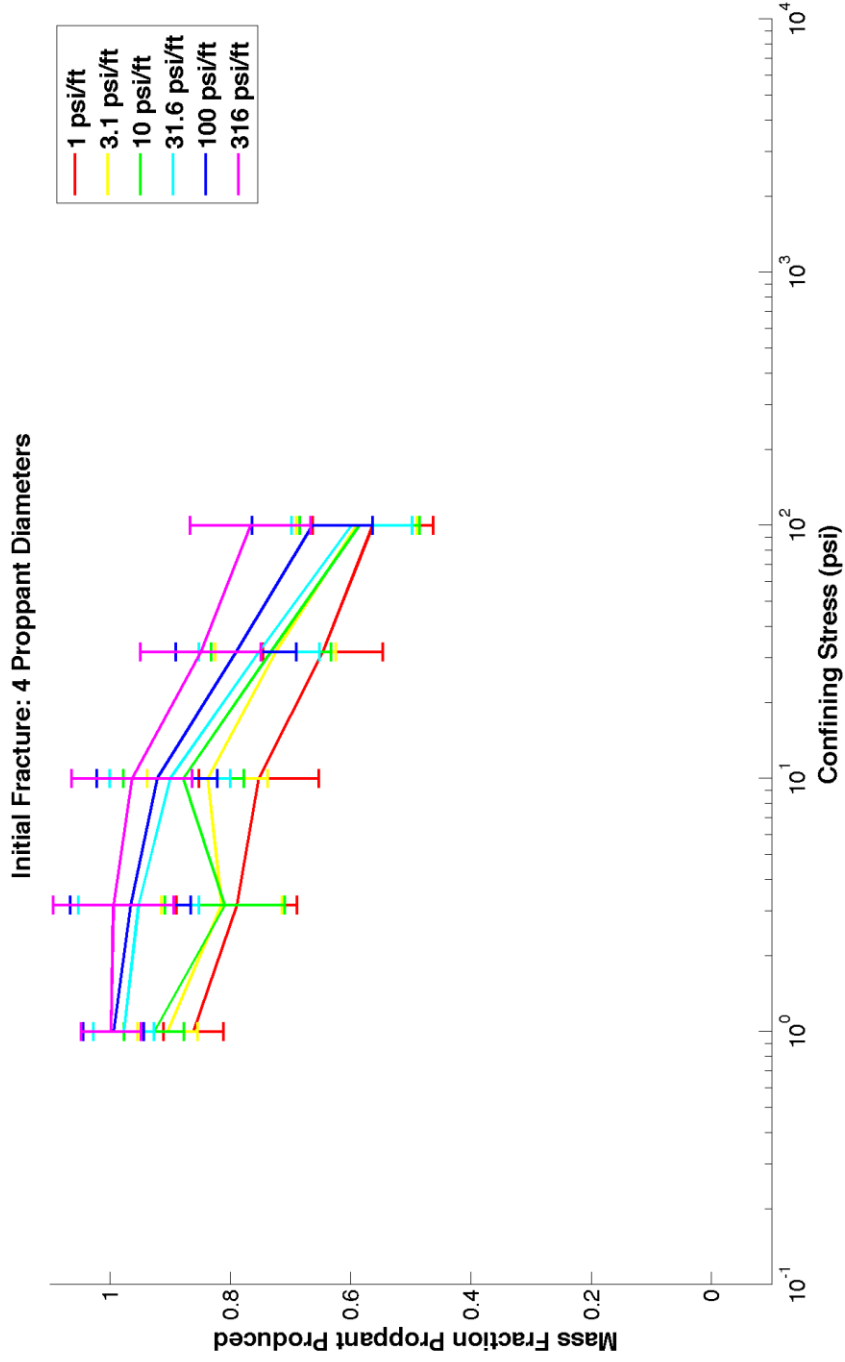
Figure 33 Mass fraction of proppant produced for a fracture initially four proppant diameters wide with a polydisperse 118 and

235 micron proppant

5.   DISCUSSION

By overlaying the plots of the final fracture width with that of proppant production, three regions can be distinguished. Two of these regions are expected: a closed, empty fracture and an open, full fracture. The first can occur when the fluid flow in the fracture overpowers the bridging tendency of the proppant pack, and the latter occurs when there is sufficient net confining stress to ensure bridging occurs. A third region is visible between these − see an example in Figure 34 − and contains fractures that remain open but have very little proppant remaining within them and are often wider than just a single proppant grain. This means a stable proppant bridge may form that can support the net confining stresses until grain breakdown occurs. An example situation is shown in Figure 35.

Beginning with a fracture that is initially three proppant diameters wide without cohesion, the final fracture widths (as shown in Figure 6) can be broadly characterized into the following regions:

1. For a net confining stress below 10 psi and a pressure gradient less than 10 psi / ft, the final fracture is wider that 2.5 proppant diameters.

2. For a net confining stress below 10 psi and a pressure gradient above 10 psi / ft, the final fracture decreases to 0 with increasing pressure gradient.

67

3. For net confining stress between 10 psi and 500 psi, the final fracture width decreases slowly from 2.5 proppant diameters to 1.5 proppant diameters.

4. For net confining stress greather than 500 psi, the fracture closes to a single proppant diameter.

The proppant production (as shown in Figure 7) can be characterized into the following, similar, regions:

1. For net confining stresses less than 2 psi, over 90% of proppant is produced

2. Between 2 and 5 psi, the fraction of proppant produced decreases from >90% for pressure gradients greater than 10 psi / ft to 50% for pressure gradients below 5 psi / ft.

3. For net confining stresses between 50 and 250 psi, only 25-40 % of proppant is produced, with a higher production at higher pressure gradients.

4. For net confining stresses higher than 250 psi, less than 25% of proppant is produced, regardless of pressure gradient.

These regions share similar boundaries and can be combined into the three fracture proppant packing regimes shown in Figure 36. For net confining stresses greater than 100 psi, a majority of proppant remains in the fracture and creates a stable proppant pack that supports the formation. For net confining stresses between 10 and 100 psi,

fracture width is generally constant but fraction of proppant produced increases, both with decreasing net confining stress and with increasing pressure gradient. Fractures in this zone are open but retain less proppant and few supporting proppant bridges. Finally, for low net confining stress, below 10 psi, and high pressure gradients, greater than 100 psi / ft, the fractures close entirely, indicating catastrophic proppant pack collapse.
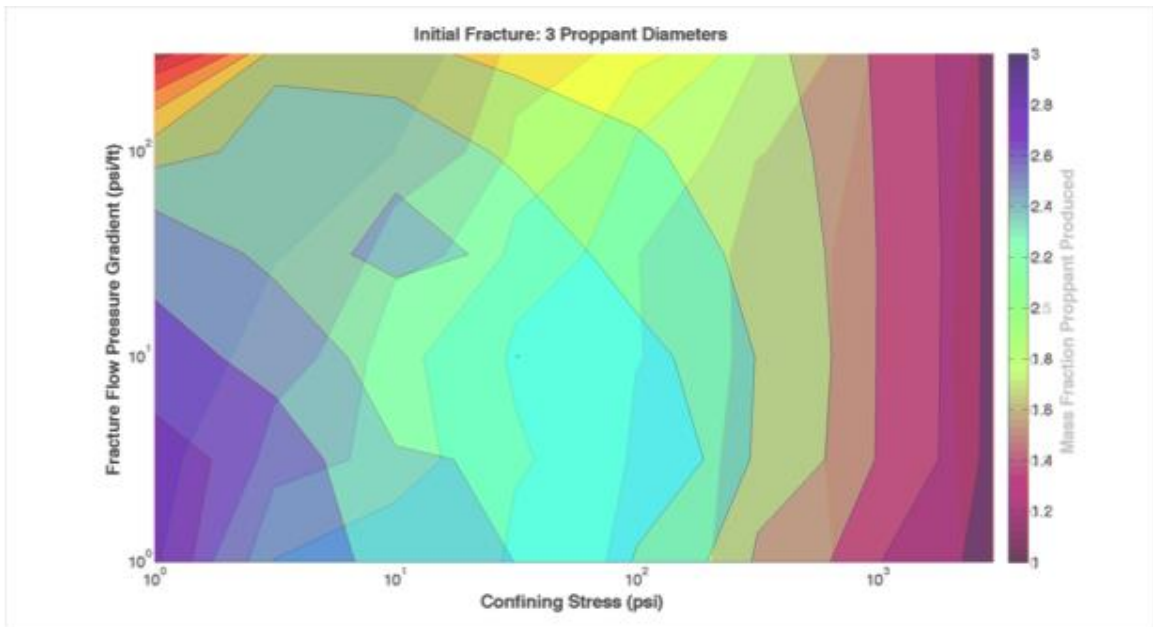
Figure 34 Overlaying the plots of final fracture width and fraction of proppant produced. The two expected regimes are easily observed on either the left or right side of the plot. On the left, an empty, closed fracture is observed while on the right; a full, propped fracture (until the point of grain crushing is reached) is observed. In the center is a third regime where a fracture remains open but still produces a majority of the proppant originally contained within it.
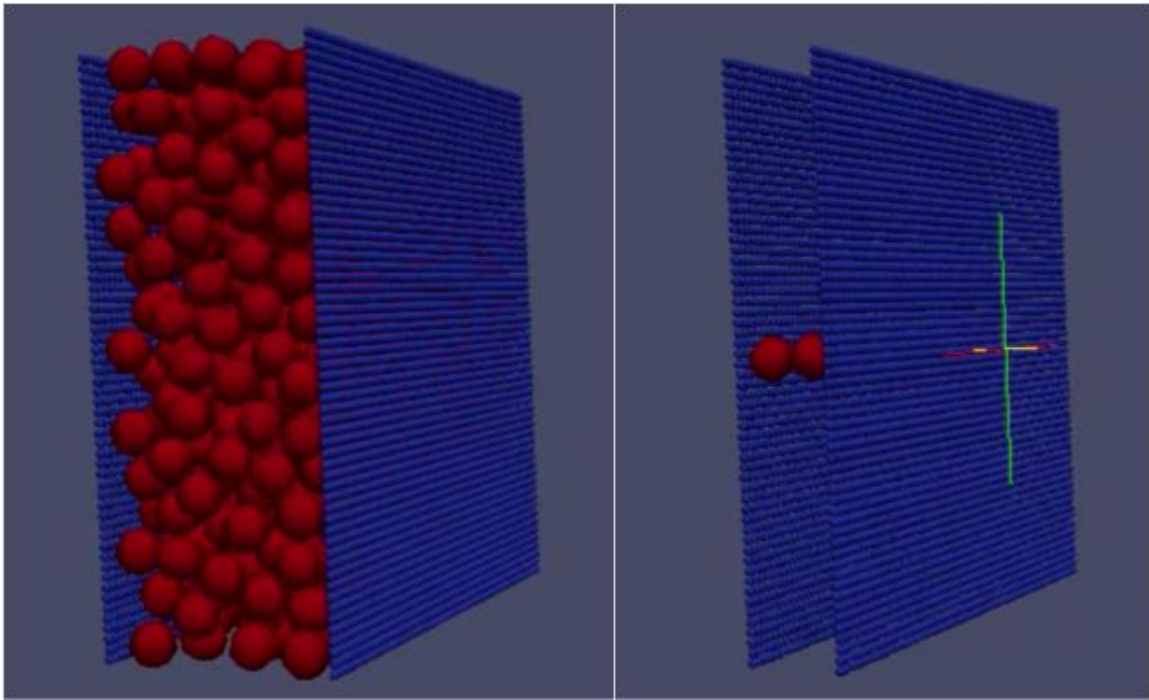
Figure 35 An example from the set of simulations of an open fracture with a single proppant bridge holding it open.

The two orthogonal forces acting on the proppant pack are the net confining stress and the point force from fluid flow. The net confining stress is transmitted between grains from the fracture walls, while the fluid force is simulated as an evenly distributed point force applied to each particle. The net confining stress from the formation acts to trap proppant grains within the fracture by creating an interlocking network that is anchored by the roughness of the grain structure of the fracture walls. The larger proppant grains settle into the low regions of the lattice structure of the fracture walls, and so long as the force normal to the walls is sufficient to hold the proppant grain against the fracture wall, the grain will not slip and will begin to anchor a bridge structure. The fluid flow acts to disturb this network of grains by providing a sideways force that will allow grains to roll, slide or bump their way down the fracture until a bridge is encountered. A bridge is formed when two or more proppant grains align across the fracture and the combination of fracture wall roughness and net confining stress are sufficient to counterbalance any tangential force from fluid flow. A sufficient force from fluid flow or a collision from a proppant grain would be able to break this bridge. An insufficient force from such a collision would instead work to increase the size of the bridge and would begin building a stable proppant pack.

5.1   Three Proppant – Fracture Packing Regimes

The three regimes can be described as: a fully collapsed fracture, an open fracture with a one or more proppant bridges holding it open, and a packed open fracture, as

illustrated as a function of stresses in Figure 36 and visually in Illustration 5. The first regime occurs with the coupling of a high pressure gradient within the fracture and a low net confining stress. The high flow rate pushes proppant out before stable bridges are able to form and catastrophic failure of the proppant pack is experienced. The second regime occurs when proppant is able to form stable bridges to prop the fracture open, but the remaining proppant escapes due to the still high flow rates and bridges remain sparse. In this case, the net confining stress is able to maintain the bridge but the bridge is unable to hold up any of the other proppant grains. The third regime occurs when sufficient bridges have formed that a majority of the proppant pack remains trapped within the fracture. This occurs at higher net confining stress and lower pressure gradients.

This second regime is the most interesting as it postulates the existence of open fractures that are not completely packed with proppant. These sections of the fracture network would have extremely high permeability, but would also be susceptible to crushing of proppant bridges at high net confining stresses, either at the completion of flowback or during production.

The formation of these three regimes can be summarized into the following basic steps

1. As fracture fluid begins to flow and to exert a point force on each proppant grain, the grains begins to move in the direction of fluid flow until a path obstruction is encountered.

a. The grain's momentum is transferred to the obstruction. If the obstruction is another free-floating grain, then the momentum transfers the first grain's velocity to the second grain. If the obstruction is part of a proppant bridge, then either the momentum imparted is sufficient to break the bridge, in which case the bridge collapses, or is insufficient, in which case the grain is held up by the bridge and the pack size increases.

b. If the obstruction is a fracture wall, then the particle simply bounces off through a reversal of its velocity normal to the fracture wall.

2. As the flow continues, depending on the fluid flow velocity, grains that have formed bridges begin to trap additional proppant grains. If flow velocity is too great for entrapment, then the flowing grains continue towards the outlet.

In the first regime, an empty fracture, the momentum of the individual grains due to the high fluid flow velocity is sufficient to knock out all bridges that are able to form, thus draining the fracture opening of all proppant and causing the fracture to close. In the second regime, at least one of the proppant bridges has sufficient strength to withstand this bombardment and remains after all the other proppant has been produced. As fluid velocity decreases, more proppant bridges survive and the fraction of proppant produced is reduced. In the final regime, the strength of the proppant bridges is sufficient to trap most, if not all, of the proppant in the fracture. This occurs since multiple bridges form near the outlet and are able to retain all upstream proppant.

The addition of a resin coating or a surface modification agent shifts the third regime, of fully packed fractures, to the left to lower net confining stresses. The increased cohesion between grains allows bridges to hold up a larger fraction of the proppant from being produced by increasing the sticking of flowing grains to existing bridges. This in turn increases the cross sectional size of the bridge and increases the trapping tendency of the bridge. At lower net confining stresses, the addition of resin increased the production of proppants due to the clumped proppants gaining velocities sufficient to destroy any bridges formed, leading to catastrophic pack failure and fracture closure. The lower net confining stress does not give enough strength to the bridge to resist the increased momentum of a clump of proppant grains. This is unlikely to be observed in true fractures due to these clumped proppants experiencing flow constrictions, such as perforations, that were not modeled.

The regimes are surprising constant regardless of initial fracture width, though a lower fraction of the proppant remains due to a higher initial input in wider fractures. The introduction of a polydisperse proppant was also observed to maintain the regimes but shifts the fraction of remaining proppant to the right, with more proppant produced under equivalent conditions. A consideration of these different proppant pack regimes needs to be included when designing a fracture treatment. To promote the creation of stable bridges within fractures and retain maximal proppant pack within the fracture, the fluid flow rate in the fracture needs to remain low while the buildup of net confining stress occurs, otherwise fractures will quickly be evacuated. In formations that would be

undamaged by fracture fluid leak-off, a shut in period followed by a ramp up of fracture fluid flowback is recommended to improve the proppant packing in fracture. In formations sensitive to fracture fluids, flowback may begin immediately but a ramp up of rate is encouraged. A rate ramp up allows the ratio of fluid flow to net confining stress to potentially remain in the packed fracture regime or would at worst maintain open fractures. Cohesive proppants are recommended to increase the proppant packing of fractures (and reduce flowback) but this may not affect the final fracture widths
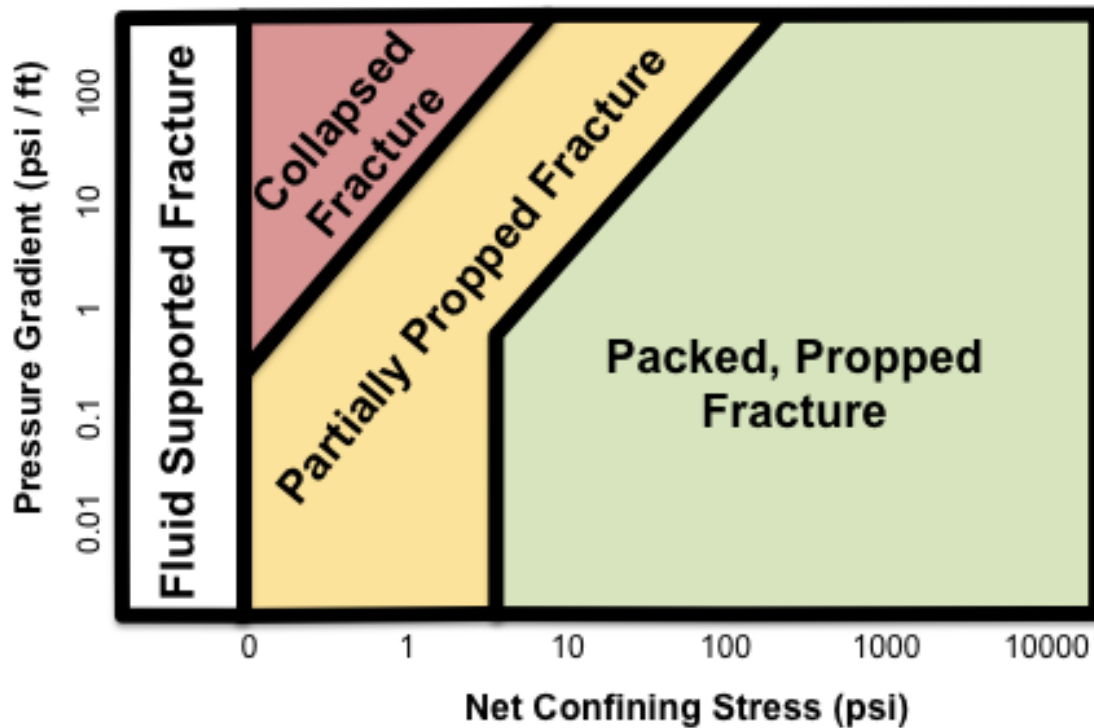
Figure 36 Three fracture – proppant pack regimes are visible in the simulations. At higher pressure gradients, the fracture is fully evacuated and collapsed. At high net confining stresses, the fracture is fully packed and propped open, but begins to collapse as the mechanical strength of the proppant or formation is exceeded. In between the two is a transition regime where the fracture is open but nearly fully evacuated.
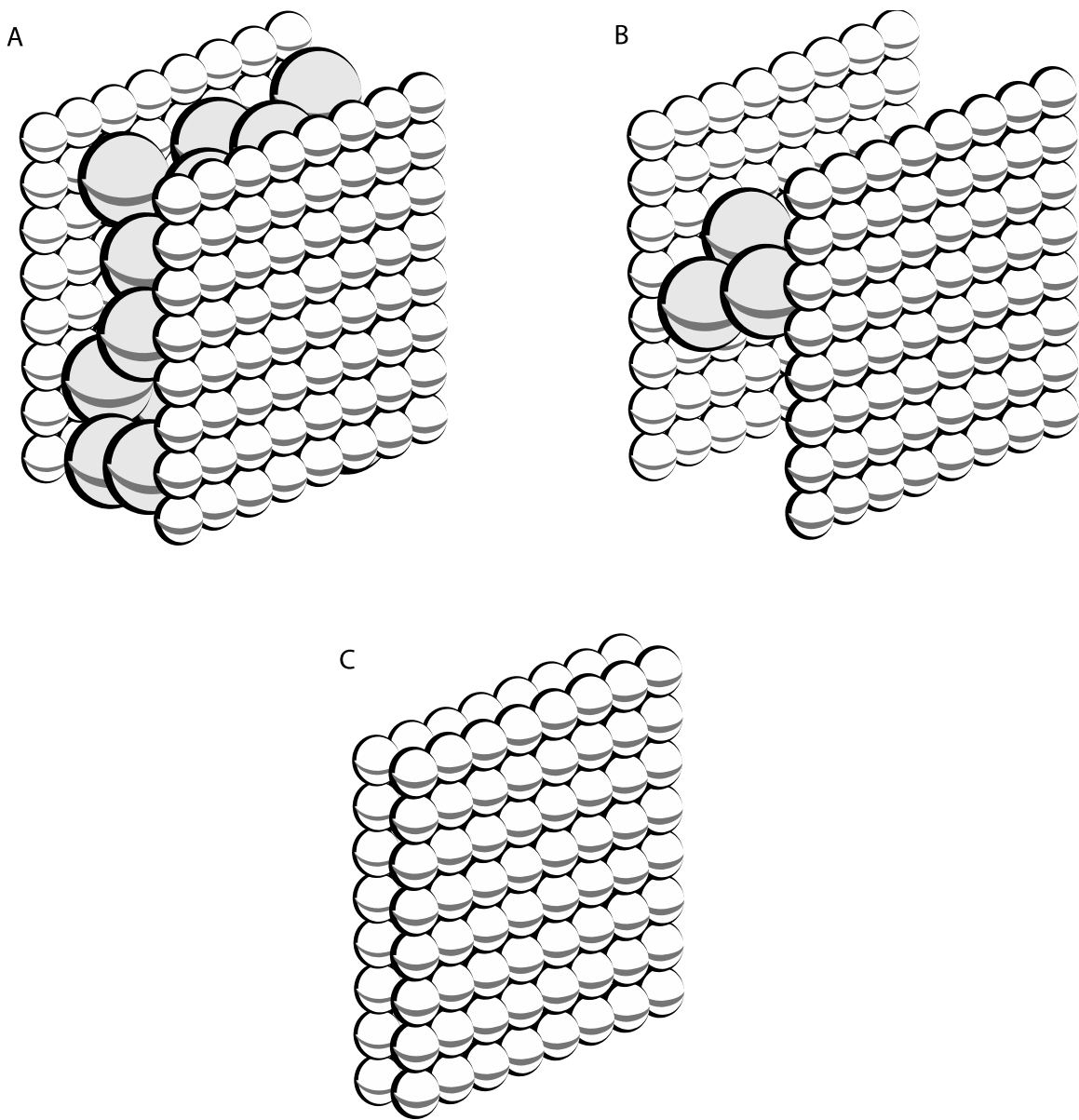
Illustration 5 Visualizing the three proppant pack regimes. (A) represents a fully packed fracture, (B) represents an open fracture with a single bridge supporting the net confining stress, but is otherwise evacuated, and (C) represents a collapsed fracture.

5.2   Application to Industry

These three proppant packing regimes need to be considered when designing and selecting a fracture treatment, especially the flowback procedures.

The first consideration is the flowback technique used to complete the fracture treatment. The two procedures utilized most widely in industry are forced closure – where fracturing fluid is rapidly produced back to surface in an effort to reduce settling, and slow flowback – where fluid velocities are minimized within the fracture to reduce erosion of the pack. The aim of forced closure is to trap proppant suspended in the fracture fluid slurry in the upper portions of the fracture and to reduce gravitational settling, but the rapid production of fluid means high fluid velocities within the fracture. During forced closure, the pressure gradient within the fracture increases rapidly as the choke at the surface is opened. The fluid in the fracture initially carries the net confining stresses before being transferred to the proppant. In Figure 37, the arrows show the evolution of the stress regime through the flowback process. With slow flowback, pressure gradients are maintained at low levels while the net confining stress is transferred from the fluid to the proppant. This means that the proppant packing will shift rapidly from an open but empty fracture to a fully propped fracture. Physically, proppant packs in the far field will flow with the fracture fluid briefly until becoming entrapped by the closure of the fracture.

As flowback rate increases, the pressure gradient within the fracture increases in early time before the net confining stress has been transferred to the proppant pack. The

more rapid the flowback treatment, the higher the pressure gradient will be within the fracture. At early time, the fracture fluid is carrying the entire confining stress of the formation, so as the pressure gradient increases, the closer the conditions come to fully evacuating the fracture of any proppant. Physically, with rapid flowback, sections of the fracture may become completely emptied of proppant and thus close once all fluid is produced.

Rapid closure of the fracture is desired to reduce the gravitational settling of the proppant suspended within the fluid, but too rapid of a flowback could result in the production of proppant and leaving sections of the fracture network unpropped. A safe middle ground that has been used with success is the gradual ramp up of flowback. By gradually increasing the pressure gradient as fluid is produced, the proppant pack can remain within the second two regimes – an open fracture with stable bridges or a fully packed fracture.
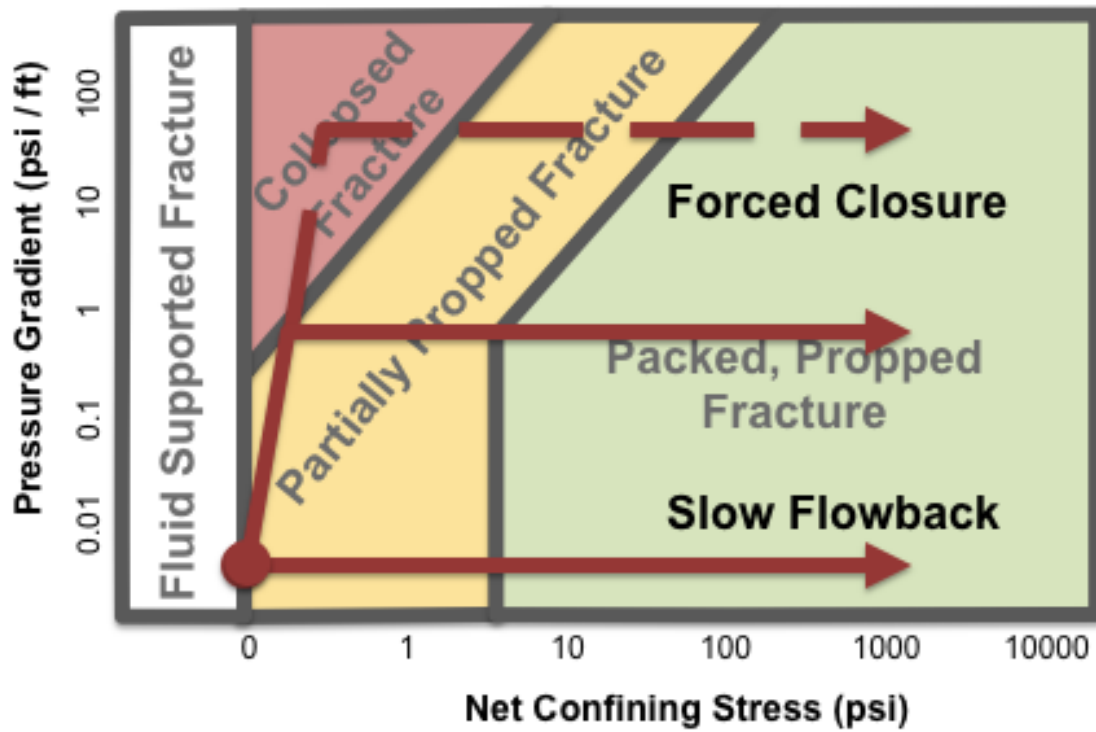
Figure 37 The effect of forced closure compared with slow flowback, as visualized on top of the three proppant pack regimes. Low fluid velocities (and low pressure gradients within the fracture) in slow flowback means that the fracture moves along the

Another consideration that must be accounted for is the gel strength, or equivalently the viscosity of the fracturing fluid. A fluid with a higher viscosity imparts a higher force on the proppant pack for the same flowback rate, so a fracture treatment that is considered 'safe' for a low viscosity fluid – a slickwater frac – may no longer be safe for a linear gel and may result in back production of proppant. And given equivalent conditions, a forced closure of a slickwater frac may give the same results as a linear or crosslinked gel – either in reduction in gravitational settling and proppant pack stability, or in catastrophic failure of the pack and massive production of proppant if the collapsed fracture regime is entered.

. In formations that would be undamaged by fracture fluid leak-off, a shut in period followed by a ramp up of fracture fluid flowback is recommended to improve the proppant packing in fracture. In formations sensitive to fracture fluids, flowback may begin immediately but a ramp up of rate is encouraged. A rate ramp up allows the ratio of fluid flow to net confining stress to potentially remain in the packed fracture regime or would at worst maintain open fractures. Cohesive proppant are recommended to increase the proppant packing of fractures but may not affect the final fracture widths.
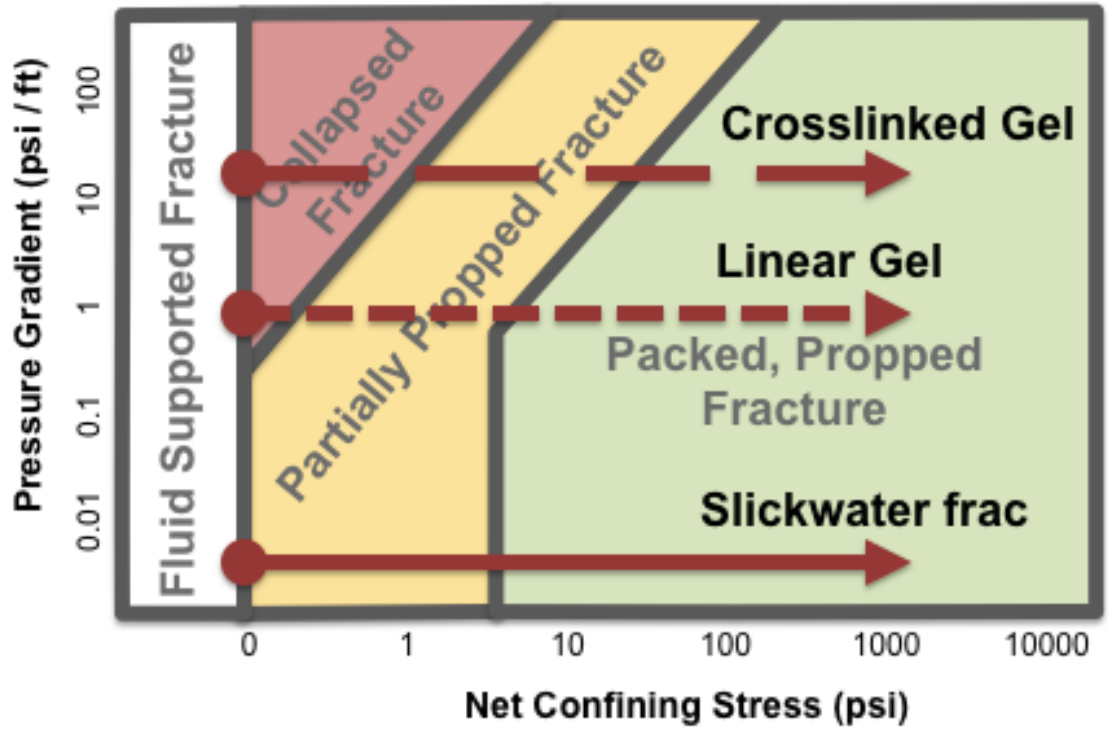
Figure 38 The effect of fracture fluid viscosity on the effect of flowing back a fracture using the slow flowback method. A high viscosity fluid increases the force experienced by the proppant pack within the fracture for the same fluid velocity, potentially leading to pack failure with equivalent flowback procedures.

6. FUTURE WORK

The natural continuation of this thesis would be to apply the coupled fluid – granular approach to more accurately model the interaction of the proppant grains and fracture fluid. Fluid abstracted as point drag forces has been applied successfully in the past, but faces limitations as particle concentration increase, as is the case in proppant packs. Fully coupled CFD – DEM simulations would be able to confirm observations presented in this thesis with a full physical model incorporating all components. Should observations be similar, as they are expected to be, the use of point drag forces instead of a full fluid simulation may be used as a time saving technique as coupled models add an order of complexity.

The full flexibility of this model may also be leveraged to understand the behavior of proppant slurries and packs in complex fracture geometries, including fractures with sharp turns or intersecting natural fractures. Turbulence occurs at these sharp changes in fracture direction, and slurries may exhibit radically different behavior than simple fracture flow. Preliminary investigations into this area have illustrated the difficulty of pumping proppants around corners and could lead to exciting results.

7. CONCLUSION

A discrete element model has successfully been applied to the evaluation of proppant pack stability and flowback. Final fracture widths are, to a first approximation, unaffected by the original fracture width if the proppant has the opportunity to be produced (as may be the case for proppant near the wellbore, but may not be the case for proppant placed far away and below the wellbore). Both final fracture widths and proppant flowback are highly dependent on net confining stress and the pressure gradient in the fracture. The dependence of proppant production on confining stress and pressure drop, as well as proppant size distribution and cohesion are quantified using the model presented here. Increasing confining stress increases the fraction of proppant retained within the fracture but reduces fracture width once proppant pack strengths begin to be exceeded. Increasing pressure gradients in the fracture, or increasing production rates, decrease pack stability and reduce the fraction of proppant remaining in a stable pack. Three broad proppant packing regimes are identified: a fully evacuated and collapsed fracture, occurring at high flow rate and low net confining stress conditions; a propped but mostly evacuated fracture, occurring at mid to high flow rates and low to intermediate net confining stresses; and fully packed and propped fractures occurring at high net confining stress and lower flow rates. From these regimes, a recommendation can be made to implement well flowback guidelines to enhance proppant pack formation or to implement forced closure in fracture treatments with gradual flow rate build ups,

85

ensuring that net confining stress is allowed to increase before high pressure gradients are

imposed on the proppant pack.

APPENDIX I - MODEL SCRIPT

LIGGGHTS executes simulation script serially, line by line, allowing variables to be utilized to track simulation progress. To begin, the simulation type is set as granular and the boundaries are set as fixed on the *y* and *z* directions and periodic in the *x* direction.

```
#particle packing by insertion and successive growing of particles

atom_style  granular
atom_modify map array
boundary    p f f
newton          off

communicate single vel yes

units       si
```

Next, the simulation volume is defined. Four regions are defined to facilitate particle insertion – the `reg` region contains the entire simulation, the `inbox` contains the original fracture opening and the `leftwall` and `rightwall`s contain the lattices for the fracture walls.

```
region           reg block -1e-5 3.0001e-3 -0.05001e-3 8e-4 -1e-8
3.0001e-3 units box
region           inbox block 0 3e-3 0 7.5e-4 0 3e-3 units box
region           leftwall block 1e-8 2.999e-3 7.5e-4 8e-4 1e-8 2.999e-
3 units box
region           rightwall block 1e-8 2.999e-3 -0.049e-3e-3 0. 1e-8
2.999e-3 units box

create_box  1 reg
```

Neighbor lists are used to determine element interaction.

```
neighbor    0.0005 bin
neigh_modify    delay 0
```

Material properties are defined for each element.

```
#Material properties required for new pair styles

fix         m1 all property/global youngsModulus peratomtype 7.e10
fix         m2 all property/global poissonsRatio peratomtype 0.20
fix         m3 all property/global coefficientRestitution
peratomtypepair 1 0.3
fix         m4 all property/global coefficientFriction peratomtypepair
1 0.5
fix          m5 all property/global coefficientRollingFriction
peratomtypepair 1 0
```

For simulations with cohesion, the 0 is replaced with a 1.

```
#New pair style
pair_style  gran/hertz/history 3 0   #Hertzian without cohesion
pair_coeff  * *
```

No flux boundaries are added in the *x*, *y* and *z* directions. The *z* plane is divided into two

planes to allow for easy removal of a boundary once fracture flow begins.

```
fix         ywall all wall/gran/hertz/history 1 0 yplane 0 8e-4 1
fix         barrier all wall/gran/hertz/history 1 0 yplane 0. 7.5e-4 1
fix          xwall all wall/gran/hertz/history 1 0 xplane -1e-5
3.0001e-3 1
fix         zwall all wall/gran/hertz/history 1 0 zplane 0 NULL 1
fix         zwall_out all wall/gran/hertz/history 1 0 zplane NULL
3.0001e-3 1

timestep      1e-9

fix           ts_check all check/timestep/gran 1000 0.2 0.2
```

Particle distribution templates dictate the mass distribution of particles that are inserted.

In this case, the original insertion pack contains 50 and 100 micron spheres.

```
#distributions for insertion
fix         pts1 all particletemplate/sphere 132 atom_type 1 density
constant 2650 radius constant 1e-4
```

```
fix          pts2 all particletemplate/sphere 132 atom_type 1 density
constant 2650 radius constant 5e-5
fix          pdd1 all particledistribution/discrete 1239  2 pts1 1.0
pts2 0.
fix          pdd2 all particledistribution/discrete 1239  2 pts1 0. pts2
1.0
```

Inserting particles is computationally intensive, thus for efficiency, smaller particles are inserted and then allowed to grow until the desired mass fraction and void fraction ratios are reached. During growth, the pack is allowed to relax physically, eliminating overlap between grains.

```
#parameters for gradually growing particle diameter
variable     alphastart equal 0.40
variable     alphatarget equal 0.65
variable     growts equal 350000
variable     growevery equal 40
variable     relaxts equal 250000

#region and insertion
group        nve_group region reg
fix          ins nve_group pour/dev/packing 1 distributiontemplate pdd1
vol ${alphastart} 200 region inbox


#apply nve integration to all particles that are inserted as single
particles
fix          integr nve_group nve/sphere
```

Useful data can be printed at specific points in the simulation to allow for simulation monitoring. In this case, every 100,000 time steps the thermodynamic properties of the system are printed to ensure proper simulation operation.

```
#output settings, include total thermal energy
compute         1 all erotate/sphere
thermo_style    custom step atoms ke c_1 vol
thermo          100000
thermo_modify   lost ignore norm no
compute_modify  thermo_temp dynamic yes
```

```
print       "Inserting Proppant Pack"
#insert the first particles
run         1
```

Simulation state may be dumped periodically into specially formatted dump files and then played back visually.

```
#dump       dmp_paraview all custom 4000
./post/dump forces limited var 7.5e-4 1e03 *.ligghts id type type x y
z ix iy iz vx vy vz fx fy fz omegax omegay omegaz radius
unfix       ins
#undump         dumpstl

#calculate grow rate
variable    Rgrowrate equal
(${alphatarget}/${alphastart})^(${growevery}/(3.*${growts}))
print       "The radius grow rate is ${Rgrowrate}"

#do the diameter grow
compute     rad all property/atom radius

variable    d_grown atom ${Rgrowrate}*2.*c_rad
fix         grow nve_group adapt ${growevery} atom diameter d_grown
neigh_modify     every ${growevery} check no


neighbor    0.000005 bin
```

The proppant pack is allowed to grow and then relax. The end product is a dense suspended slurry with a proppant volume fraction approaching 0.5.

```
#run
run         ${growts}

#let the packing relax
unfix       grow

neigh_modify     check yes


run             ${relaxts}

variable    pack equal ${growts}+${relaxts}
```

90

Fracture walls are generated as rigid square lattices on either side of the proppant pack.

```
print        "Creating Fracture Walls"

neighbor     0.0005 bin

lattice          sc 5e-5
create_atoms     1 region leftwall units box
group        leftwall_group region leftwall
set          group leftwall_group diameter 5e-5 density 2650

create_atoms     1 region rightwall units box
group        rightwall_group region rightwall
set          group rightwall_group diameter 5e-5 density 2650
velocity     rightwall_group zero linear
fix          2 rightwall_group nve/noforce
fix          3 rightwall_group freeze
```

Since the walls are rigid bodies, granular interactions between grains of the same wall may be ignored. The walls are assume to remain parallel due to the small volume being simulated, so only normal forces are allowed and torques are ignored.

```
#Granular Wall
fix          1 leftwall_group rigid group 1 leftwall_group force * on on
off torque * off off off
neigh_modify     exclude group leftwall_group leftwall_group
neigh_modify     exclude group rightwall_group rightwall_group
neigh_modify     exclude group leftwall_group rightwall_group

thermo           1000

#run         100000
```

The barrier between the proppant pack and the walls is removed and the system is allowed to come to equilibrium. Data of interest is then specified and saved to a file every 4000 time steps.

```
unfix        barrier

#save data
```

91

```
variable    massleft equal mass(nve_group,inbox)
variable    totalmass equal mass(nve_group,inbox)
variable    averagevelocity equal vcm(nve_group,z,reg)
variable    fracturewidth equal xcm(leftwall_group,y,reg)-
xcm(rightwall_group,y,reg)
variable    pressureleft equal fcm(leftwall_group,y,reg)
variable    pressureright equal fcm(rightwall_group,y,reg)


fix         screen all print 100000 "${massleft}, ${totalmass},
${averagevelocity}, ${fracturewidth}, ${pressureleft},
${pressureright}"
fix         extra all print 4000 "${massleft}, ${totalmass},
${averagevelocity}, ${fracturewidth}, ${pressureleft},
${pressureright}" file flowingMAXs_203.txt

#relax

run         100000
```

Net confining stress is applied and the proppant pack is allowed to compact between the

fracture walls. All boundaries are still closed, so no proppant is yet produced. Viscous

dampening is applied to reduce the energy of the system, simulating the effects of the

presence of a carrier fluid.

```
#compact

print       "Compacting Proppant Pack"

fix         shmin leftwall_group addforce 0.0 0 0.0


run         400000

fix             damp nve_group viscous 0.189
run             200000
unfix           damp
```

The *z* boundary is removed and a point drag force is applied to each proppant grain in the

direction of fluid flow.

```
unfix       zwall_out
```

```
print       "Applying Fracture Flow"

fix          gr nve_group addforce 0. 0. 8.6167e-3


run         1000000
```

The equilibrium loop is entered and the mass of the system is checked until mass remains
constant over a large period of time steps. This condition met, the system is assumed to
be at equilibrium.

```
label            loop

print       "Entering mass loop"

variable    masspres equal ${massleft}

run         40000

variable    deltam equal v_masspres-v_massleft

if          $deltam=<0.00000001 then

            "jump in.var_width_MAXp7.5e408.6167e3 continuing"

variable    masspres delete
variable    deltam delete


jump        in.var_width_MAXp7.5e408.6167e3 loop


label       continuing

run         100000

print       "Done"
```

On completion a text file created with model state throughout the simulation, and Matlab
script is used to load this data and compare it as model parameters are varied.

BIBLIOGRAPHY

Asgian, M., Cundall, P., & Brady, B. (1995). Mechanical Stability of Propped Hydraulic Fractures: A Numerical Study. *Journal of Petroleum Technology* , 203-208.

Baker, V., & Pyne, S. (1978). G.K. Gilbert and modern geomorphology. *American Journal of Science* , *278*, 97-123.

Barree, R., & Conway, M. (2007). Multiphase Non-Darcy Flow in Proppant Packs. *SPE ATCE*. Anaheim, CA: Society of Petroleum Engineers.

Barree, R., & Conway, M. (2001). Proppant Holdup, Bridging, and Screenout Behavior in Naturally Fractured Reservoirs. *SPE Production and Operations Symposium*. Oklahoma City: Society of Petroleum Engineers.

Brannon, H., Rickards, A., & Stephenson, C. (2003). Exceptional Proppant Flowback Control for the Most Extreme Well Environments: The Shape of Things to Come. *SPE Asia Pacific Oil and Gas Conference and Exhibition*. Jakarta, Indonesia: Society of Petroleum Engineers.

Cleary, M., & Fonseca, A. (1992). Proppant Convection and Encapsulation in Hydraulic Fracturing: Practical Implications of Compuater and Laboratory Simulations. *SPE ATCE*. Washington, D.C.: Society of Petroleum Engineers.

Crafton, J. (2008). Modeling Flowback Behavior or Flowback Equals "Slowback". *SPE Shale Gas Production Conference*. Fort Worth, TX: Society of Petroleum Engineers.

Cundall, P., & Strack, O. (1979). A discrete numerical model for granular assemblies. *Geotechnique* , *29* (1), 47-65.

Dartevelle, S. (2004). Numerical modeling of geophysical granular flows: A comprehensive approach to granular rheologies and geophysical multiphase flows. *Geochemistry Geophysics Geosystems* , *5* (8).

Dewprashad, B., Abass, H., Meadows, D., Weaver, J., & Bennet, B. (1993). A Method to Select Resin-Coated Proppants. *SPE ATCE*. Houston, TX: Society of Petroleum Engineers.

Ely, J. (1996). Experience proves forced fracture closure works. *World Oil* , *217* (1), 37-41.

Gadde, P., & Sharma, M. (2005). The Impact of Proppant Retardation on Propped Fracture Lengths. *SPE Annual Technical Conference and Exhibition*. Dallas: Society of Petroleum Engineers.

Gadde, P., & Sharma, M. (2005). The Impact of Proppant Retardation on Propped Fracture Lengths. *Annual Technical Conference and Exhibition*. Dallas, TX: Society of Petroleum Engineers.

Herrmann, H., & Luding, S. (1998). Modeling granular media on the computer. *Continuum Mechanical Thermodynamics* , *10*, 189-231.

Kabilamany, K., & Ishihara, K. (1990). Stress dilatancy and hardening laws for rigid granular model of sand. *Soil Dynamics and Earthquake Engineering* , *9* (2), 66-77.

Kloss, C., & Goniva, C. LIGGGHTS - Open Source Discrete Element simulations of Granular Materials based on LAMMPS. *Annual Meeting and Exhibition*. *2*. Minerals, Metals and Materials Society.

Lai, B., Miskimins, J., & Wu, Y. (2012). Non-Darcy Porous-Media Flow According to the Barree and Conway Model: Laboratory and Numerical-Modeling Studies . *SPE Rocky Mountain Petroleum Technology Conference*. Denver: Society of Petroleum Engineers.

Liu, Y., Gaddem, P., & Sharma, M. (2007). Proppant Placement Using Reverse-Hybrid Fracs. *Production & Operations* , *22* (3), 348-356.

Malhotra, S., Lehman, E., & Sharma, M. (2013). Proppant Placement Using Alternate-Slug Fracturing. *Hydraulic Fracturing Technology Conference*. The Woodlands, TX: Society of Petroleum Engineers.

Mangeney, A., Bouchut, F., Thomas, N., Vilotte, J., & Bristeau, M. (2007). Numerical modeling of self-channeling granular flows and of their levee-channel deposits. *Journal of Geophysical Research* , *112*.

Milton-Tayler, D., Stephenson, C., & Asgian, M. (1992). Factors Affecting the Stability of Proppant in Propped Fractures: Results of a Laboratory Study. *SPE ATCE*. Washington, D.C.: Society of Petroleum Engineers.

Mondal, S., Sharma, M., Hodge, R., Chanpura, R., Parlar, M., & Ayoub, J. (2011). A New Method for the Design and Selection of Premium / Woven Sand Screens.

Annual Technical Conference and Exhibition. Denver, CO: Society of Petroleum Engineers.

Nguyen, P., & Jaripatke, O. (2009). Controlling Solids Flowback to Maintain Production of Hydrocarbons: A Review of Successful Chemical Technologies in the Last Decade. *International Petroleum Technology Conference*. Doha, Quatar: IPTC.

Nguyen, P., Weaver, J., Dewprashad, B., Parker, M., & Terracina, J. (1998). Enhancing Fracture Conductivity Through Surface Modification of Proppant. *Formation Damage Control Conference*. Lafayette, LA: Society of Petroleum Engineers.

Novotny, E. (1977). Proppant Transport. *SPE ATCE*. Denver, CO: Society of Petroleum Engineers.

O'Connor, R., Torczynski, J., Preece, D., Klosek, J., & Williams, J. (1997). Discrete Element Modeling of Sand Production. *International Journal of Rock Mechanics and Mineral Science*. *34*, pp. 3-4. Elsevier Science.

Parker, M., Weaver, J., & van Batenburg, D. (1999). Understanding Proppant Flowback. *SPE Annual Technical Conference and Exhibition*. Houston, TX: Society of Petroleum Engineers.

Pitakbunkate, T., Yang, M., & Valko, P. (2011). Hydraulic Fracture Optimization with a p-3D Model . *SPE Production and Operations Symposium*. Oklahoma City: Society of Petroleum Engineers.

Shor, R.J. & Sharma, M.M. (2014). Reducing Proppant Flowback From Fractures: Factors Affecting the Maximum Flowback Rate. *SPE Hydraulic Fracturing Conference*. The Woodlands, TX: Society of Petroleum Engineers.

Settari, A., & Cleary, M. (1984). Three-Dimensional Simulation of Hydraulic Fracturing. Society of Petroleum Engineers.

Stephenson, C., Crabb, T., Orrego, G., & Khachatrian, M. (2003). Effective Proppant Flowback Control Following Hydraulic Fracturing Treatments in Shallow Reservoirs. *SPE ATCE*. Denver: Society of Petroleum Engineers.

Stephenson, C., Crabb, T., Villa Orrego, G., & Kharchatrian, M. (2003). Effective Proppant Flowback Control Following Hydraulic Fracturing Treatments in Shallow Reservoirs. *SPE Annual Technical Conference and Exhibition*. Denver: Society of Petroleum Engineers.

Stephenson, C., Ward, B., Milton-Taylor, D., Brannon, H., & Rickards, A. (2002). Exceptional Proppant Flowback Control for the Most Extreme Well Environments: The Shape of Things to Come. *SPE ATCE*. San Antonio, TX: Society of Petroleum Engineers.

Tamura, S., Aizawa, T., & Kihara, J. (1994). Three-dimensional granular modeling for metallic powder compaction and flow analysis. *Journal of Materials Processing Technology , 42*, 197-207.

Trela, J., Nguyen, P., & Smith, B. (2008). Controlling Proppant Flowback to Maintain Fracture Conductivity and Minimize Workovers: Lessons Learned from 1,500

Fracturing Treatments. *SPE International Symposium and Exhibition on Formation Damage Control*. Lafayette, LA: Society of Petroleum Engineers.

van Batenburg, D., Biezen, E., & Weaver, J. (1999). Towards Proppant Back-Production Prediction. *SPE European Formation Damage Conference*. The Hague, The Netherlands: Society of Petroleum Engineers.

Weaver, J., Baker, J., Woolverton, S., & Parker, M. (1999). Application of Surface Modification Agent in Wells with High Flow Rates. *Latin American and Caribbean Petroleum Engineering Conference*. Caracas, Venezuela: Society of Petroleum Engineers.

Weng, X., & Klein, H. (1998). Numerical Simulation of Proppant Accumulation at Fracture Wall due to Fluid Leak-off. *SPE Rocky Mountain Regional/Low-Permeability Reservoirs Symposium and Exhibtion*. Denver, CO: Society of Petroleum Engineers.

Ye, X., Tonmukayakul, N., Weaver, J., & Morris, J. (2012). Experiment and Simulation Study of Proppant Pack Compression. *SPE International Symposium and Exhibition on Formation Damage Control*. Layfayette, LA: Society of Petroleum Engineers.

Zhang, Y., Marongiu-Porcu, M., Ehlig-Economides, C., Tosic, S., & Economides, M. (2010, November). Comprehensive Model for Flow Behavior of High-Performance-Fracture Completions . *SPE Production & Operations* .